

**TCC Training Seminar on  
Climate Analysis Information on  
Extreme Climate Events**

**25 – 29 November 2019**

**Tokyo, Japan**

**Tokyo Climate Center  
Japan Meteorological Agency**



# **TCC Training Seminar on Climate Analysis Information on Extreme Climate Events**

**25 – 29 November 2019**

**Tokyo, Japan**

## **Contents**

<b>Schedule of the Training Seminar</b>	<b>i</b>
<b>List of Participants</b>	<b>ii</b>
<b>Item 3: “Introduction to Climatology” for experts on climate analysis information</b>	<b>1</b>
<b>Item 4: Introduction of reanalysis and JRA-55</b>	<b>17</b>
<b>Item 7: Climate Analysis information</b>	<b>29</b>
<b>Item 9: Tokyo Climate Center Website and its products – for monitoring the world climate and ocean –</b>	<b>41</b>
<b>Item 10: Climate condition at extreme climate events</b>	<b>51</b>
<b>Item 11: Climate analysis information – Examples of analysis of past extreme events –</b>	<b>63</b>
<b>Annex: Introduction and Operation of iTacs</b>	



**Schedule  
and  
List of Participants**



**TCC Training Seminar on Climate Analysis Information on Extreme Climate Events  
JMA Headquarters, Tokyo, Japan, 25 - 29 November 2019**

**Schedule**

<b>Day 1 - Monday, 25 November</b>	
10:00-10:30	1. Opening - Welcome Address - Self-introduction by participants - Group photo shooting - Courtesy call on JMA's Director-General
10:30-10:45	Coffee Break
10:45-11:15	2. Introduction: Outline and scope of the Training Seminar, and Introduction of the Tokyo Climate Center (TCC)
11:15-12:30	3. Lecture: "Introduction to Climatology" for experts on climate analysis information
12:30-14:00	Lunch
14:00-15:30	3. Lecture: "Introduction to Climatology" for experts on climate analysis information (cont.)
15:30-15:50	Coffee Break
15:50-16:20	4. Lecture: Introduction of reanalysis and JRA-55
16:20-17:00	5. Exercise: Introduction and operation of iTacs (Basic)
17:00-17:20	Coffee Break
17:20-18:00	5. Exercise: Introduction and operation of iTacs (Basic, cont.)
18:30-20:00	Reception at KKR Hotel Tokyo
<b>Day 2 - Tuesday, 26 November</b>	
09:30-10:30	6. Lecture: Interannual to decadal variability in the tropical oceans
10:30-11:00	7. Lecture: Climate Analysis information
11:00-11:20	Coffee Break
11:20-12:00	7. Lecture: Climate Analysis information (cont.) and an example for your presentation
12:00-12:30	8. Exercise: Introduction and operation of iTacs (Advanced)
12:30-14:00	Lunch
14:00-15:30	8. Exercise: Introduction and operation of iTacs (Advanced, cont.)
15:30-15:50	Coffee Break
15:50-17:00	9. Lecture: Tokyo Climate Center Website and its products - for monitoring the world climate and ocean -
17:00-17:20	Coffee Break
17:20-18:00	9. Lecture: Tokyo Climate Center Website and its products - for monitoring the world climate and ocean - (cont.)
<b>Day 3 - Wednesday, 27 November</b>	
9:30-11:00	10. Exercise: Climate condition at extreme climate events
11:00-11:20	Coffee Break
11:20-12:30	11. Lecture and Exercise: Climate Analysis information - example of analysis of past extreme events -
12:30-14:00	Lunch
14:00-16:00	12. Exercise: Analyzing past extreme climate events for your country and preparation for presentation
16:00-16:20	Coffee Break
16:20-18:00	12. Exercise: Analyzing past extreme climate events for your country and preparation for presentation (cont.)
<b>Day 4 - Thursday, 28 November</b>	
9:30-11:00	12. Exercise: Analyzing past extreme climate events for your country and preparation for presentation (cont.)
11:00-11:20	Coffee Break
11:20-12:30	12. Exercise: Analyzing past extreme climate events for your country and preparation for presentation (cont.)
12:30-14:00	Lunch
14:00-15:20	13. Presentation by participants (4 participants) - Presentation (15 min.) followed by Q&A (5 min.) -
15:20-15:40	Coffee Break
15:40-17:00	13. Presentation by participants (cont.) (4 participants)
17:00-17:20	Coffee Break
17:20-18:00	13. Presentation by participants (cont.) (2 participants)
<b>Day 5 - Friday, 29 November</b>	
9:30-10:30	13. Presentation by participants (cont.) (3 participants)
10:30-10:50	Coffee Break
10:50-11:30	13. Presentation by participants (cont.) (2 participants)
11:30-12:15	14. Wrap up and closing
12:30-14:00	Lunch
14:00-18:00	Technical tour

## List of participants

### Bangladesh

Mr A.K.M Ruhul KUDDUS  
Meteorologist  
Storm Warning Centre  
Bangladesh Meteorological Department  
Agargaon, Dhaka - 1207  
People's Republic of Bangladesh  
TEL: +88029135742, +88029141437  
FAX: +88029119230, +880258152019  
E-mail: ruhulk1975@gmail.com

### Lao People's Democratic Republic

Mr Phapasit KHAMPHOUMY  
Weather forecaster  
Department of Meteorology and Hydrology  
Ban Akad, Avenue Souphanouvong Sikhottabong  
Dist., P.O. Box 2903, Vientiane  
Lao People's Democratic Republic  
TEL: +856-21 215010, 263657  
FAX: +856-21 223446, 520038  
E-mail: kai.khamphoumy@gmail.com,  
dmhvte@etllao.com

### Bhutan

Ms Phuntsho WANGMO  
Assistant Environment Officer  
Weather and Climate Services Division, National  
Center for Hydrology and Meteorology of Bhutan,  
Kingdom of Bhutan  
TEL: +975 02 323703, mobile +975-178-41-659  
FAX: +975-02-327202  
E-mail: pwangmo@nchm.gov.bt

### Malaysia

Ms Siti Noor Faizan MUHAMAD FADZIL  
Meteorological Officer  
National Climate Center  
Malaysian Meteorological Department  
Jalan Sultan, 46667 Petaling Jaya, Selangor  
Malaysia  
TEL: +603-79678207  
FAX: +603-79563621  
E-mail: faizan@met.gov.my

### Hong Kong, China

Mr. Wing Hang CHAN  
Experimental Officer  
Hong Kong Observatory  
134A Nathan Road, Tsim Sha Tsui, Kowloon  
Hong Kong, China  
TEL: +852 29263104  
FAX: +852 23752645  
E-mail: whchan@hko.gov.hk

### Mongolia

Ms Doljinsuren MYAGMAR  
Senior Engineer  
Weather Forecasting Division,  
National Agency for Meteorology and  
Environmental Monitoring (NAMEM)  
15160 Juulchny gudamj-5, Ulaanbaatar  
Mongolia  
TEL: 976-11-326609, 976-11-326611,  
976-90560218  
FAX: +976-11-326611  
E-mail: dosharty@gmail.com

### Indonesia

Dr (Mr) Supari  
Head of Climate Early Warning Sub Division,  
Center for Climate Change Information,  
Indonesia Agency for Meteorology Climatology  
and Geophysics (BMKG)  
Jl. Angkasa 1, No.2, Kemayoran, Jakarta 10720  
Republic of Indonesia  
TEL: +62 81995251300  
E-mail: supari.bmg@gmail.com

### Myanmar

Ms May Khin CHAW  
Director  
Department of Meteorology and Hydrology  
Officw No (5), Nay Pyi Taw  
Republic of the Union of Myanmar  
TEL: +95 9 969814238  
FAX: +95 673411250  
E-mail: mkhinc@gmail.com

**Nepal**

Mr Bishnu Prasad NEUPANE  
Assistant Meteorologist  
Department of Hydrology and Meteorology  
P.O. Box 406, Babarmahal, Kathmandu, Nepal  
+977-01-4258276(office)  
E-mail: climate.reader@gmail.com

**Pakistan**

Mr Fayyaz AHMED  
Assistant Meteorologist  
Meteorological Office, Multan Airport  
Pakistan Meteorological Department  
Islamic Republic of Pakistan  
TEL: + 92-334-3327415  
FAX: + 92-61-9202597  
E-mail: fayyazpmd@gmail.com

**Papua New Guinea**

Mr Gabriel Tuno  
Climate Data Processing Officer,  
Papua New Guinea National Weather Service,  
Department of Transport  
P. O. Box 1240, Boroko, National Capital District,  
111  
Independent State of Papua New Guinea  
Tel +675 3255925  
Fax +675 3255544  
E-mail: aizotuno@gmail.com

**Philippines**

Ms. Jorybell A. MASALLO  
Senior Weather specialist I, Philippine  
Atmospheric, Geophysical and Astronomical  
Services Administration (PAGASA)  
Science Garden, Agham Road, Diliman, Quezon  
City 1100  
Republic of the Philippines  
TEL: +632-284-0800-LOCAL 906  
E-mail: jorybell.masallo@yahoo.com  
jorybell.masallo@gmail.com

**Sri Lanka**

Ms Aluthgama Hewage Pabodini Priyanka  
KARUNAPALA  
Meteorologist  
Department of Meteorology  
No. 383, Baudhaloka Mawatha, Colombo 07  
Democratic Socialist Republic of Sri Lanka  
TEL: +94 11 2252721, +94717999840  
FAX: +94112698311  
E-mail: pabodini.karunapala@gmail.com

**Thailand**

Ms Krittika SUEBSAK  
Meteorologist  
Meteorologist, Climate Center, Meteorological  
Development Division  
Thai Meteorological Department  
4353 Sukhumvit Road, Bangna,  
Bangkok 10260  
Kingdom of Thailand  
TEL: +66-084-7582959  
E-mail: pinajika@hotmail.com

**Viet Nam**

Ms NGUYEN Thi Diem Huong  
Climatologist at Climate Prediction Division  
National Center for Hydro-Meteorological  
Forecasting,  
Viet Nam Meteorological and Hydrological  
Administration  
No. 08, Phao Dai Lang str., Ha Noi  
Socialist Republic of Viet Nam  
TEL: +84397545856  
E-mail: huongdiem.nchmf@gmail.com



**“Introduction to Climatology”  
for experts on climate analysis information**



# “Introduction to Climatology” for experts on climate analysis information

Tomoaki OSE (tomoaose@mri-jma.go.jp)

Climate Research Department, Meteorological Research Institute (MRI/JMA)

1-1 Nagamine, Tsukuba, 305-0052, JAPAN

## 1. Climate and Climate system

According to WMO website, “on the simplest level the weather is what is happening to the atmosphere at any given time. Climate, in a narrow sense, can be considered as the ‘average weather,’ or in a more scientifically accurate way, it can be defined as ‘the statistical description in terms of the mean and variability of relevant quantities over a period of time.’” Although climate is the synthesis of the weather, climate is not maintained only by atmosphere itself but is formed in the interactions among many components of the Earth. This system is named as a climate system. The global climate system consists of atmosphere including its composition and circulation, the ocean, hydrosphere, land surface, biosphere, snow and ice, solar and volcanic activities (Fig.1). These components interact on various spatial and temporal scales through the exchanges of heat, momentum, radiation, water and other materials.

The purpose of the lecture is to know how climate is formed and its variability is caused. In the lecture, the global warming or anthropogenic “climate change” defined by United Nations Framework Convention on Climate Change (UNFCCC) is also included.

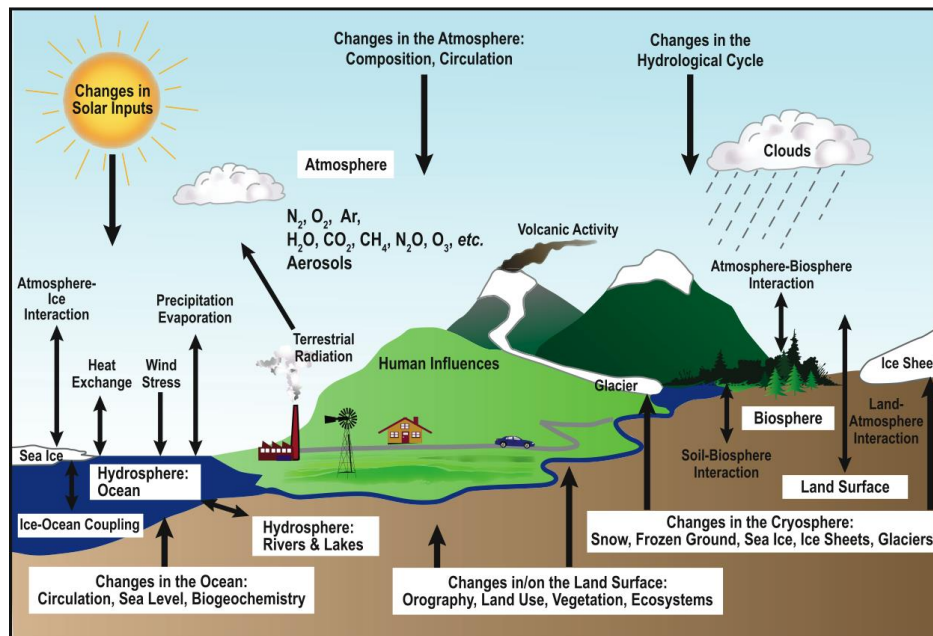


Figure 1 Schematic view of the components of the climate system, their processes and interactions. From IPCC (2007).

## 2. Global mean temperature and Radiative balance

Global mean temperature of planets, which is the temperature “observed from space”, is estimated by global radiation balance between absorbed solar radiation and terrestrial emission from the planet. Incoming solar radiation is reflected back to space by a fraction of the planetary albedo. For the Earth, the observed mean ground temperature ( $15^{\circ}\text{C}$ ) is warmer by  $34^{\circ}\text{C}$  than the estimated temperature ( $-19^{\circ}\text{C}$ ). The reason is explained by radiative absorption by greenhouse gas in atmosphere which is another important factor to determine mean ground temperature besides planetary albedo.

The Earth’s atmosphere has different characteristics for shortwave and longwave radiations (Fig.2). It is transparent (about 50%) for shortwave radiative flux from the sun as an approximation except for the reflection due to clouds (about 20%). On the other hand, the longwave or thermal radiation flux emitted from the Earth’s ground is absorbed (about 90%) once in the atmosphere approximately and then mostly emitted back to the ground (greenhouse effect). Upper cold atmosphere and clouds emit less longwave flux to space than the ground emits. As a net, surface ground is heated by shortwave radiation from the sun, and atmosphere is cooled by longwave emission to space. The vertical contrast of the heating between ground and atmosphere creates thermal instability, which is compensated by vertical transport processes of sensible and latent heat energy due to turbulences, convections and waves. The global warming is caused by radiative imbalance between incoming solar radiation and outgoing thermal radiation at the top of the atmosphere.

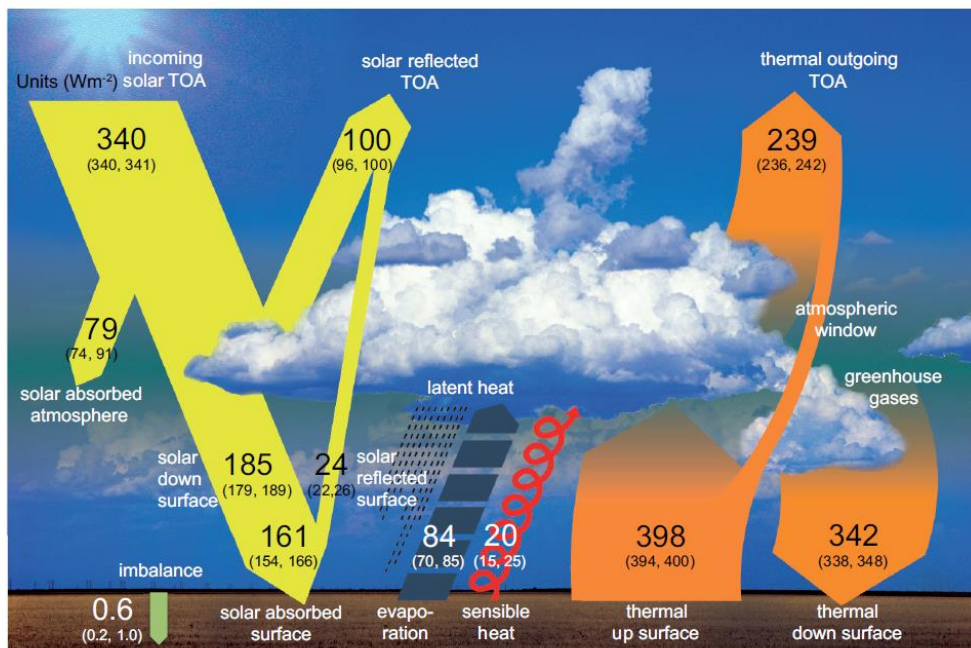
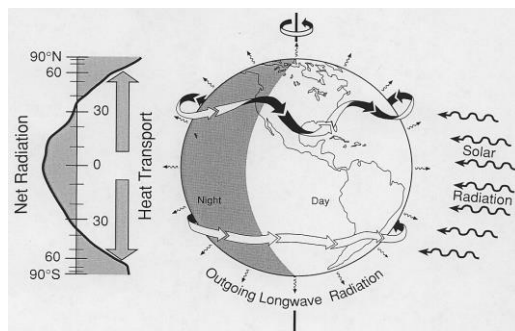


Figure 2 Schematic diagram of the global mean energy balance of the Earth. Numbers indicate best estimates for the magnitudes of the globally averaged energy balance components together with their uncertainty ranges, representing present day climate conditions at the beginning of the twenty first century. Units  $\text{W}/\text{m}^2$ . From IPCC (2014).

### 3. Annual mean circulation and Horizontal heating contrast

Longitudinal contrast of radiative heating is created between day and night (Fig.3). Latitudinal heating contrast on the Earth is created on seasonal time-scale by the different incoming shortwave radiation between near the poles and the tropics (Fig.3). Local surface temperature determining outgoing longwave radiation is not adjusted instantly enough to compensate for the shortwave radiation contrast. A part of absorbed radiative energy in low latitudes is transported poleward by meridional circulations and waves in atmosphere and ocean, and these heat transports keep high-latitudes warmer than the radiative equilibrium.

Poleward/equatorward air motions form westerly/easterly wind in the upper/lower subtropics (Fig.4) through Coriolis force due to the rotation of the Earth (or the angular momentum conservation about the Earth's rotation axis). Extra-tropical waves are also responsible for creating mid- to high latitude's westerly jets.



**Figure 3 Horizontal radiative imbalance and energy transport by the atmosphere and ocean. From IPCC (1995).**

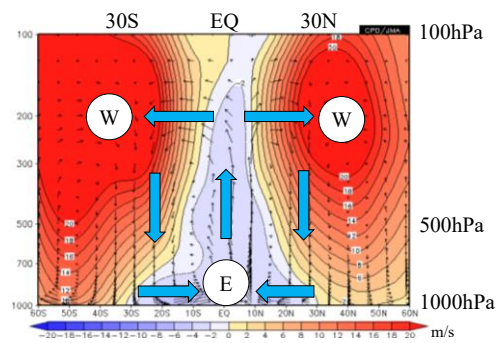


**Figure 4 Annual and zonal mean wind. Shade: zonal wind, and arrow: meridional and vertical wind.**

### 4. Seasonal change and Heat capacity

Seasonal change is definitely produced by the seasonally changing solar incidence with its maxima at the South Pole in December and at the North Pole in June (Fig.5 left). However, zonally averaged features of temperature are not drastically changed in the troposphere (lower than about 100hPa) through the whole year, maintaining hot tropics and cold poles (Fig.5 right). This fact is attributed to basically unchanged distribution of sea surface temperature (SST) due to large heat capacity of the oceans; in the Earth, heat capacity of the ocean is about 1,000 times of that of the atmosphere. SSTs roughly determine the location of deep cumulus occurrences, which leads to vertical energy mixing in the troposphere and drives global circulations (Webster, 1994). Stratospheric climate above 100hPa varies following the seasonal march of the sun (Fig.5 middle) because of the seasonal change of ozone-related shortwave heating and small heat capacity of thin stratospheric atmosphere.

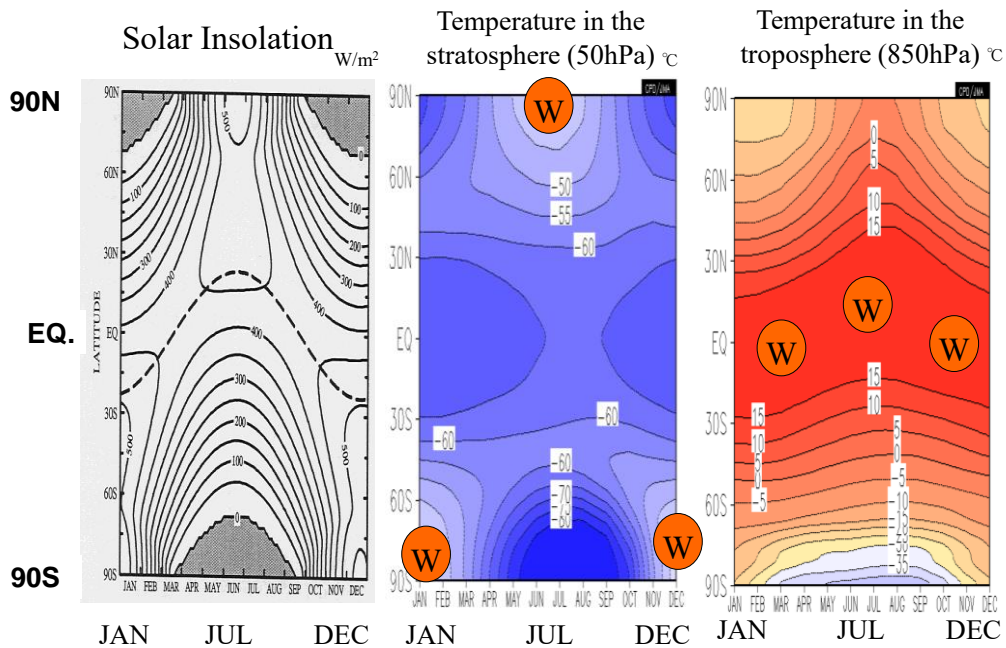


**Figure 5** Seasonal change of (left) solar insolation, zonally averaged temperature (middle) at 50hPa and (right) at 850hPa. The figure for solar insolation is from IPCC (1995).

Heat capacity of land surface is also small as compared with that of the oceans. Surface air temperature over the northern continents is much higher than SSTs at the same latitudes in the northern summer (especially in daytime) and much colder in the northern winter (Fig.6). The large contrasts of surface air temperature between the continents and the oceans add a significant feature to regional seasonal changes of rainfall and wind around the continents in low and mid-latitudes, which is named as monsoon. A concentrated subtropical rainfall forms a typical summer monsoon system consisting of an upper-level anti-cyclonic circulation, a monsoon trough, a low-level jet, a subtropical rainfall band expanding north eastward (south eastward) and extensive downward motions causing dry region in the north westward (south westward) area of the Northern (Southern) Hemisphere (Rodwell and Hoskins, 1996), as shown in the Asian region of Fig.6 and Fig. 7.

**Jan-Jul contrast of surface temperature/precipitation**

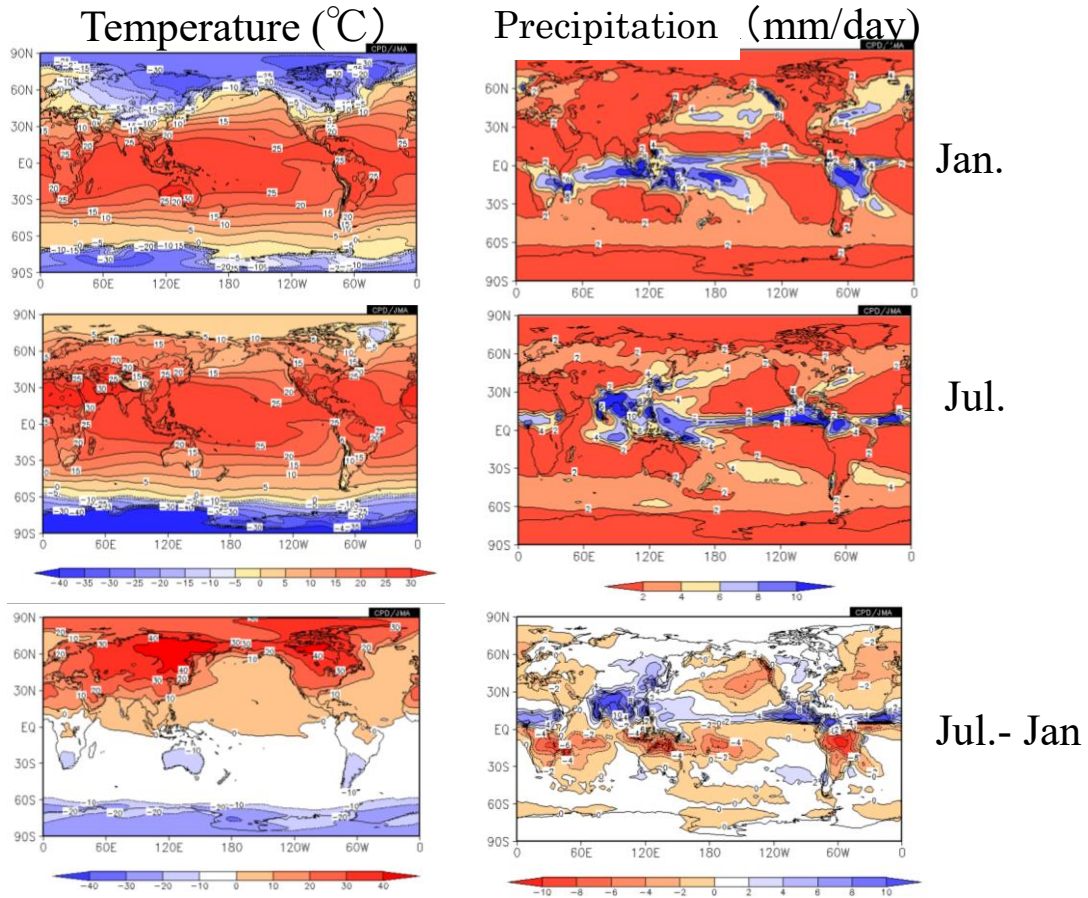


**Figure 6** (Left) surface are temperature and (right) precipitation in (upper) January, (middle) July, and (bottom) difference between the two months.

**Northern Summer Monsoon circulation**

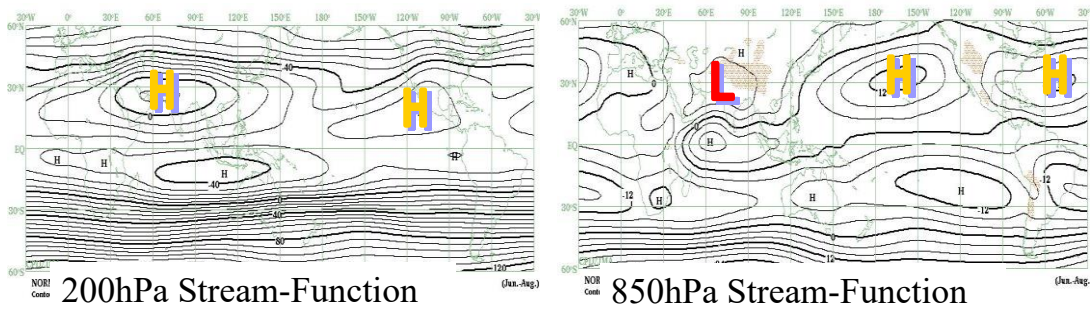


**Figure 7** (Left) 200hPa stream function and (right) 850hPa stream function in JJA.

Mountains have also impact on seasonal changes in local climate through thermal and dynamical processes. A good way to understand climate system is to modify or remove some elements of the climate system (Fig. 1). It is not easy to modify a real climate system of the Earth by changing the Earth orbit or removing mountains. Instead, we can easily modify virtual climate systems simulated numerically in climate models based on physics and other fundamental sciences. From the comparison between with/without mountain model experiments (Fig. 8), we can see that mountains would be responsible for the real world climate of humid summer and somewhat cold winter in the eastern parts of the continents.

## Effect of mountain: Koppen climate

Kitoh(2005)

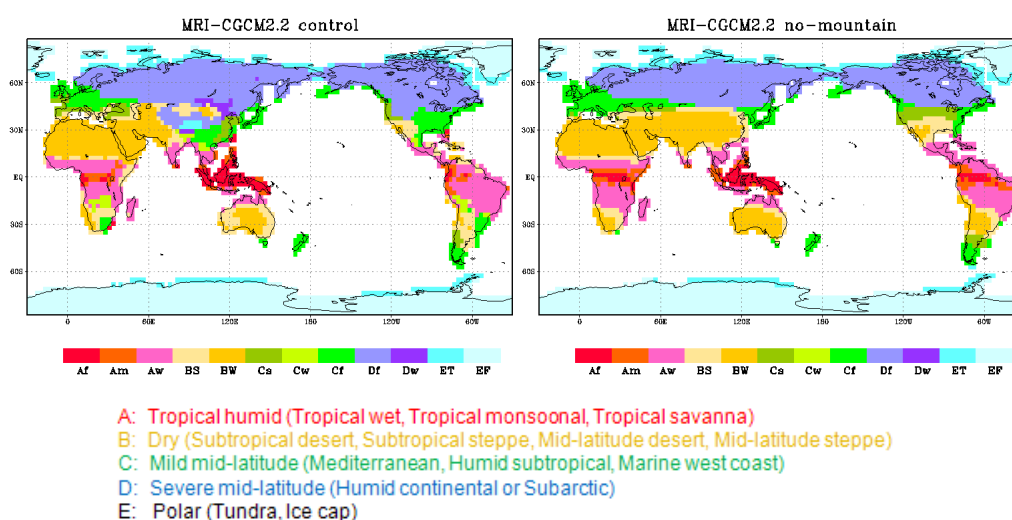


Figure 8 Koppen climate maps simulated by a climate model (left) with mountains and (right) without mountains. From Kitoh (2005) in Japanese.

## 5. Intra-seasonal variability

Atmosphere itself includes internal instability mechanisms, typically the baroclinic instability around the extratropical westerly jets (Vallis, 2006). Therefore, atmosphere itself is considered as chaotic or unpredictable beyond a few weeks. However, there are some long-lived phenomena useful for one-month prediction. Long-term mean atmosphere (climate) varies naturally with various space and time (Fig. 9) besides the global warming. Some atmospheric low-frequency (>10days) teleconnections are analyzed such as wave patterns along the westerly jet waveguides, which are consistent with the Rossby-wave propagation theory (Fig. 10). Numerical ensemble predictions from many disturbed atmospheric initials are a reasonable tool to capture mean weathers in next few weeks.

■ Atmospheric and Oceanic variability related to seasonal forecasting

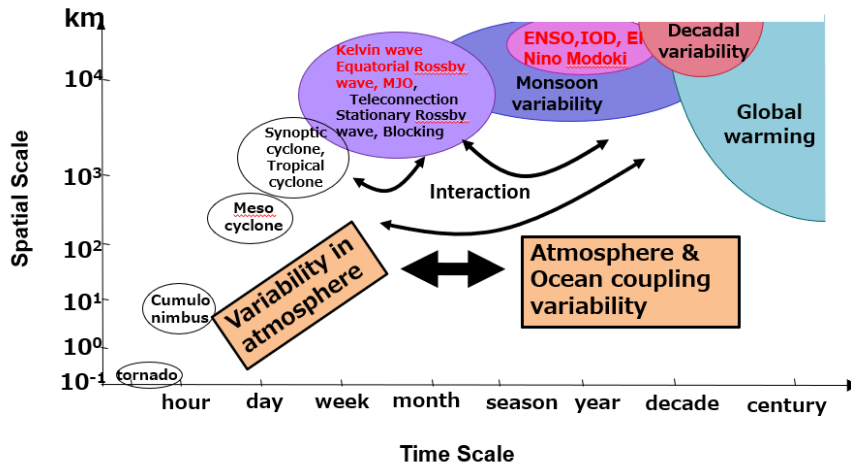
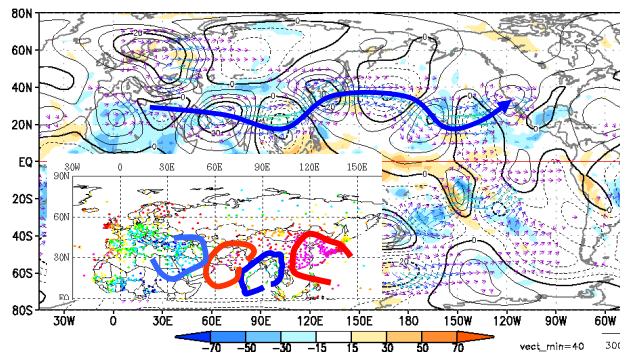


Figure 9 Schematic picture for atmospheric and oceanic variability with various spatial and temporal scales.

Wave train along the Asian jet

1.11 – 1.15



Observed 5-day mean stream function anomalies at 200hPa (contours) 2002.1.11-1.15

15

Figure 10 An example of atmospheric wave trains along Asian jet in the northern winter.

In the tropics, some peaks in spatial and temporal power-spectrums, indicating organized atmospheric variability coupled with convective activity, are imbedded in red noise backgrounds. Weekly to intra-seasonal variabilities of outgoing longwave radiation (OLR) associated with equatorial waves, such as Kelvin waves, equatorial Rossby waves (ER) and mixed Rossby-Gravity waves (MRG), can be detected in Fig. 11 as well as the Madden-Julian Oscillation (MJO).

## ■ (Low frequency) equatorial waves in the atmosphere

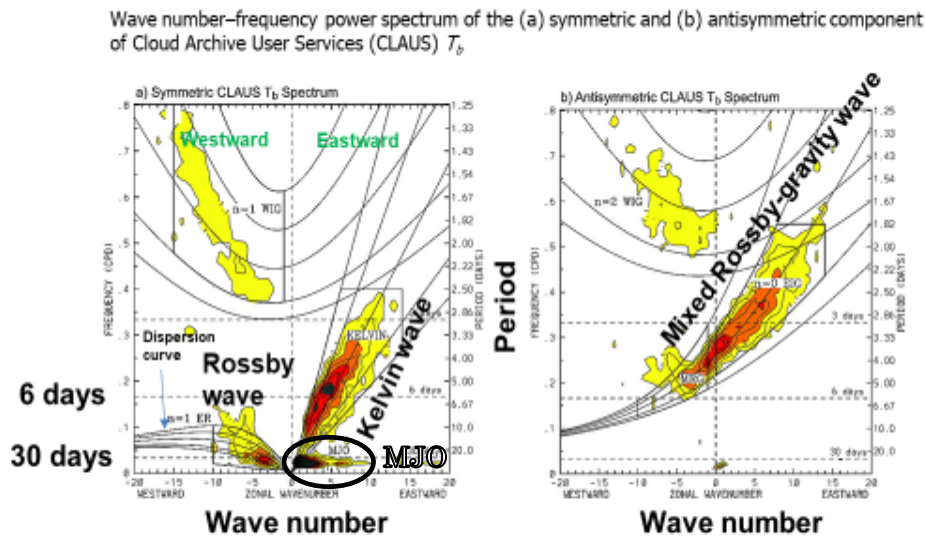


**Figure 11** Equatorial waves in the atmosphere represented by wave-number-frequency spectrum of (a) symmetric and (b) antisymmetric component of clouds.

The Madden-Julian Oscillation (MJO) is an eastward-moving oscillation of surface pressure, precipitation (or cloud) and winds along the equator with the period of 30–60 days and planetary scale wavenumbers (Fig. 11). Monitoring MJO or watching OLR and velocity potential anomalies may be very helpful for intra-seasonal prediction in the tropics to the subtropics and even in the mid-latitudes (Fig. 12). Improvement of MJO prediction skill is one of key topics for operational numerical prediction centers in the world.

The MJO and related OLR or convection anomalies are symmetry around the equator for the northern winter (Fig. 12 left) whereas those migrate northward toward Asian monsoon regions over the Indian Ocean and the western Pacific for the northern summer (Fig. 12 right).

### 6. Inter-annual variability

Atmosphere-ocean couplings are able to produce longer time-scale natural variability in atmosphere with periods beyond months up to several and decadal years. A typical example is ENSO (El Niño / Southern Oscillation) with the period of 2–7 years, which is the most dominant interannual climate variability in the climate system and has huge sociological and economic impacts globally. El Niño events themselves, and related surface air temperature and precipitation anomalies are predicted successfully on seasonal to inter-annual scales (Fig.13). The SST anomalies with El Niño tend to keep seasonally steady precipitation (heating) anomalies over the equatorial central Pacific. The response of the upper and lower-level tropical

atmosphere to these steady heating anomalies can be explained based on forced equatorial waves or the Gill-pattern (or Matsuno-Gill pattern) (Gill 1980; James 1995). These anomalous steady heating in the tropics forces modification of Walker circulation and occurrence of stationary Rossby waves in the subtropics, which propagate to mid-latitudes and form teleconnection patterns such as the Pacific North America (PNA) pattern.

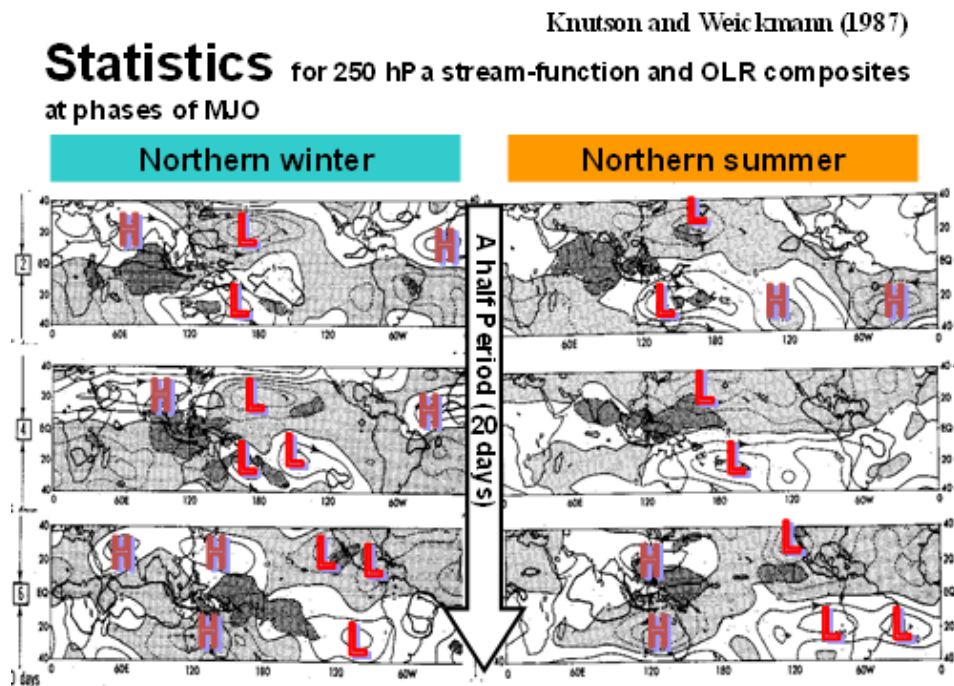


Figure 12 Composite maps of OLR (shades) and 250hPa stream function anomaly (contours) at MJO phases (left) for the northern winter and (right) for the northern summer (from Knutson and Weickmann 1987).

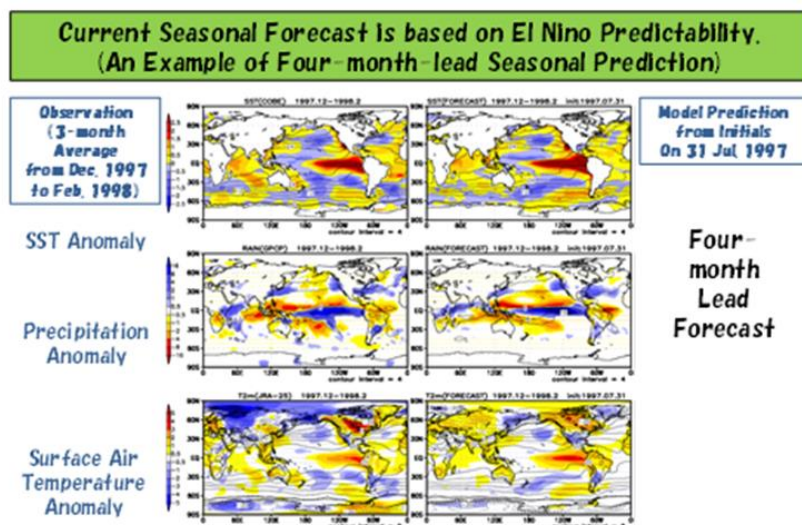
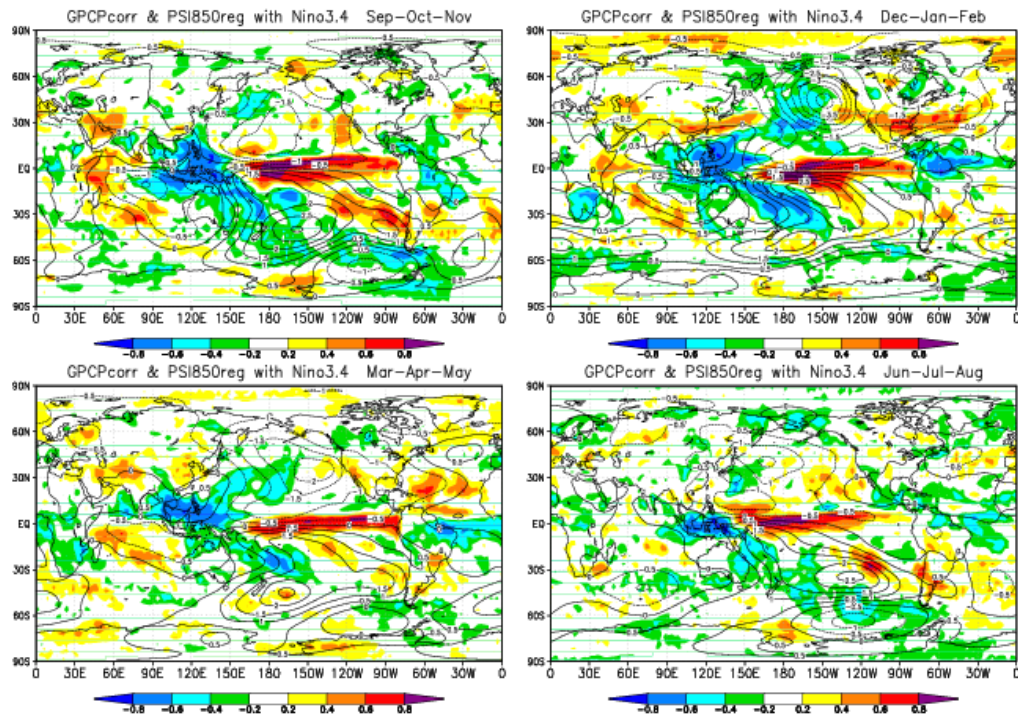


Figure 13 (Left) observed SST, precipitation and surface air temperature anomalies for DJF 1997-98. (Right) the same except for four-month lead prediction.



**Figure 14** (Shades) statistical correlations between 3-month-mean precipitation anomaly and Nino3.4 SST anomaly for September to November (upper-left), December to February (upper-right), March to May (lower-left) and June to August (lower-right). Contours indicate the statistical regression of 850hPa stream-function anomaly onto Nino3.4 SST anomaly. The JRA-25(Onogi et al. 2006), GPCP (Adler et al. 2003) and COBE SST (Ishii et al. 2005) data during 25 years of Sep1979 to Aug2004 is used. The 95% significance for the correlations corresponds to roughly more than 0.4 or less than -0.4.

Therefore, atmospheric responses to El Niño, including precipitation anomaly, are distributed worldwide, especially strong over the western Pacific in the tropics. Those responses have statistically common but seasonally dependent regional distributions among El Niño events (Fig.14).

Recently, terms of “El Niño Modoki” or “Central Pacific (CP)-El Niño” are used to distinguish them from normal El Niño events or Eastern Pacific (EP)-El Niño. They consist of the equatorial Pacific phenomena with warm SST anomalies and enhanced precipitation in the central Pacific, and cold SST anomalies and suppressed precipitation in the eastern Pacific, on contrast (Fig.15). The remote effect of El Niño during the mature stage is stored in the Indian Ocean capacity and still influential to the Indo-western Pacific climate even during summer following the ENSO (Fig.16). A dipole mode with an east-west SST anomaly contrast sometimes occurs around September and October in the tropical Indian Ocean, which is at least partially independent from ENSO events (Fig. 17). Occurrence of this mode affects climate over various regions including tropical eastern Africa and the maritime continent.

## ■ El Niño Modoki & CP El Niño

Nature, 2009  
**The El Niño with a difference**  
 Karumuri Ashok and Toshio Yamagata

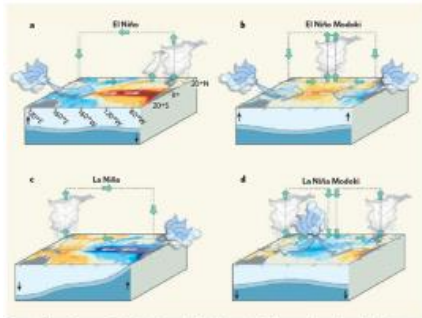


Figure 2 | Anomalous conditions in the tropical Pacific. a, An El Niño event is produced when the easterly winds weaken, sometimes, in the west, westerlies prevail. This condition is categorized by warmer than normal sea surface temperatures (SSTs) in the east of the ocean, and is associated with alterations in the thermocline and in the atmospheric circulation that make the east wetter and the west drier. b, An El Niño Modoki event is an anomalous condition of a distinctly different kind. The warmest SSTs occur in the central Pacific, flanked by colder waters to the east and west, and are associated with distinct patterns of atmospheric convection. c, d, The opposite (La Niña) phases of the El Niño and El Niño Modoki respectively. Yeh *et al.* argue that the increasing frequency of the Modoki condition is due to anthropogenic warming, and that these events in the central Pacific will occur more frequently if global warming increases.

Nature, 2009  
**El Niño in a changing climate**  
 Sang-Wook Yeh<sup>1</sup>, Jong-Seong Kug<sup>2</sup>, Boris Dewitte<sup>3</sup>, Min-Ho Kwon<sup>3</sup>, Ben P. Kirtman<sup>4</sup> & Fai-Fai Jin

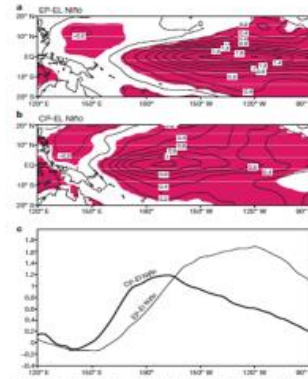


Figure 3 | Deviations of mean SST for the two characteristics of El Niño from the 1950-2006 observations. a, The EP-El Niño; b, the CP-El Niño. The contour interval is 0.2 °C, and shading denotes a statistical confidence at 95% confidence level based on a Student's *t*-test. c, The seasonal structure for the composite EP-El Niño (thin line) and CP-El Niño (thick line) averaged over 2°N to 2°S.

51

Figure 15 El Niño Modoki (Ashok and Yamagata 2009) and CP El Niño (Yeh et al. 2009).

## Indian Ocean Capacitor Effect on Indo-Western Pacific Climate during the Summer following El Niño

SHANG-PING XIE,<sup>\*,†</sup> KAIMING HU,<sup>#</sup> JAN HAFNER,<sup>\*</sup> HIROKI TOKINAGA,<sup>\*</sup> YAN DU,<sup>\*,@</sup>  
 GANG HUANG,<sup>#</sup> AND TAKEAKI SAMPE<sup>\*</sup>

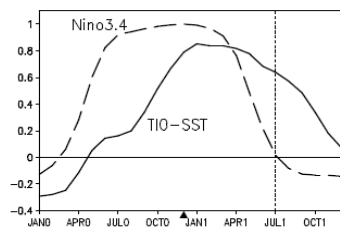


Fig. 1. Correlation of tropical Indian Ocean (40-100°E, 20°S-20°N) SSTA (solid) with the Nino 3.4 (170°W-120°W, 5°S-5°N) SSTA index for Nov(0)-Dec(0)-Jan(1). Numerals in parentheses denote years relative to El Niño: 0 for its developing and 1 for decay year. The dashed curve is the Nino 3.4 SSTA auto-correlation as a function of lag. The black triangle denotes Dec(0), the peak phase of ENSO.

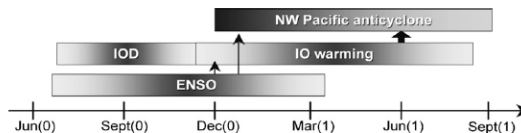


FIG. 13. Seasonality of major modes of Indo-western Pacific climate variability. Vertical arrows indicate causality, and the block arrow emphasizes the TIO capacitor effect, the major finding of the present study.

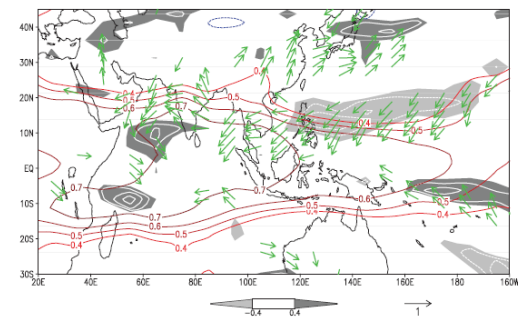


FIG. 6. JJA(1) correlation with the NDJ(0) Niño-3.4 SST index: tropospheric (850-250 hPa) temperature (contours), precipitation (white contours at intervals of 0.1; dark shade > 0.4; light < -0.4), and surface wind velocity (vectors).

Figure 16 Indian Ocean capacitor effect. (Left) lagged correlation of tropical Indian Ocean SSTA with Nino 3.4 SSTA for Nov(0)-Dec(0)-Jan(1). (Upper-right) seasonality of major modes. (Lower-right) correlation of the Nov(0)-Dec(0)-Jan(1) Nino3.4 SSTA with the following Jun(1)-July(1)-Aug(1) tropospheric temperature (contours), precipitation (shades) and surface wind (vectors). From Xie et al. (2009).

## A dipole mode in the tropical Indian Ocean

N. H. Saji\*, B. N. Goswami†, P. N. Vinayachandran\* & T. Yamagata‡

Saji et al., Nature 1999

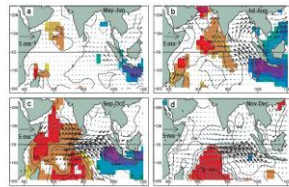


Figure 2 A composite dipole mode event,  $n=4$ . Evolution of composite SST and surface wind anomalies from May–June (a) to Nov–Dec (d). The statistical significance of the analyzed anomalies were estimated by the two-tailed  $t$ -test. Anomalies of SSTs and winds exceeding 90% significance are indicated by shading and best arrows, respectively.

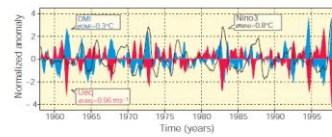


Figure 1 Dipole mode and El Niño events since 1950. Plotted in blue, the dipole mode index (DMI) exhibits a pattern of evolution distinctly different from that of the El Niño, which is represented by the Niño-3 sea surface temperature (SST) anomalies (black line). On the other hand, equatorial zonal wind anomalies ( $U_{eq}$ , plotted in red) coevolves with the DM. All the three time series have been normalized by their respective standard deviations. We have removed variability with periods of 7 years or longer, based on harmonic analysis, from all the data sets used in this analysis. In addition, we have smoothed the time series using a 5-month running mean.

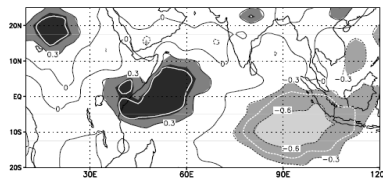
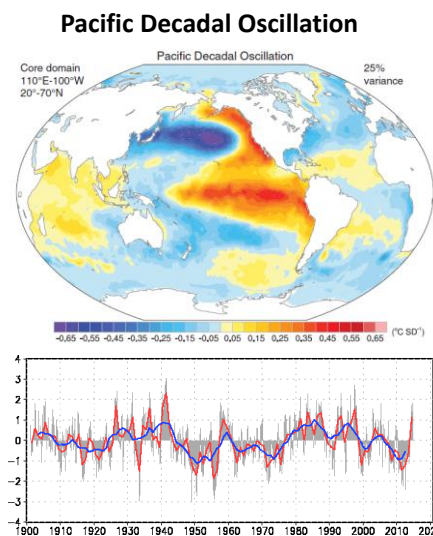


Figure 4 Rainfall shifts northwest of the OTCZ during dipole mode events. The map correlates the DMI and rainfall to illustrate these shifts. The areas within the white curve exceed the 90% level of confidence for non-zero correlation (using a two-tailed  $F$ -test).

Figure 17 A dipole mode in the tropical Indian Ocean. (Upper-left) time-evolution of the dipole mode SST anomaly, (lower-left) rainfall shift during the dipole mode, (right) historical records for dipole mode and El Niño events. From Saji et al. (1999).

## 7. Decadal variability

One of decadal variabilities is found in SST anomaly from the North Pacific to the tropics (Fig. 18) which is named Pacific Decadal Oscillation (PDO) or Interdecadal Pacific Oscillation (IPO). A possible mechanism of PDO is the subduction hypothesis; high latitudes' cold surface water is subducted in the North Pacific and flows into the subtropical deeper ocean along the surfaces of constant density, and then emerges again to the surface of the equatorial Pacific by upwelling (Deser et al. 1996).



Trenberth and Fasullo (2013)

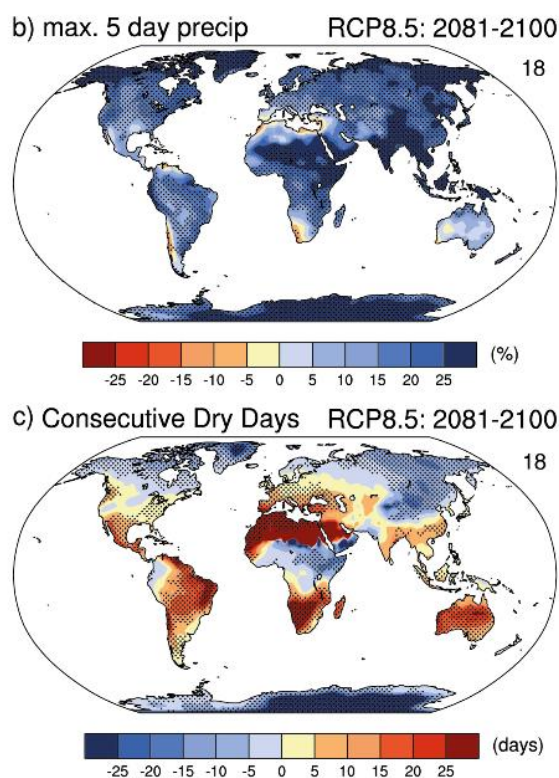
PDO index (From JMA HP)

Figure 18 (Upper) SST anomaly pattern in the positive phase of Pacific Decadal Oscillation (PDO)(from Trenberth and Fasullo, 2013) and (lower) PDO index (from <http://ds.data.jma.go.jp/tcc/tcc/products/elniño/decadal/pdo.html>).

This is consistent with the analysis showing that the decadal SST variability in the central North Pacific spreads into the deep ocean. PDO has impact on ENSO characteristics and regional climate on decadal scales. Several studies indicated that the negative phase of PDO played the major role in the slowdown of the global averaged surface air temperature raise in recent years (Meehl, 2015).

## 8. Global warming

Human activity also changes external conditions of the climate system, typically the increase of greenhouse gases which lead to warmer climate. The influences of global warming appear not only in global mean temperature but also in local precipitation, tropical cyclones and weather extremes including extreme precipitation rate and consecutive dry days (Fig. 19). Sea level rise comes from thermal expansion of water in the ocean, as well as retreating glaciers and ice sheet (Fig.20).



**Figure 19** (Upper) projected percent changes of the annual maximum five-day precipitation accumulation over the 2081-2100 in the RCP8.5 scenario relative to the 1981-2000 from the CMIP5 models and (lower) the same as the upper figure expect for the annual maximum number of consecutive dry days when precipitation is less than 1 mm/day. Stippling indicates gridpoints with changes that are significant at 5% level using a Wilcoxon signed-ranked test. (From WGI\_AR5\_Fig12-26b and c).

## ■ Sea Level Rise

Sea level rise comes from thermal expansion, as well as retreating glaciers and ice sheet

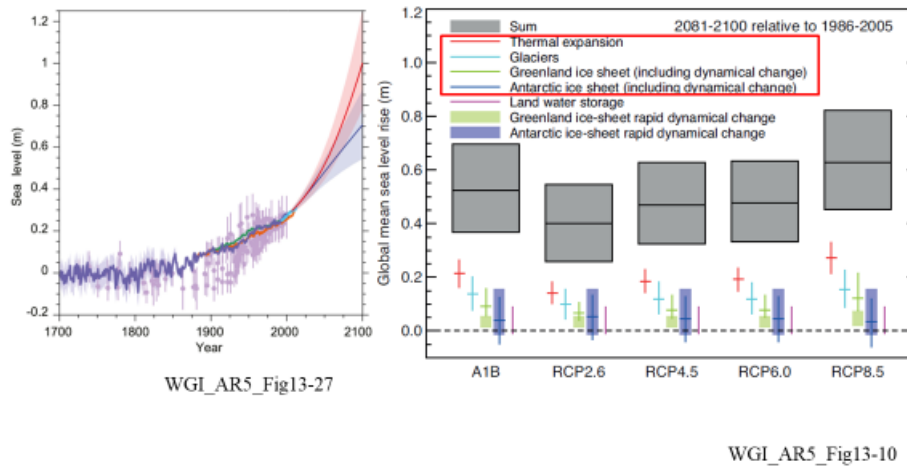


**Figure 20** Sea level rise projection (From WGI\_AR5\_Fig13-27 and Fig13-10).

## 9. Summary

Unusual weather and climate are attributed to unusual atmospheric flows, storms and convective disturbance. Diagnostic analysis shows that those disturbances are often related to atmospheric intrinsic waves and phenomena. Numerical ensemble predictions from many disturbed atmospheric initials are a reasonable tool to capture mean weathers in next few weeks.

However, atmospheric environment is maintained and influenced by other elements consisting of the climate system. Unusual and steady convective activity is sometimes connected to long-term SST anomalies related to ocean variability. Numerical ensemble atmosphere-ocean simulations starting from many disturbed atmospheric and oceanic initials are a reasonable tool to capture the mean state of weathers and climate in a timescale from weeks to seasons.

Radiative processes including longwave absorption by greenhouse gases and shortwave reflection by snow, ice, clouds and aerosols determine the local Earth's ground temperature. The distribution of ground temperature is influential to vertical and horizontal atmospheric and oceanic stabilities, the amount of water vapor and the speed of water cycle. Then, those can affect atmospheric and oceanic flows, the features of storms and convections and eventually our daily lives.

Extreme precipitation and weathers are directly connected to disasters. The extremes tend to be caused when unusual weather and various climate variability happen at the same time while the global warming is gradually strengthened. Therefore, we need to continue careful watches and diagnostics for global and local climate systems (Fig.1), as well as its decadal to historical predictions using the Earth or climate system models starting from many disturbed oceanic initials.

## References

- Ashok, K. and T. Yamagata, 2009: The El Niño with a difference. *Nature*, 461, 481-484.
- Deser, C., M. A. Alexander and M. S. Timlin, 1996: Upper-ocean thermal variations in the North Pacific during 1970-1991. *J. Climate*, **9**, 1840-1855.
- Gill, A. E., 1980: Some simple solutions for heat-induced tropical circulation. *Quart. J. Meteor. Soc.*, **106**, 447-462.
- IPCC Second Assessment Report (SAR) Climate Change 1995: The Science of Climate Change.
- IPCC Fourth Assessment Report (AR4) Climate Change 2007: The Physical Science Basis.
- IPCC Fifth Assessment Report (AR5) Climate Change 2014: The Physical Science Basis.
- Kiladis, G. N., M. C. Wheeler, P. T. Haertel, K. H. Straub, and P. E. Roundy, 2009: Convectively coupled equatorial waves. *Rev. Geophys.*, **47**, RG2003, doi:10.1029/2008RG000266.
- Kitoh, A., 2005: Climate model simulation on the role of mountain uplift on Asian monsoon. *The Geological Society of Japan*, 111, XIX.
- Knutson, T. R. and K. M. Weickmann, 1987: 30-60 day atmospheric oscillations: composite life cycles of convection and circulation anomalies. *Monthly Wea. Rev.* **115**, 1407-1436.
- Madden, R. A. and P. R. Julian, 1994: Observations of the 40–50-day tropical oscillation—A review, *Monthly Wea. Rev.*, **122**, 814–37.
- Meehl G. A., 2015: Decadal climate variability and the early-2000s hiatus. *US CLIVAR*, **13**, No.3, 1-6.
- Rodwell, M.J. and B. I Hoskins, 1996: Monsoons and the dynamics of deserts. *Q. J. R. Meteor. Soc.*, **122**, 1385-1404.
- Saji, N. H., B. N. Goswami, P. N. Vinayachandran and T. Yamagata, 2009: A dipole mode in the tropical Indian Ocean. *Nature*, **401**, 360-363.
- Trenberth, K.E and J. T. Fasullo, 2013: An apparent hiatus in global warming?. *Earth's Future* **1**, 19-32.
- Webster, P. J., 1994: The role of hydrological processes in ocean-atmosphere interactions, *Review of Geophysics*, **32**,427-476.
- Xie, S.-P., K. Hu, J. Hafner, H. Tokinaga, Y. Du, G. Huang and T. Sampe, 2009: Indian Ocean capacitor effect on Indo-western Pacific climate during the summer following El Niño. *J. Climate*, **22**, 730-747.
- Yeh, S.-W., J.-S. Kug, B. Dewitte, M.-H. Kwon, B. Kirtman and F.-F. Jin, 2009: El Niño in a changing climate. *Nature*, **461**, 511-514.

## Text books

- James, I. N., 1995: Introduction to Circulating Atmospheres. Cambridge University Press, 422pp.
- Trenberth, K.E. (ed.), 1992: Climate System Modeling. Cambridge University Press, 788pp.
- Vallis G. K., 2006: Atmospheric and oceanic fluid dynamics. Cambridge University Press, 7454pp.
- Wallace, J.M. and P. V. Hobbs, 2006: Atmospheric Science. Academic Press, 483pp.



# **Introduction of Reanalysis and JRA-55**



# Introduction of Reanalysis and JRA-55

Yuki KOSAKA (Climate Prediction Division, JMA)

## 1. Background and basis of reanalysis

### 1.1 Background

Important quantities for climate monitoring and analysis are climatology (long-term mean) and anomaly (deviation from the climatology). In JMA's operational climate monitoring, 1981-2010 average of meteorological variables are used as the climatology, and long-term trends and variations of the anomaly are usually monitored. As the basis for these operations, the climate dataset must be (a) covering the globe for several decades, (b) including as many variables as possible. Furthermore, the dataset needs to be (c) spatially and temporally consistent and highly qualified because the biases in temporal and/or spatial spaces make it difficult to distinguish natural trends and variations of the climate system from artificial ones.

### 1.2 Approaches for producing climate dataset

One approach for producing such a climate dataset is a direct use of observational data. Currently, historical in situ surface and upper air observational data have been accumulated for several decades or a century in many organizations, which could be a reliable data source to investigate the past climate. Indeed, based on historical observations, a variety of land surface temperature and sea surface temperature (SST) datasets have been developed and used for the climate monitoring. However, conditions (a) and (b) in Section 1.1 are not satisfied in most cases for observational dataset, i.e., (1) observational dataset has a coverage limitation (not distributed uniformly over the globe) and (2) the observed meteorological variables are limited. Consequently, observational dataset alone is generally not sufficient for comprehensive monitoring and analysis of climate.

The other approach is based on a method used in operational numerical weather prediction (NWP). Let us now assume that atmospheric condition at a certain time is estimated by the NWP model with some errors, and observational data before and after the time are given (Fig. 1). For convenience, we further suppose that the observational data are located on grid points of the NWP model. Although it is impossible to know the actual state of the atmosphere, statistical estimation of the atmospheric state by the data assimilation method is possible if we had information on error characteristics of the NWP model and observations. By using the estimated state (hereafter, the analysis) as the initial field for the NWP model, future state can be predicted, which in turn be used as a priori state (hereafter, the first guess) of the next assimilation step.

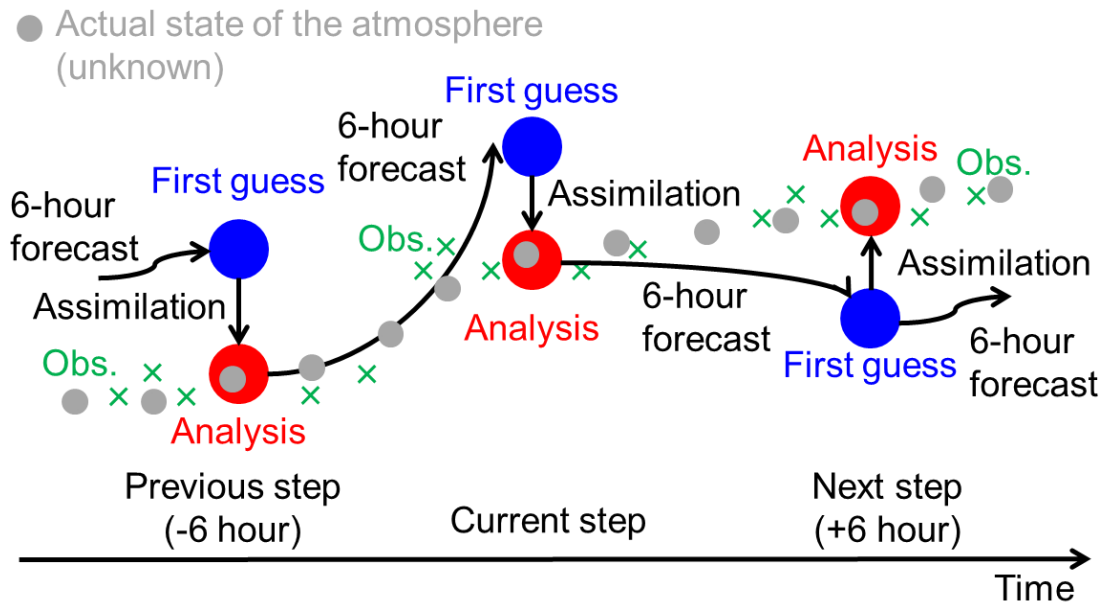


**Fig 1.** Schematic diagram of the analysis cycle. See text for details.

These processes, so-called the analysis cycle, are a continuous repetition of data assimilation and short-term forecasts which aim to estimate the state of the atmosphere as accurate as possible. The accumulated operational analysis dataset contains periodic, three-dimensional, high-quality, and global grid point values (GPV) of many kinds of meteorological variables. Thus, the dataset seems to satisfy the conditions (a), (b) and (c) described above and gives us the most reliable data for meteorology and climate at the target time. In particular, for climate monitoring, daily global dataset containing many kinds of meteorological variables for several decades are necessary as the basic data.

However, the operational analysis system has two problems from the viewpoint of climate monitoring. The first problem is changes of the NWP model characteristics due to its updates. In the operational NWP centers including JMA, the NWP models are frequently modified to improve its short-term forecast skills. Since the quality of analysis largely depends on performance of the model, changes in the NWP system are problematic for climate monitoring. Thus, the analysis produced with the latest operational system can have a quite different quality from that produced with the older systems. The second problem is a compromised accuracy due to a limited availability of observational data at the time of the operational analysis. Because of time constraints in the near real-time NWP operation, operational systems in general make compromises to cut off belated observational data, which would be available after the cut-off. It is possible that inclusion of these observational data in a delayed analysis could improve the accuracy compared with the operational analysis.

### 1.3 The reanalysis

In order to overcome the problems pointed out in section 2.2, the analysis to produce climate dataset apart from the operational NWP analysis has been conducted at some of the major NWP centers such as the European Center for Medium-Range Weather Forecasts (ECMWF), the National Center for Environmental Prediction (NCEP) and JMA. Here, we define the reanalysis for climate dataset as “*analysis of the past atmospheric conditions using a constant, state-of-the-art NWP and data assimilation system with the latest observation to produce a high-quality, spatially and temporally consistent climate dataset*”.

It should be noted that the NWP model used in the reanalysis are not always the latest one practically because it takes a long time to construct an analysis system and to conduct preliminary investigations before its calculation. Therefore, the “*state-of-the-art*” in the previous paragraph should be added “*as much as possible*” to reserve the time for preparation. In regard to observational data, not all the available observational data are used at the time of reanalysis, but some data are excluded due to the Quality Control (QC) or requirements from the data assimilation system<sup>1</sup>. Hence, “*the latest observation*” in the previous paragraph should also be added as “*quality-controlled and efficient from the viewpoint of assimilation system*”.

## 2. Reanalysis at JMA

Reanalysis has been conducted at a number of major NWP center. In Japan, the Japan Meteorological Agency (JMA) and the Central Research Institute of Electric Power Industry (CRIEPI) jointly produced the Japanese 25-year Reanalysis (JRA-25; Onogi et al. 2007) which covers from 1978 to 2004. In the second reanalysis by JMA called the Japanese 55-year Reanalysis (JRA-55; Kobayashi et al. 2015), updated DA system and newly prepared observations since the JRA-25 are used to improve the quality of dataset. The JRA-55 covers from 1958 to present and currently used as a basic dataset for climate services at JMA.

The JRA-55 has been based on the TL319 version of JMA’s operational NWP system as of December 2009 (JMA 2013). Both the DA system and forecast model (Global spectral model; GSM) have been extensively improved since the JRA-25. Observations used in JRA-55 primarily consist of those used in ERA-40 (Uppala et al. 2005) and those archived at JMA. Observations after 1979 are basically the same as those used in JRA-25, but newly available observation data were collected and introduced whenever possible. Detailed list of the DA system, NWP model, and observation data are shown in tables 1, 2, and 3 of Appendix,

---

<sup>1</sup> JMA’s data assimilation system ignores spatial correlation of observational data (non-diagonal elements of the observation error covariance in the data assimilation theory; Kalnay 2003) for computational reasons. Thus, in regions where observational are spatially dense, some data are excluded before the analysis so that the spatial correlation sufficiently decreases (data thinning process).

respectively.

### 3. Basic performance of JRA-55

Kobayashi et al. (2015) examined performance of JRA-55 in the aspect of reproducing temporal and spatial variability of basic variables such as temperature, precipitation, and sea-level pressure. Harada et al. (2016) extended their investigation to include stratospheric circulation, tropical cyclones, the Madden-Julian oscillation, and mid-latitude storm tracks. Both studies concluded that quality of the JRA-55 improved significantly compared with that of the JRA-25. Some examples from these studies are introduced in this section.

#### 3.1 Two-day forecast scores

To evaluate the temporal consistency of the product, short-range forecast was carried out in JRA-55. Figure 2 shows time series of root-mean-square (RMS) errors in 2-day forecasts at a geopotential height of 500hPa averaged over the extratropical northern and southern hemisphere from JRA-25, JRA-55, and the JMA operational system, as verified against their own analyses. The scores from JRA-55 and JRA-25 are temporally steady compared with that of the operational system, indicating that quality of the operational system strongly depends on frequent upgrades of the system. It is also found that the scores of the JRA-55 improved significantly from those of the JRA-25, which reflects updates of the system and observations since JRA-25. The improvement is particularly significant in the southern hemisphere, probably due to the availability of new satellite observations as well as to the improvement of the DA system.

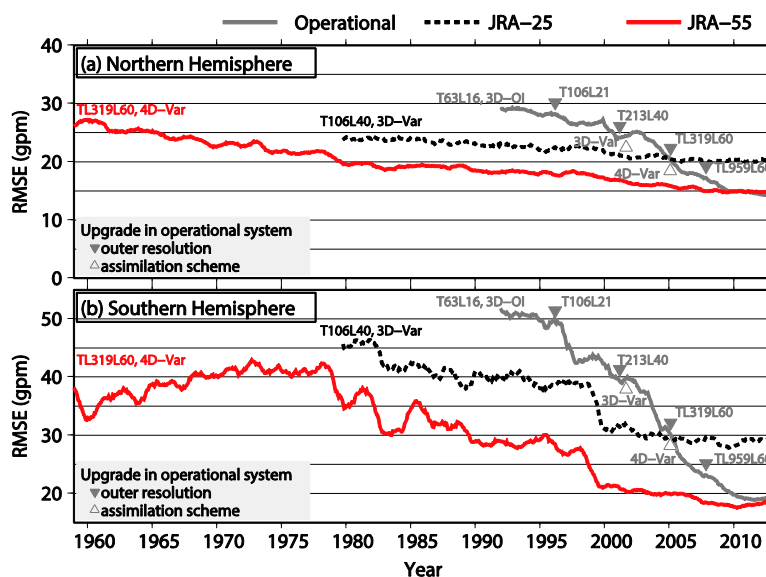


**Fig. 2.** RMS errors of 2-day forecasts at a geopotential height of 500hPa averaged over the extratropics of the (a) Northern and (b) Southern Hemispheres from JRA-25, JRA-55 and JMA operational system, verified against their own analyses. Changes in

the assimilation scheme and resolution of the outer model are also noted. Each value represents the average for the last 12 months.

### 3.2 Temperature

Figure 3 compares monthly mean land-surface air temperature anomalies from the Climatic Research Unit (CRU) temperature database (CRUTEM4, Jones et al. 2012), the NCEP/National Center for Atmospheric Research (NCAR) reanalysis, ERA-40, JRA-25, and JRA-55, averaged over the globe. The low-frequency variability of 2-m temperature anomalies over land is fairly similar between JRA-55 and JRA-25. Compared with ERA-40, the trend reproduced in JRA-55 is closer to that in CRUTEM4 but there is a difference of less than 0.1 K between CRUTEM4 and JRA-55 after the 1990s.

The difference might be related to a difference in how observations are used between CRUTEM4 and JRA-55. In JRA-55, observations on islands and the coast are not used in the screen-level analysis of JRA-55 and analysis in those areas could be affected by observations in coastal waters such as reports of surface observation from sea stations (SHIP) and buoy observations (BUOY), and by Sea Surface Temperature (SST) through background fields. On the other hand, CRUTEM4 is based on observations over land only, which include those on islands and on the coast.

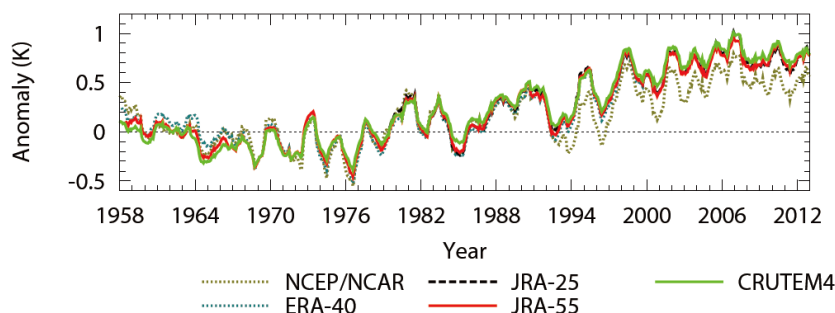


**Fig. 3.** Twelve-month running mean land-surface air temperature anomalies from CRUTEM4, the NCEP/NCAR reanalysis, ERA-40, JRA-25, and JRA-55, averaged over the globe. Anomalies for each dataset were defined relative to their own climatological monthly means over 1961–1990, except JRA-25, for which anomalies were first computed relative to its own climatological monthly means over 1981–2010 and then adjusted so that their average over 1979–1990 gave the same value as that of JRA-55. Reanalyses are sampled with the same spatial and temporal coverage as CRUTEM4.

### 3.3 Precipitation

Figure 4 shows the climatology of precipitation distribution in JRA-55, JRA-25, ERA-Interim (Dee et al. 2011), ERA-40, the Modern-Era Retrospective Analysis for Research and Applications (MERRA, Rienecker et al. 2011), and the Global Precipitation Climatology Project (GPCP) version 2.2 (Adler et al. 2003) as an observational dataset. While precipitation in middle and high latitudes are underestimated in most reanalysis, JRA-55 well reproduce these feature, especially in the Pacific and Atlantic Oceans north of 30°N. On the other hand, JRA-55

overestimates precipitation in the tropics compared with GPCP. The regions where JRA-55 overestimates precipitation tend to exhibit the spin-down problem<sup>2</sup> (not shown). Therefore, the excessive precipitation in the tropics in JRA-55 is most likely related to the dry bias and the spin-down problem of the forecast model in regions of deep convection.

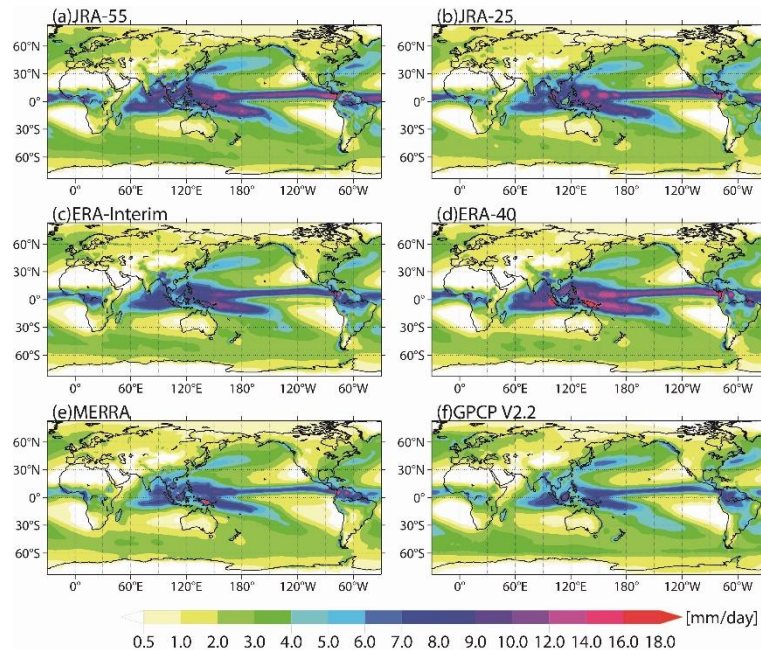


**Fig. 4.** Climatological annual mean precipitations in (a) JRA-55, (b) JRA-25, (c) ERA-Interim, (d) ERA-40, (e) MERRA, and (f) GPCP V2.2, averaged over 1980–2001.

#### 4. JRA-55 user application and homepage

The JRA-55 data are available from the JMA Data Dissemination System (JDDS) for registered users. Application for JRA-55 data access can be made via the JRA-55 homepage by filling in necessary information such as name, affiliation, and purpose of use. The dataset is also available from the Data Integration and Analysis System (DIAS) managed by the University of Tokyo, the Center for Computational Sciences (CCS) of University of Tsukuba, NCAR in the U.S.A., and the Earth System Grid Federation (ESGF) at the National Aeronautics and Space Administration (NASA). Note that registration at the JRA-55 homepage is valid only at JDDS and separate registration is required for downloading from these collaborative organizations.

The JRA-55 homepage also provides detailed information on JRA-55 data (JRA-55 Product User’s Handbook) and its quality issues. In addition, the homepage displays climate maps for a variety of meteorological variables ranging from basic metrics to technical considerations for climate research (JRA-55 Atlas). It is expected to be widely useful in research and education.

**JRA-55 homepage:** [http://jra.kishou.go.jp/JRA-55/index\\_en.html](http://jra.kishou.go.jp/JRA-55/index_en.html)

<sup>2</sup> Precipitation is excessive immediately after the start of forecasts and then gradually decreases.

JRA-55 Atlas: <http://ds.data.jma.go.jp/gmd/jra/atlas/en/index.html>

## 5. Next Japanese reanalysis: JRA-3Q

JMA is currently conducting the third Japanese reanalysis called JRA-3Q (Japanese Reanalysis for Three Quarters of a century), which covers over 75 years from 1947 to present. The JRA-3Q is produced by utilizing the latest NWP system as of December 2018, as well as newly added observation since the JRA-55, to update quality of the reanalysis products. The production of JRA-3Q has been started in August 2019 and will be ended by the end of 2021. Detail of the plan and schedule will be presented in the lecture.

## Appendix: Detail of the DA system, NWP model, and observation data for JRA-25 and JRA-55.

**Table 1.** Data assimilation systems used for JRA-25 and JRA-55.

	JRA-25	JRA-55
Basic system	JMA's operational system as of March 2004 (JMA 2002)	JMA's operational system as of December 2009 (JMA 2007, 2013b)
Horizontal grid system	Gaussian	Reduced Gaussian
Horizontal resolution	T106 (~110 km)	TL319 (~55 km)
<b>Atmospheric analysis</b>		
Vertical levels	Surface and 40 levels up to 0.4 hPa	Surface and 60 levels up to 0.1 hPa (Iwamura and Kitagawa 2008; Nakagawa 2009)
Analysis scheme	3D-Var with the T106 inner resolution	4D-Var with the T106 inner resolution
Background error covariances	Static	Static with the simple inflation factor of 1.8 applied before 1972
Bias correction for satellite radiances	<i>TOVS</i> Adaptive scheme using 1D-Var analysis departures (Sakamoto and Christy 2009) <i>ATOVS</i> Static (until July 2009) and adaptive (thereafter) schemes using radiosonde and supplemental background fields (Kazumori et al. 2004)	VarBC (Derber and Wu 1998; Dee and Uppala 2009; JMA 2013)
Radiative transfer model for satellite radiances	<i>TOVS</i> : RTTOV-6 <i>ATOVS</i> : RTTOV-7	RTTOV-9.3
<b>Surface analysis</b>		
Screen-level analysis	2D-OI	2D-OI with the FGAT approach
Land surface analysis	Offline SiB with 6-hourly atmospheric forcing	Offline SiB with 3-hourly atmospheric forcing
Snow depth analysis	2D-OI	2D-OI

**Table 2.** Forecast models used for JRA-25 and JRA-55.

	JRA-25	JRA-55
Base model	JMA GSM as of March 2004 (JMA 2002)	JMA GSM as of December 2009 (JMA 2007, 2013b)
Horizontal resolution	T106 (~110 km)	TL319 (~55 km)
Vertical levels	Surface and 40 levels up to 0.4 hPa	Surface and 60 levels up to 0.1 hPa (Iwamura and Kitagawa 2008; Nakagawa

		2009)
<b>Dynamics</b>		
Horizontal grid system	Gaussian	Reduced Gaussian
Advection scheme	Euralian	Semi-Lagrangian
<b>Radiation</b>		
Longwave radiation	<i>Line absorptions</i> Random band model of Goody (1952) <i>Water vapor continuum (e-type)</i> Roberts et al. (1976) <i>Radiatively active gases</i> H <sub>2</sub> O, O <sub>3</sub> and CO <sub>2</sub> (constant at 375 ppmv)	<i>Line absorptions</i> Pre-computed transmittance tables and <i>k</i> -distribution (Chou et al. 2001) <i>Water vapor continuum (e-type and p-type)</i> Zhong and Haigh (1995) with MK_CKD (Clough et al. 2005) <i>Radiatively active gases</i> H <sub>2</sub> O, O <sub>3</sub> , CO <sub>2</sub> , CH <sub>4</sub> , N <sub>2</sub> O, CFC-11, CFC-12 and HCFC-22
Shortwave radiation	<i>Absorptions by H<sub>2</sub>O, O<sub>2</sub>, O<sub>3</sub> and CO<sub>2</sub></i> Briegleb (1992)	<i>Absorptions by H<sub>2</sub>O</i> Briegleb (1992) <i>Absorptions by O<sub>2</sub>, O<sub>3</sub> and CO<sub>2</sub></i> Freidenreich and Ramaswamy (1999)
Cloud radiation	<i>Longwave</i> Maximum-random overlap <i>Shortwave</i> Random overlap	<i>Longwave</i> Maximum-random overlap with the method of Räisänen (1998) <i>Shortwave</i> Random overlap
Aerosols	Atmospheric aerosol profiles from WMO (1986) (CONT-I over land and MAR-I over sea)	Atmospheric aerosol profiles from WMO (1986) (CONT-I over land and MAR-I over sea) with optical depths adjusted to 2-dimensional monthly climatology
<b>Cumulus convection</b>	Prognostic Arakawa-Schubert	Prognostic Arakawa-Schubert with DCAPE
<b>Initialization</b>	Nonlinear normal mode initialization	Not used
<b>Boundary conditions and forcing fields</b>		
SST and sea ice	COBE-SST (Ishii et al. 2005)	COBE-SST (Ishii et al. 2005)
Ozone	T42L45 version of MRI-CCM1 (Shibata et al. 2005)	<i>Until 1978: Climatology</i> <i>From 1979 onward:</i> T42L68 version of MRI-CCM1 (Shibata et al. 2005)

**Table 3.** Observational data sources for JRA-55. Observations shown in plain cells were added or reprocessed after JRA-25, whereas those in shaded cells are the same as those used in JRA-25. Acronyms in this table are summarized in Appendix B. of Kobayashi et al. (2015).

Data supplier	Data type and supplier's identifiers	Period	Note
<b>Conventional data</b>			
ECMWF		Jan 1958-Aug 2002	Uppala et al. (2005)
JMA		Jan 1961-	
	GAME and SCSMEX	Apr 1998-Oct 1998	
NCEP/NCAR	SYNOP and upper-level observation	Jan 1979-Dec 1979	Kalnay et al. (1996) Kistler et al. (2001)
M. Yamanaka	Radiosondes from Indonesia	Jan 1958-	Okamoto et al. (2003)
M. Fiorino	TCRs	Jan 1958-	Fiorino (2002)
RIHMI	Snow depths from Russia	Jan 1958-Dec 2008	
UCAR	Snow depths from USA	Jan 1958-Aug 2011	NCDC et al. (1981)
Monthly Surface Meteorological Data in China	Snow depths from China	Jan 1971-Dec 2006	Digitized from printed matters
IMH	Snow depths from Mongolia	Jan 1975-Dec 2007	
<b>Satellite radiances</b>			
ECMWF	VTPR	Jan 1973-Feb 1976	Uppala et al. (2005)
	HIRS and SSU	Nov 1978-Dec 2000	
	MSU and AMSU	Nov 1978-May 2003	

NOAA/NCDC	SSM/I	Jun 1987-Dec 2004	
NOAA/CLASS	AMSU and MHS	Aug 1998-	
	SSM/I	Jul 1987-	
JMA	AMSU and MHS	Jun 2003-	
	SSM/I and SSMIS	Mar 2006-	
	TMI	Dec 2011-	
	CSR	Jun 2005-	
JMA/MSC	Reprocessed CSRs from GMS-5, GOES 9 and MTSAT-1R	Jul 1995-Dec 2009	
JAXA, NASA	Reprocessed TMI version 7	Feb 1998-Dec 2011	
JAXA	Reprocessed AMSR-E Version 3	Jun 2002-Oct 2011	
EUMETSAT	CSRs from the Meteosat series	Jan 2001-Aug 2009	
<b>AMVs</b>			
ECMWF	GMS, Meteosat and GOES	Jan 1979-Dec 1997	Uppala et al. (2005)
JMA	GMS, MTSAT, Meteosat and GOES	Dec 1979-Dec1980, Jan 1998-	
	MODIS	Jun 2004-	
JMA/MSC	Reprocessed GMS, GOES 9 and MTSAT-1R	Jan 1979-Nov 1979 Nar 1987-Sep 2009	
EUMETSAT	Reprocessed Meteosat-2	May 1982-Aug 1988	van de Berg et al. (2002)
	Reprocessed Meteosat-3 and -7	Jan 1989-Dec 2000 Aug 1988-Nov 1998	
	Meteosat-5 and -7	Jan 2001-Feb 2001	
<b>Scatterometer ocean surface winds</b>			
ESA	Reprocessed AMI (ERS.ASPS20.N)	May 1997-Jan2001	De Chiara et al. (2007)
Hersbach (2008)			
JPL	Reprocessed SeaWinds from QuickSCAT (QSCAT LEVEL 2B V2)	Jul 1999-Nov 2009	Dunbar et al. (2006)
JMA	ASCAT	Jan 2008-	
<b>GNSS-RO refractivities</b>			
CDAAC	Reprocessed CHAMP, SAC-C, COSMIC, GRACE, Metop-A, TerraSAR-X, and C/NOFS	Jul 2006-Jun 2012	
JMA	COSMIC, GRACE, Metop, TerraSAR-X, and C/NOFS		

## References

- Adler, R.F., G. J. Huffman, A. Chang, R. Ferraro, P.-P. Xie, J. Janowiak, B. Rudolf, U. Schneider, S. Curtis, D. Bolvin, A. Gruber, J. Susskind, P. Arkin, and E. Nelkin, 2003: The Version-2 Global Precipitation Climatology Project (GPCP) monthly precipitation analysis (1979-present). *J. Hydrometeor.*, 4, 1147-1167.
- Briegleb, B. P., 1992: Delta-Eddington approximation for solar radiation in the NCAR community climate model. *J. Geophys. Res.*, 97, 7603–7612.
- Chou, M.-D., M. J. Suarez, X.-Z. Liang, and M. M.-H. Yan, 2001: A thermal infrared radiation parameterization for atmospheric studies. Technical report series on global modeling and data assimilation, NASA/TM-2001-104606, 19, National Aeronautics and Space Administration (NASA) Goddard Space Flight Center, USA, 68 pp.
- Clough, S. A., M. W. Shephard, E. J. Mlawer, J. S. Delamere, M. J. Iacono, K. Cady-Pereira, S. Boukabara, and P. D. Brown, 2005: Atmospheric radiative transfer modeling: a summary of the AER codes. *J. Quant. Spectrosc. Radiat. Transfer*, 91, 233–244.
- De Chiara, G., R. Crapolicchio, and P. Lecomte, 2007: ERS-1/2 scatterometer new products: mission reprocessing and data quality improvement. Paper presented at the 2nd Space for Hydrology Workshop, Geneva, Switzerland, November, 12-14, 2007.
- Dee, D. P., S. M. Uppala, A. J. Simmons, P. Berrisford, P. Poli, S. Kobayashi, U. Andrae, M. A. Balmaseda, G. Balsamo, P. Bauer, P. Bechtold, A. C. M. Beljaars, L. van de Berg, J. Bidlot, N. Bormann, C. Delsol, R. Dragani, M. Fuentes, A. J. Geer, L. Haimberger, S. B. Healy, H. Hersbach, E. V. Hólm, L. Isaksen, P. Kållberg, M. Köhler, M. Matricardi, A. P. McNally, B. M.

- Monge-Sanz, J.-J. Morcrette, B.-K. Park, C. Peubey, P. de Rosnay, C. Tavalato, J.-N. Thépaut, and F. Vitart, 2011: The ERA-Interim reanalysis: configuration and performance of the data assimilation system. *Quart. J. Roy. Meteor. Soc.*, 137, 553-597.
- Dunbar, R. S., T. Lungu, B. Weiss, B. Stiles, J. Huddleston, P. S. Callahan, G. Shirliff, K. L. Perry, C. Hsu, C. Mears, F. Wentz, and D. Smith, 2006: QuikSCAT science data product user's manual. Version 3.0, D-18053 - Rev A, Jet Propulsion Laboratory (JPL), USA, 85 pp.
- Fiorino, M., 2002: Analysis and forecasts of tropical cyclones in the ECMWF 40-year reanalysis (ERA-40). 25th Conference on Hurricanes and Tropical Meteorology, CA, USA, 261-264.
- Freidenreich, S. M., and V. Ramaswamy, 1999: A new multiple-band solar radiative parameterization for general circulation models. *J. Geophys. Res.*, 104, 31389-31409.
- Goody, R. M., 1952: A statistical model for water-vapour absorption. *Quart. J. Roy. Meteor. Soc.*, 78, 165-169.
- Harada, Y., H. Kamahori, C. Kobayashi, H. Endo, S. Kobayashi, Y. Ota, H. Onoda, K. Onogi, K. Miyaoka, and K. Takahashi, 2016: The JRA-55 Reanalysis: Representation of atmospheric circulation and climate variability, *J. Meteor. Soc. Japan*, 94, 269-302.
- Iwamura, K., and H. Kitagawa, 2008: An upgrade of the JMA operational global NWP model. *CAS/JSC WGNE Res. Activ. Atmos. Oceanic Modell.*, 38, 3-4.
- Ishii, M., A. Shouji, S. Sugimoto, and T. Matsumoto, 2005: Objective analyses of sea-surface temperature and marine meteorological variables for the 20th century using ICOADS and the KOBE collection. *Int. J. Climatol.*, 25, 865-879.
- JMA, 2002: Outline of the operational numerical weather prediction at the Japan Meteorological Agency. WMO Numerical Weather Prediction Progress Report. JMA, Japan, 158 pp.
- JMA, 2007: Outline of the operational numerical weather prediction at the Japan Meteorological Agency. WMO Technical Progress Report on the Global Data-Processing and Forecasting System and Numerical Weather Prediction, JMA, Japan, 194 pp.
- JMA, 2013: Outline of the operational numerical weather prediction at the Japan Meteorological Agency. Appendix to WMO Technical Progress Report on the Global Data-processing and Forecasting System (GDPFS) and Numerical Weather Prediction (NWP) Research, JMA, Japan, 188 pp.
- Jones, P. D., D. H. Lister, T. J. Osborn, C. Harpham, M. Salmon, and C. P. Morice, 2012: Hemispheric and large-scale land surface air temperature variations: An extensive revision and an update to 2010. *J. Geophys. Res.*, 117, D05127, doi:10.1029/2011JD017139.
- Kalnay, E., M. Kanamitsu, R. Kistler, W. Collins, D. Deaven, L. Gandin, M. Iredell, S. Saha, G. White, J. Woollen, Y. Zhu, M. Chelliah, W. Ebisuzaki, W. Higgins, J. Janowiak, K. C. Mo, C. Ropelewski, J. Wang, A. Leetmaa, R. Reynolds, R. Jenne, and D. Joseph, 1996: The NCEP/NCAR 40-year reanalysis project. *Bull. Amer. Meteor. Soc.*, 77, 437-471.
- Kazumori, M., H. Owada, and K. Okamoto, 2004: Improvements of ATOVS radiance-bias correction scheme at JMA. *CAS/JSC WGNE Res. Activ. Atmos. Oceanic Modell.*, 34, 15-16.
- Kistler, R., E. Kalnay, W. Collins, S. Saha, G. White, J. Woollen, M. Chelliah, W. Ebisuzaki, M. Kanamitsu, V. Kousky, H. van den Dool, R. Jenne, and M. Fiorino, 2001: The NCEP-NCAR 50-year reanalysis: Monthly means CD-ROM and documentation. *Bull. Amer. Meteor. Soc.*, 82, 247-267.
- Kobayashi, S., Y. Ota, Y. Harada, A. Ebita, M. Moriya, H. Onoda, K. Onogi, H. Kamahori, C. Kobayashi, H. Endo, K. Miyaoka, and K. Takahashi, 2015: The JRA-55 reanalysis: General specifications and basic characteristics. *J. Meteor. Soc. Japan*, 93, 5-48.
- Nakagawa, M., 2009: Outline of the high resolution global model at the Japan Meteorological Agency. RSMC Tokyo-Typhoon Center Technical Review, 11, JMA, Japan, 1-13.
- NCDC, NWS, and FAA, 1981: NCDC TD3200 U.S. cooperative summary of day, 1890(1948)-cont. Research Data Archive at NCAR, Computational and Information Systems Laboratory, USA.
- Okamoto, N., M. D. Yamanaka, S.-Y. Ogino, H. Hashiguchi, N. Nishi, T. Sribimawati, and A. Numaguchi, 2003: Seasonal variations of tropospheric wind over Indonesia: comparison between collected operational radiosonde data and NCEP reanalysis for 1992-99. *J. Meteor. Soc. Japan*, 81, 829-850.
- Onogi, K., J. Tsutsui, H. Koide, M. Sakamoto, S. Kobayashi, H. Hatsushika, T. Matsumoto, N.

- Yamazaki, H. Kamahori, K. Takahashi, S. Kadokura, K. Wada, K. Kato, R. Oyama, T. Ose, N. Mannoji, and R. Taira, 2007: The JRA-25 reanalysis. *J. Meteor. Soc. Japan*, 85, 369-432.
- Rienecker M. M., M. J. Suarez, R. Gelaro, R. Todling, J. Bacmeister, E. Liu, M. G. Bosilovich, S. D. Schubert, L. Takacs, G.-K. Kim, S. Bloom, J. Chen, D. Collins, A. Conaty, A. da Silva, W. Gu, J. Joiner, R. D. Koster, R. Lucchesi, A. Molod, T. Owens, S. Pawson, P. Pegion, C. R. Redder, R. Reichle, F. R. Robertson, A. G. Ruddick, M. Sienkiewicz, and J. Woollen. 2011: MERRA: NASA's Modern-Era Retrospective Analysis for Research and Applications. *J. Climate*, 24, 3624-3648.
- Räisänen, P., 1998: Effective longwave cloud fraction and maximum-random overlap of clouds: a problem and a solution. *Mon. Wea. Rev.*, 126, 3336–3340.
- Roberts, R. E., J. E. A. Selby, and L. M. Biberman, 1976: Infrared continuum absorption by atmospheric water vapor in the 8-12- $\mu$ m window. *Appl. Opt.*, 15, 2085–2090.
- Shibata, K., M. Deushi, T. T. Sekiyama, and H. Yoshimura, 2005: Development of an MRI chemical transport model for the study of stratospheric chemistry. *Pap. Geophys. Meteor.*, 55, 75–119.
- Uppala, S. M., P. W. Kållberg, A. J. Simmons, U. Andrae, V. Da Costa Bechtold, M. Fiorino, J. K. Gibson, J. Haseler, A. Hernandez, G. A. Kelly, X. Li, K. Onogi, S. Saarinen, N. Sokka, R. P. Allan, E. Andersson, K. Arpe, M. A. Balmaseda, A. C. M. Beljaars, L. Van De Berg, J. Bidlot, N. Bormann, S. Caires, F. Chevallier, A. Dethof, M. Dragosavac, M. Fisher, M. Fuentes, S. Hagemann, E. Hólm, B. J. Hoskins, L. Isaksen, P. A. E. M. Janssen, R. Jenne, A. P. McNally, J.-F. Mahfouf, J.-J. Morcrette, N. A. Rayner, R. W. Saunders, P. Simon, A. Sterl, K. E. Trenberth, A. Untch, D. Vasiljevic, P. Viterbo, and J. Woollen, 2005: The ERA-40 re-analysis. *Quart. J. Roy. Meteor. Soc.*, 131, 2961-3012.
- van de Berg, L., J. Gustafsson, and A. Yildirim, 2002: Reprocessing of atmospheric motion vectors from Meteosat image data. ECMWF ERA-40 Project Report Series, 3, ECMWF, UK, 159–168.
- WMO, 1986: A preliminary cloudless standard atmosphere for radiation computation, World Climate Programme (WCP), 112, 53 pp.
- Zhong, W., and J. D. Haigh, 1995: Improved broadband emissivity parameterization for water vapor cooling rate calculations. *J. Atmos. Sci.*, 52, 124–138.



# **Climate Analysis Information**



# Climate Analysis Information

Hitoshi Sato  
Tokyo Climate Center (TCC)  
Japan Meteorological Agency (JMA)

---

## Outline

1. Introduction to climate analysis information
2. Climate system monitoring and analysis
  - 2-1. Basic knowledge
  - 2-2. Activities at JMA
3. Example of climate analysis information

# 1. Introduction to climate analysis information

3

---

## Background

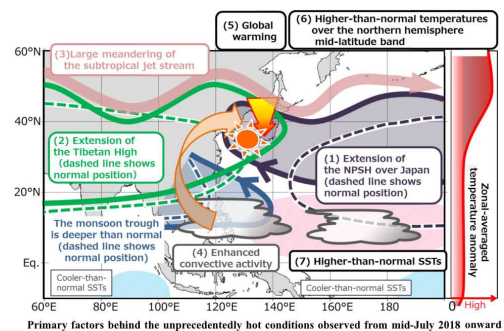
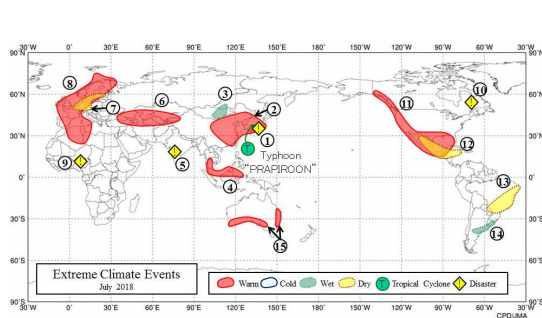
- The climate system has strong impact on socio-economic activities in the world through extreme climate events (e.g., heat/cold waves, droughts and heavy rainfall).
- It is important for society and people to appropriately deal with climate variability and extreme climate events for maximizing climate benefits and minimizing climate risks.



- It is necessary for us to understand **present climate conditions, backgrounds and factors**, and to prepare for possible impact in the future.

# Mission

- National Meteorological and Hydrological Services (NMHSs) are responsible for implementing climate system monitoring services (in addition to climate prediction services) including:
  - Diagnosing and assessing conditions of the climate system.
  - Providing scientifically accurate climate information and products to the public timely and in appropriate formats.



5

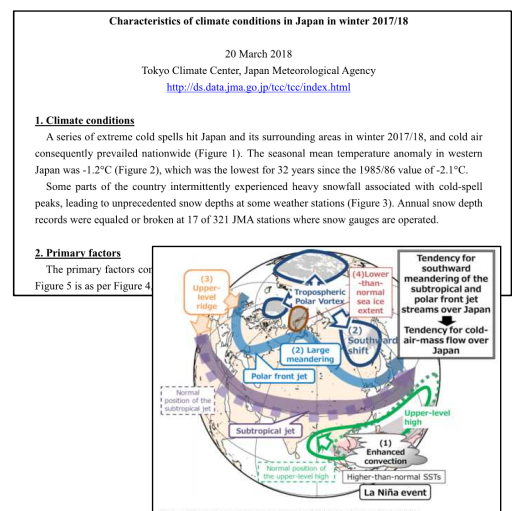
## Type of information

### 1. Information for non-experts

- Easy-to-understand information that is summarized and interpreted without jargon for decision making,
- Tailored information based on users' needs.

### 2. Information for experts

- Information requiring special and professional knowledge to be understood,
- Detailed information that includes climate system conditions associated with climate events and factor analysis.



6

# Basic structure of the information

1. Surface climate conditions and impacts
2. Characteristics of atmospheric circulation directly contributing to the surface climate conditions
3. (if possible) Primary factors associated with the characteristic atmospheric circulation

7

## Procedure

### ● Analyzing

**Step 1** : Assess surface climate conditions and impacts.

**Step 2** : Identify atmospheric circulation directly contributing to the targeted surface climate conditions.

**Step 3** : Investigate the possible factors associated with the identified atmospheric circulation directly contributing to the targeted surface climate conditions.

### ● Producing information

- **Information for non-experts** : Step 1 and summary of Steps 2 and 3.

- **Information for experts** : Step 1, Step 2 and Step 3.

## 2. Climate system monitoring and analysis

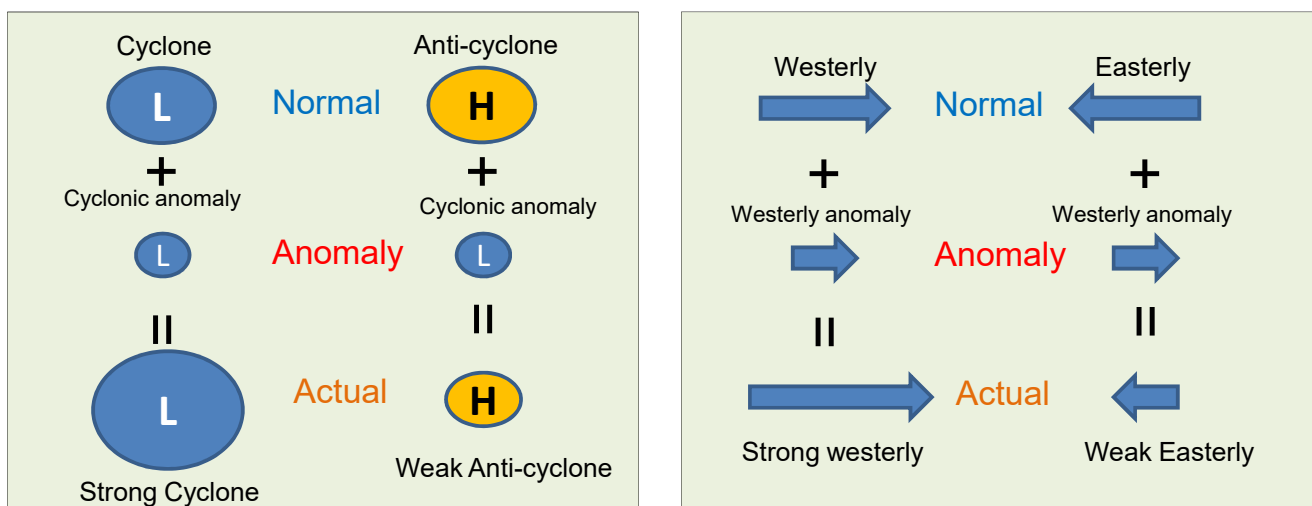
### 2-1. Basic knowledge

9

### Climatological normal and anomaly

**Normal** is the average over a sufficiently long period (typically 30 years).

**Anomaly** is the deviation of an observed atmospheric or oceanic condition from the climatological normal.



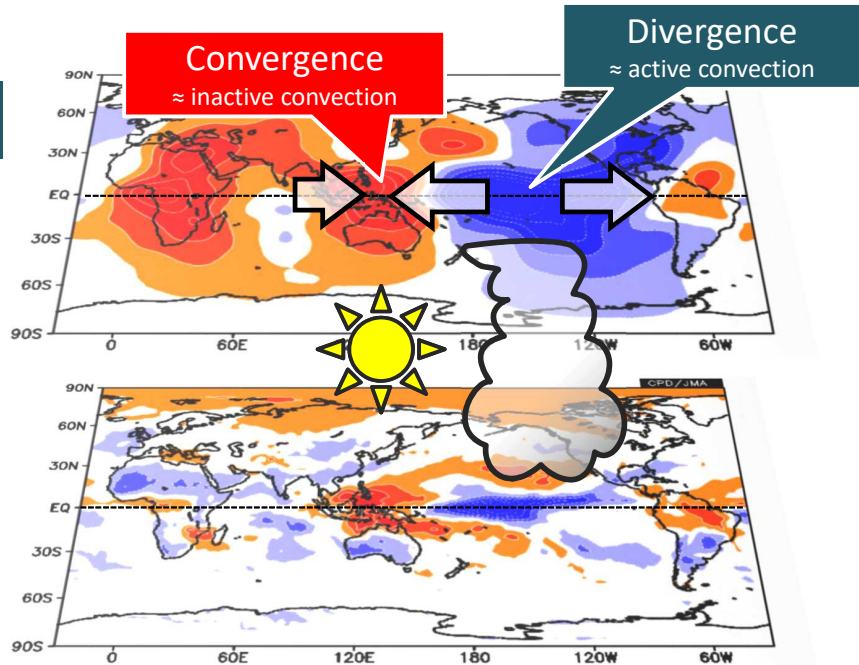
Same anomalies, but different meanings.

# Tropical convection and divergence

- In association with the enhanced (suppressed) convective activity, upper-tropospheric divergence (convergence) anomalies were seen over the central-to-eastern (western) Pacific during El Niño boreal winter 2015/16.

$\chi_{200}$  anom.

OLR anom.



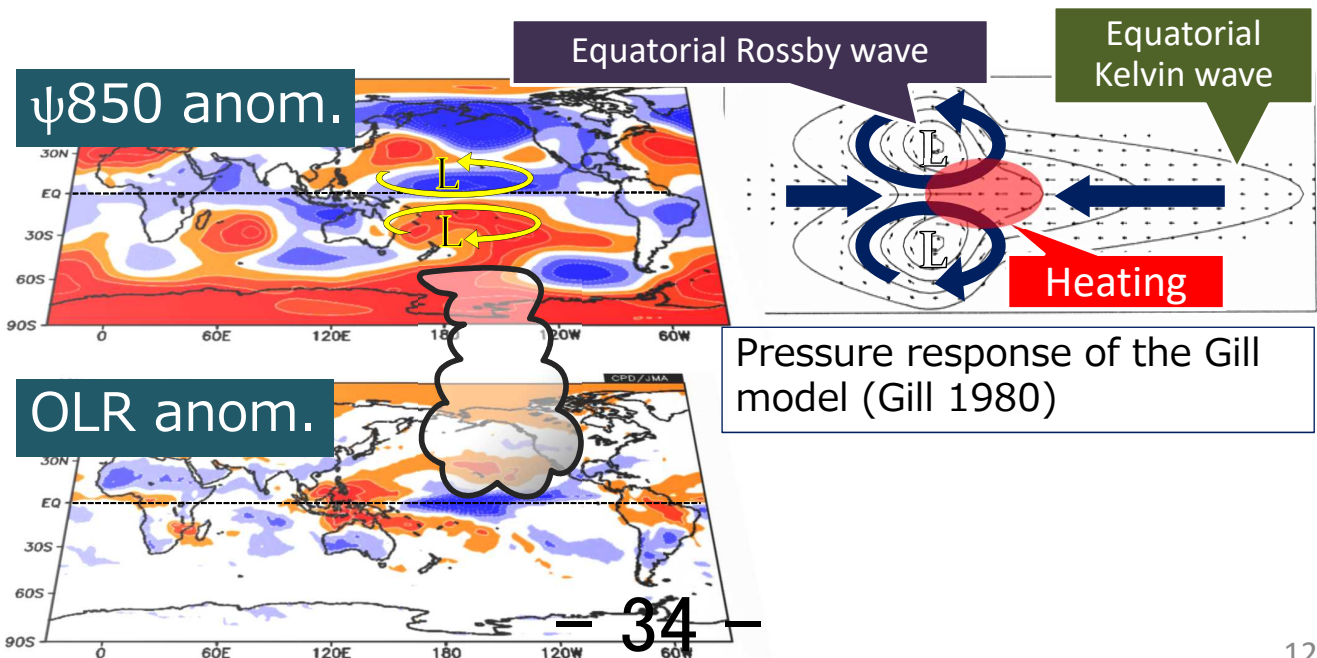
11

# Tropical convection and circulation

- In association with the enhanced (suppressed) convective activity, cyclonic (anti-cyclonic) circulation anomalies straddling the equator are seen, indicating the appearance of the Matsuno–Gill response.

$\psi_{850}$  anom.

OLR anom.



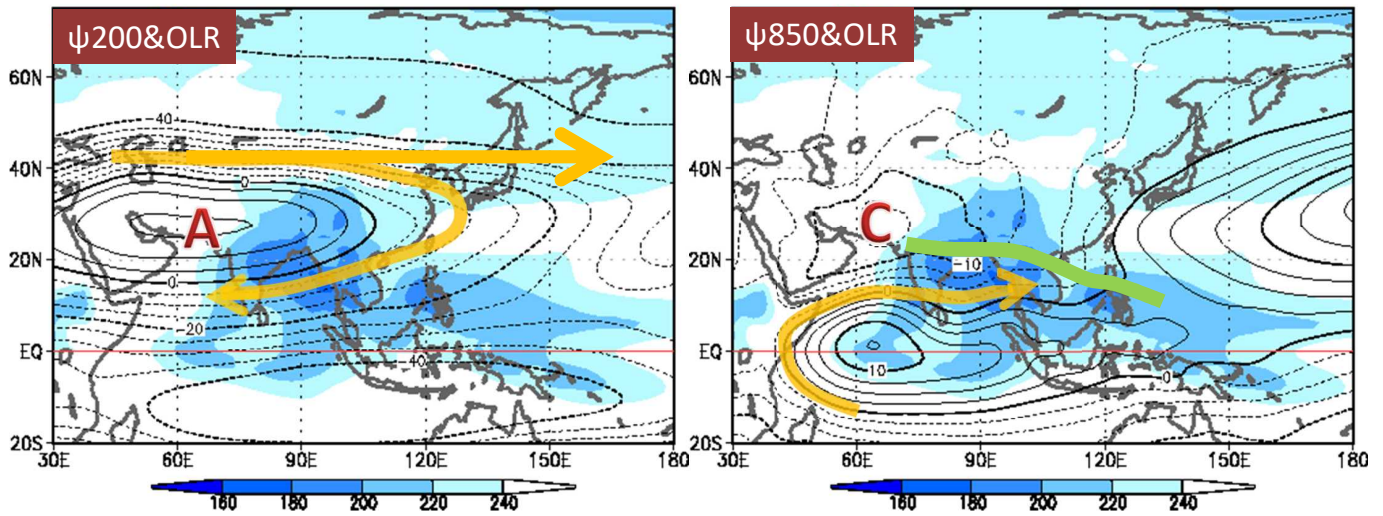
Pressure response of the Gill model (Gill 1980)

12

# Summer monsoon circulation

01Jul. – 30Jul.

01Jul. – 30Jul.



## Climatological normals of atmospheric circulation and convection (July)

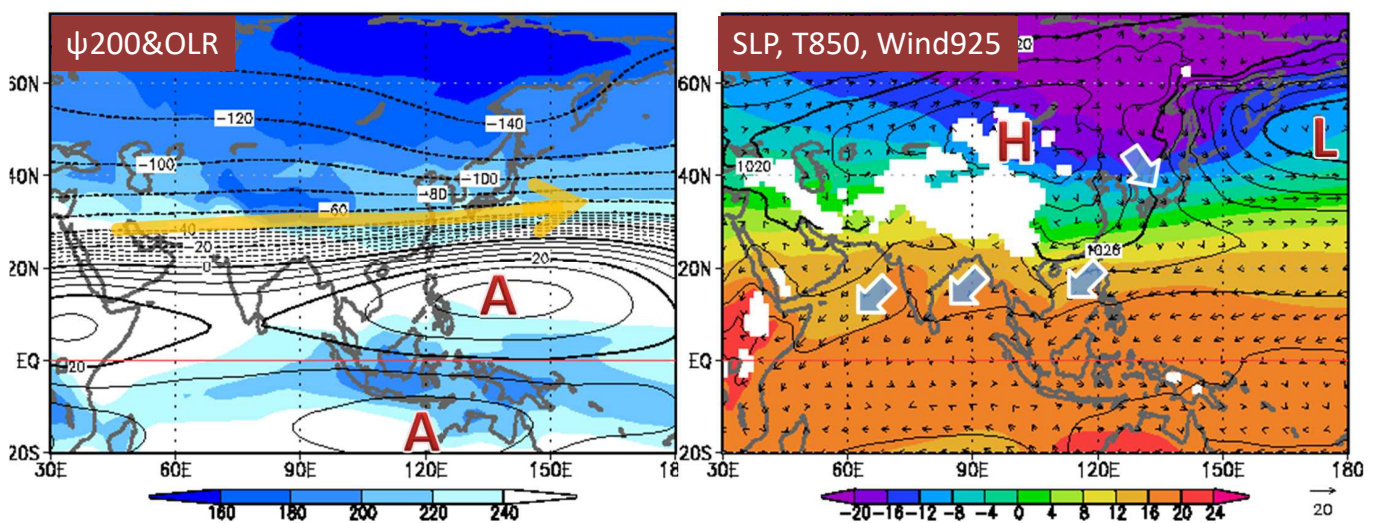
Contours: 200-hPa (left) and 850-hPa (right) stream function  
 Shading: OLR  
 Base period for normal: 1981 – 2010

13

# Winter monsoon circulation

01Jan. – 30Jan.

01Jan. – 30Jan.



## Climatological normals of atmospheric circulation and convection (January)

Left: 200-hPa stream function (contour) and OLR (shading)  
 Right: Sea level pressure (contour), 850-hPa temperature (shading) and 925-hPa wind vectors  
 Base period for normal: 1981 – 2010

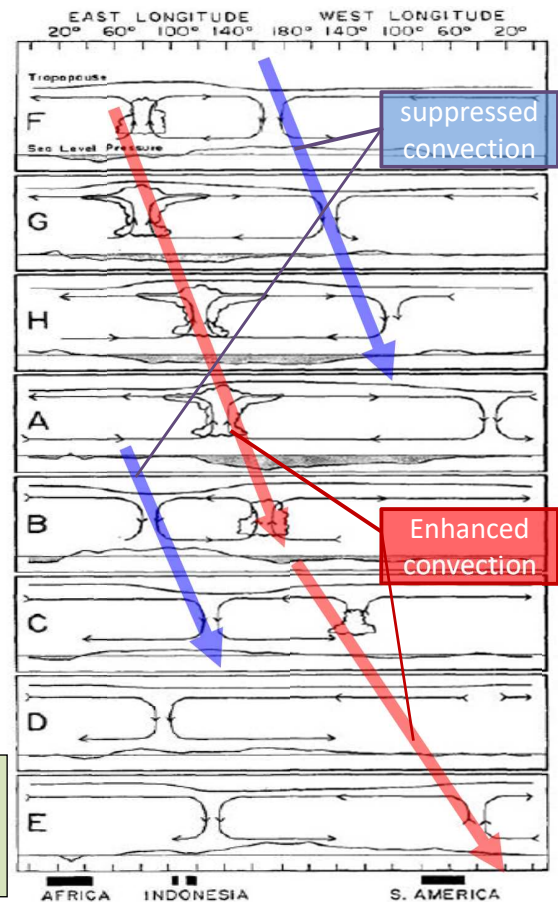
14

# General features of MJO

MJO:

- Is a major intraseasonal oscillation in the tropics,
- Propagates eastward along the equator with periods of 30 – 60 days,
- Is a large-scale coupled pattern between deep convection and atmospheric circulation,
- Has a clearer signal in convection over the Indian Ocean and the western Pacific than the other tropical regions.

Schematic of MJO  
Time increasing downward  
(Madden and Julian 1972)



15

## 2. Climate system monitoring and analysis

### 2-2. Activities at JMA

# Monitoring and analysis for the climate system

- JMA monitors the global atmospheric circulation, convection, ocean conditions and snow/ice coverage.
- JMA issues monthly and seasonal bulletins focusing on the monthly and seasonal highlights of the monitoring results.

HOME > Climate System Monitoring > Monthly Highlights on the Climate System

## Monthly Highlights on the Climate System

'Monthly Highlights on the Climate System' has been issued in PDF format since March 2007 as a monthly bulletin focusing on the monthly highlights of the monitoring results.

### Highlights in September 2019

- Monthly mean temperatures were significantly above normal from northern to southern Japan, from the western part of Western Africa to the western part of Middle Africa, from the eastern USA to southern Mexico, and in and around central Brazil.
- In the equatorial Pacific, remarkably positive SST anomalies were observed in the western equatorial Indian Ocean, the seas northeast of the Philippines, and the eastern Pacific, and was suppressed from the southeastern tropical Indian Ocean to the western equatorial Indian Ocean.
- In the 500-hPa height field, positive anomalies were seen over the northern polar region, the seas south of Alaska, the eastern USA, and the seas west of Europe, and northeast of the Caspian Sea and over Eastern Siberia.

### Full version (PDF)

▶ Monthly Highlights on the Climate System (September 2019)

▶ Back Number

Back Number (PDF) ▾

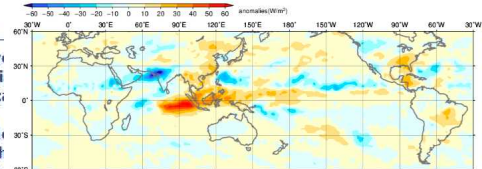


Fig. 6 Monthly mean Outgoing Longwave Radiation (OLR) anomaly (September 2019)

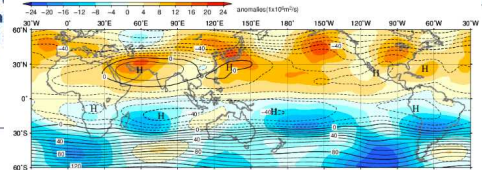


Fig. 8 Monthly mean 200-hPa stream function and anomaly (September 2019). The contour interval is  $10 \times 10^{10} \text{ m}^2/\text{s}$ . The base period for the normal is 1981-2010.

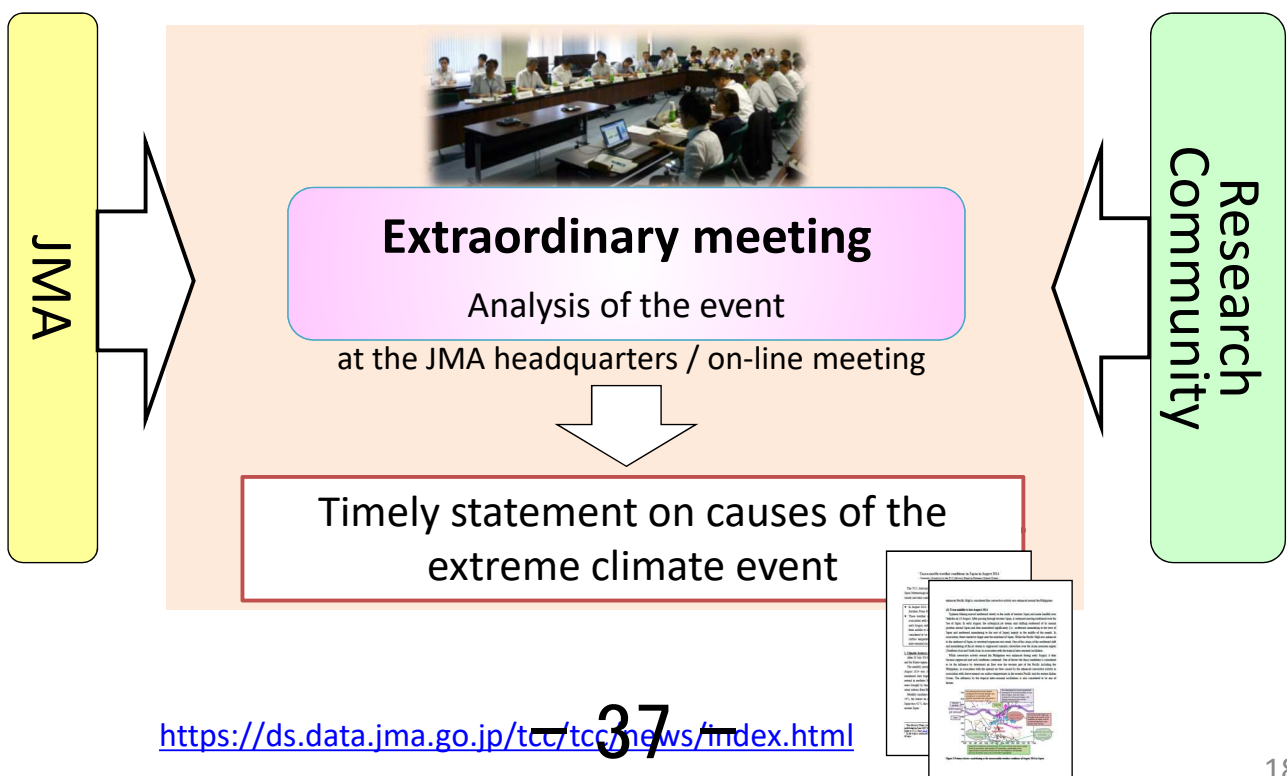
Monthly Highlights: <https://ds.data.jma.go.jp/tcc/tcc/products/clisys/highlights/index.html>

Seasonal Highlights: [https://ds.data.jma.go.jp/tcc/tcc/products/clisys/season\\_highlights/index.html](https://ds.data.jma.go.jp/tcc/tcc/products/clisys/season_highlights/index.html)

17

# Advisory Panel on Extreme Climate Events

When an extreme climate event has occurred or is expected



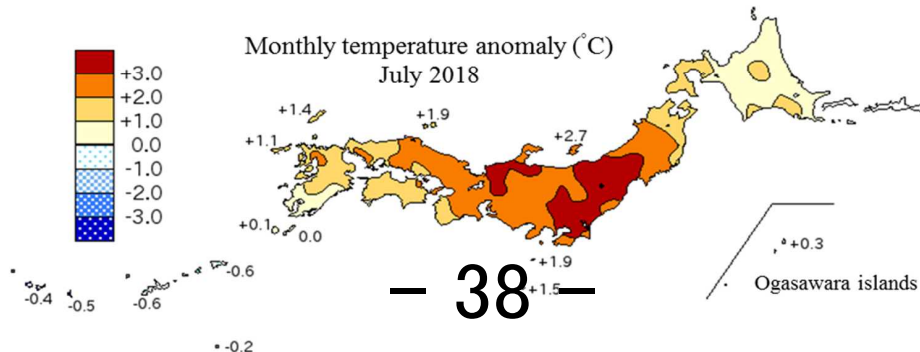
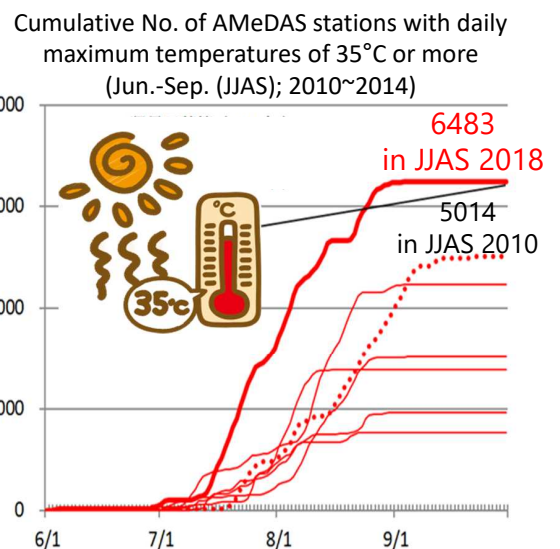
# 3. Example of climate analysis information

- Heatwave in Japan in boreal summer 2018 -

## 1. Surface climate conditions

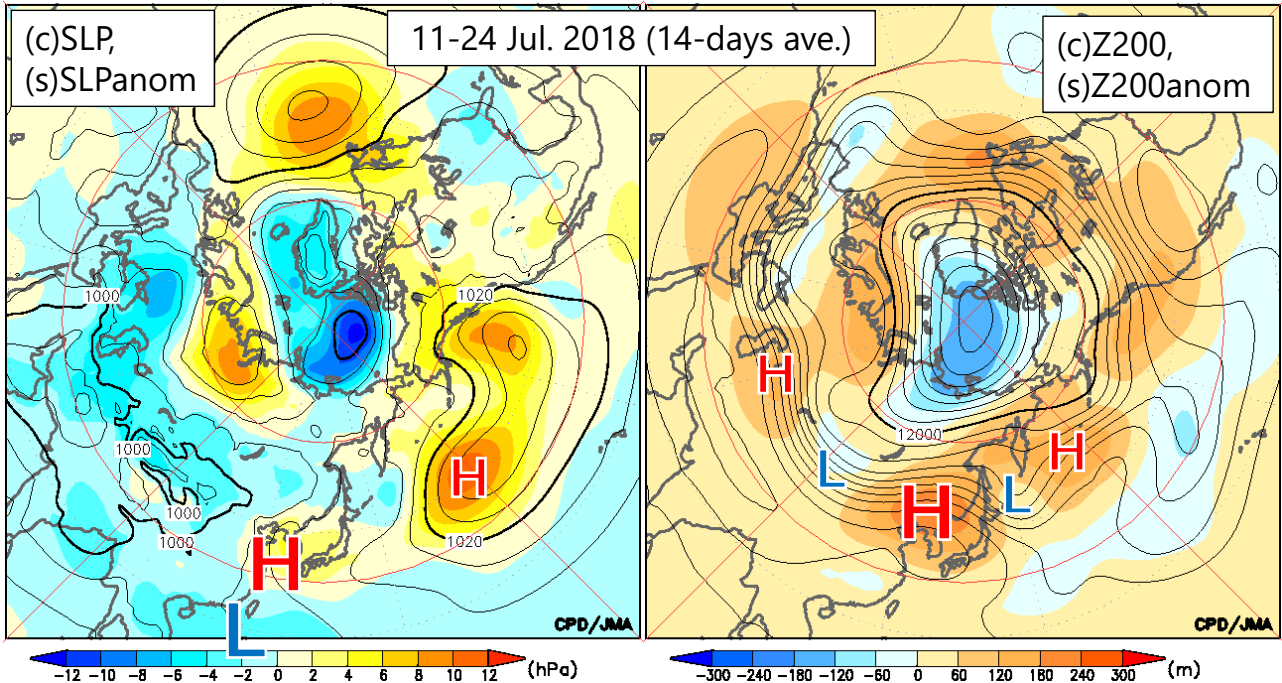
Heatwave in Japan in boreal summer 2018

- The monthly mean temperature anomalies for July 2018 (+2.8°C) and JJA 2018 (+1.7°C) in eastern Japan were the highest on record for July and JJA since 1946, respectively.
- On 23rd July a new national record maximum temperature of 41.1°C was recorded at Kumagaya in Saitama Pref.
- Cumulative number with daily temperatures of 35°C or more from June to September was the highest since 2010.

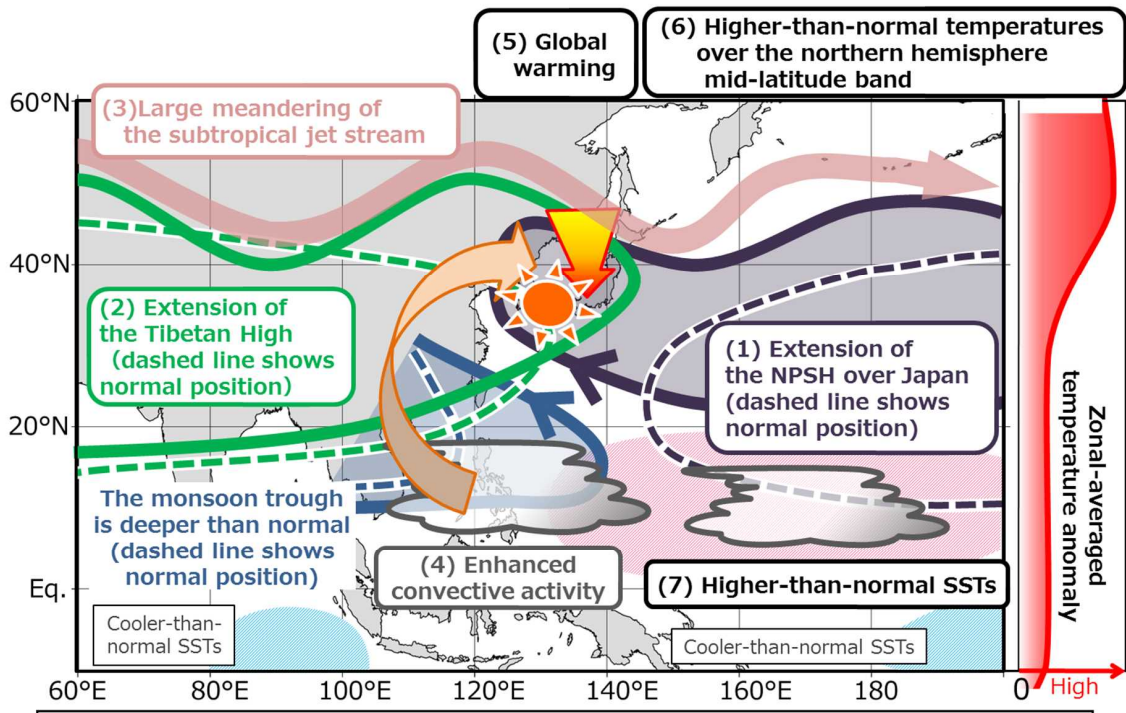


## 2. Atmospheric circulation

- Both the North Pacific Subtropical High and the Tibetan High expanded to the main islands of Japan and persisted.
- Surface temperatures in Japan increased, due mainly to high-pressure systems with warmer-than-normal air covering the islands, predominant sunny conditions and downward flow associated with the pressure systems, influenced by northward meandering of the subtropical jetstream in the vicinity of Japan.



### Primary factors behind the unprecedentedly hot conditions observed in boreal summer 2018



**Extension of the North Pacific Subtropical High (NPSH) and the Tibetan High over Japan brought extreme high temperatures there through strengthening downward air flow and above-normal sunshine duration.**



**Tokyo Climate Center Website  
and its products**

**- for monitoring the world climate and ocean -**



# Tokyo Climate Center Website and its products

- for monitoring the world climate and ocean -

Hitoshi Sato  
Tokyo Climate Center (TCC)  
Japan Meteorological Agency (JMA)

## TCC Website

The screenshot shows the Tokyo Climate Center website interface. A red box highlights the main navigation menu. Callout boxes identify the following sections:

- 1. World Climate**: Points to the 'World Climate' menu item.
- 2. Climate System Monitoring**: Points to the 'Climate System Monitoring' menu item.
- 3. El Niño Monitoring**: Points to the 'El Niño Monitoring' menu item.
- Global Warming**: Points to the 'Global Warming' menu item.
- NWP Model Prediction**: Points to the 'NWP Model Prediction' menu item.
- Climate in Japan**: Points to the 'Climate in Japan' menu item.
- Training Materials**: Points to the 'Training Module' menu item.
- Press release**: Points to the 'Press release' menu item.

The main content area includes a 'Latest Updates' section with a 'World Climate' update from 13 October 2019, a 'Climate System Monitoring' update from 16 October 2019, and an 'El Niño Monitoring' update from 10 October 2019. A 'Monthly Discussion on Seasonal Climate Outlook No.68' is also featured, issued on 25 October 2019. The 'What's New' section includes an announcement for the 2018/2019 Winter Season Forecast Provision and a launch of a two-week temperature forecast for Japan.

# 1. World Climate

HOME > World Climate

## World Climate

JMA monitors the global climate with CLIMAT and SYNOP reports from NMHSs through the Global Telecommunication System (GTS) of WMO. Quality-checked data on temperature and precipitation are assembled to assess extreme climate events. Weekly, monthly and seasonal monitoring reports on extreme climate events with brief descriptions of disastrous events are available on this page, along with world distribution maps of temperature and precipitation.

Climatological normals for temperature and precipitation are based on the period 1981-2010.

### Main Products

#### Extreme Climate Monitoring

- ▶ Weekly Report(30 Oct 2019) ▶ Reports on Specific Events (11 Apr 2019)
- ▶ Monthly Report(15 Oct 2019)
- ▶ Seasonal Report(30 Sep 2019)
- ▶ Annual Report(15 Feb 2019)

Extreme Climate Monitoring

#### Normal & Historical Data

- ▶ World Climate Chart
- ▶ ClimatView: Monthly Historical & Normal Data (All available stations)
- ▶ 10-day/Half-monthly Mean Temperature and Precipitation (Regional Map)
- ▶ Monthly Normals Data (Principal Stations)(8 Dec 2011)

Normal & Historical Data

#### Data Descriptions & Analysis Procedures

- ▶ Extreme Climate Report
- ▶ Weekly, 10-day and half-monthly data
- ▶ Monthly Normals

Data Descriptions & Analysis Procedures

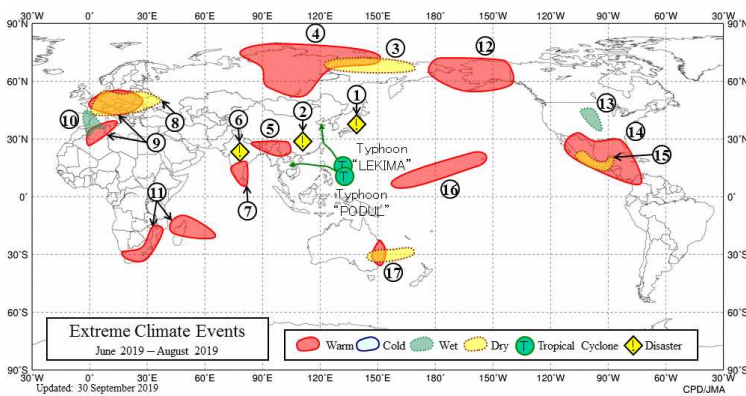
#### Statistical Research

- ▶ Impacts of Tropical SST Variability on the Global Climate

Statistical Research

## Seasonal report on global extreme climate events

Seasonal Report on GLOBAL Extreme Climate Events ----- Period: < > Jun 2019 - Aug 2019 Show

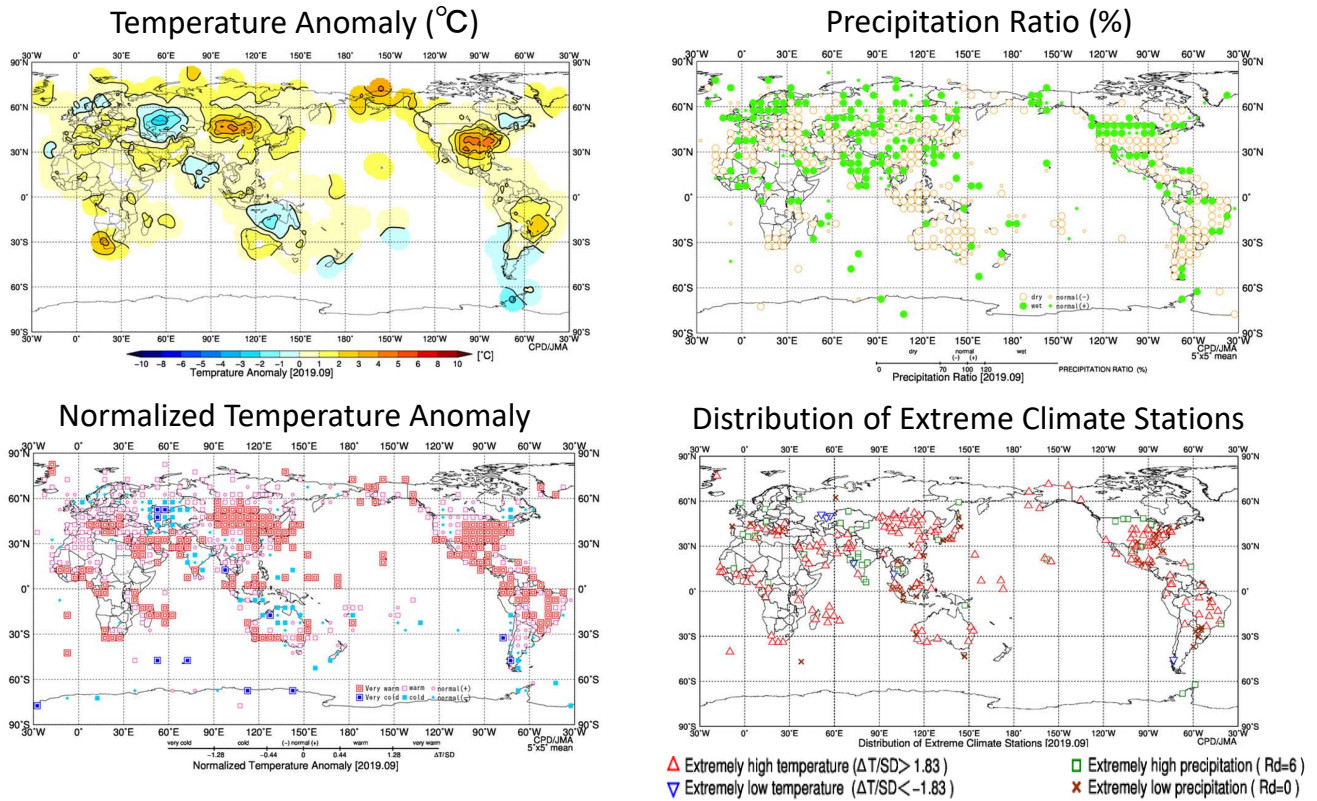


	Type	Area	Remarks
1	Heat Wave	From northern to western Japan	• It was reported that heat waves from late July to mid August caused more than 100 fatalities from northern to western Japan (Fire and Disaster Management Agency of Japan, as of 3 September).
2	Heavy Rain - Typhoon	From eastern China to northern Thailand	• It was reported that heavy rains, Typhoon "LEKIMA" and "PODUL" caused more than 200 fatalities from eastern China to northern Thailand (the government of China, the government of Viet Nam, European Commission).
3	Dry	The northern part of Eastern Siberia	
4	Warm	In and around Central Siberia	
5	Warm	From southern China to Nepal	
6	Heavy Rain	In and around South Asia	• It was reported that heavy rains from July to August caused more than 1900 fatalities in and around South Asia (the government of India, the government of Pakistan, European Commission).
7	Warm	Southern India	• It was reported that heat waves in June caused more than 110 fatalities in India (European Commission).

### Highlight

- Seasonal mean temperatures were extremely high in and around Central Siberia, from southern China to Nepal, in southern India, from eastern Europe to the western part of Northern Africa, from the Comoros to Mauritius, from Mozambique to South Africa, in and around Alaska, in and around Central America, from northern Polynesia to central Micronesia, and in eastern Australia.
- Seasonal precipitation amounts were extremely high from western Europe to the western part of Northern Africa and the central USA.
- Seasonal precipitation amounts were extremely low in the northern part of Eastern Siberia, in and around the central Europe, and in southern Mexico.

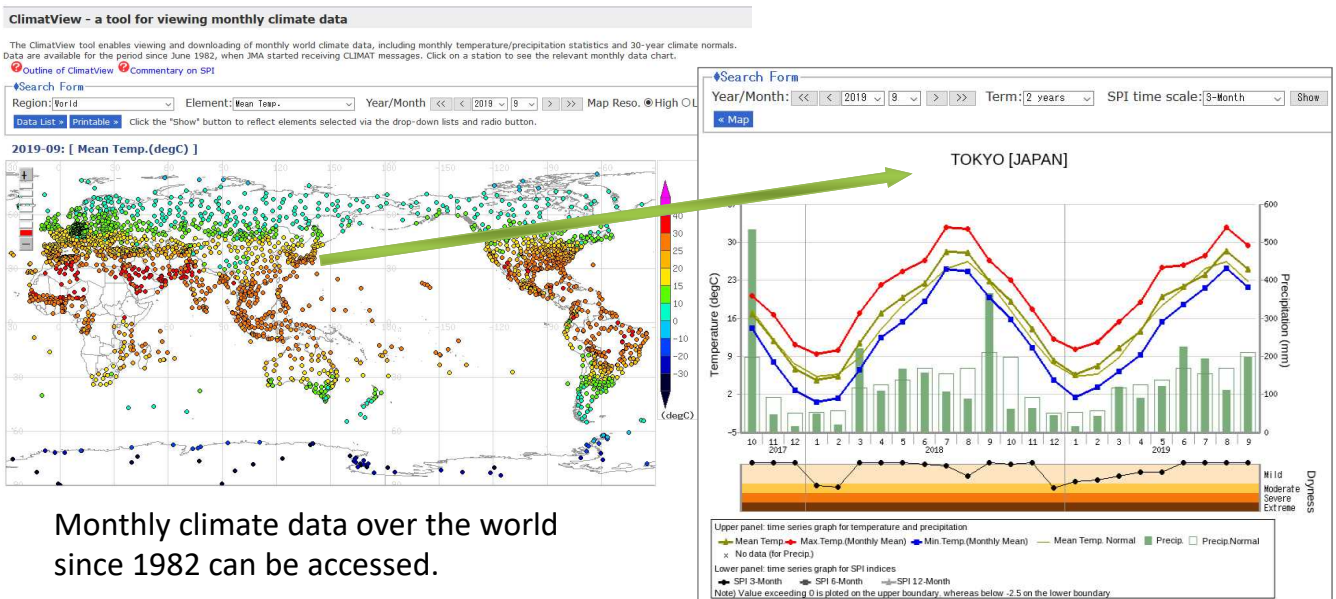
# Monthly world climate chart (September 2019)



<https://ds.data.jma.go.jp/tcc/tcc/products/climate/climfig/?tm=monthly>

## ClimatView

The ClimatView tool enables viewing and downloading of monthly world climate data, giving users access to statistics on monthly mean temperatures, monthly total precipitation amounts and related anomalies or ratios for all available stations.



Monthly climate data over the world since 1982 can be accessed.

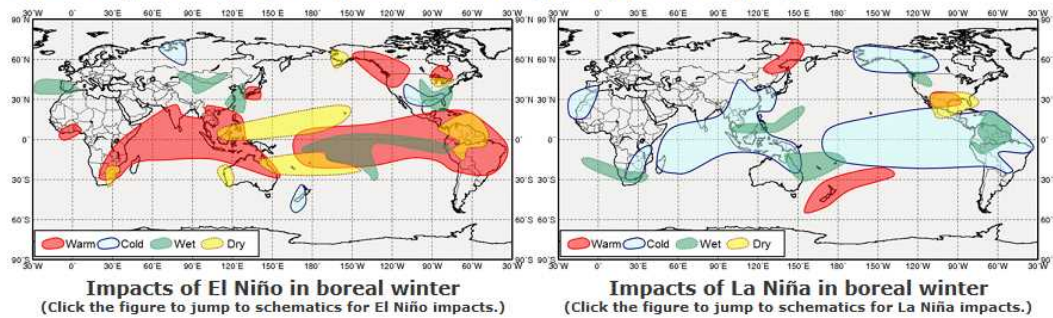
Time series of monthly temperatures, precipitation and SPI (Standardized Precipitation Index)

<https://ds.data.jma.go.jp/tcc/tcc/products/climate/climatview/frame.php>

# Statistical research: Impacts of tropical SST variability on the global climate

## Schematic Charts

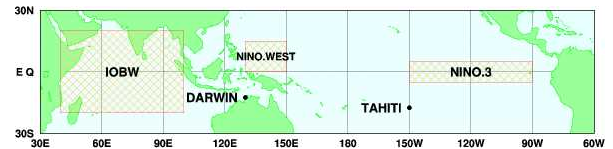
Schematic charts indicate typical anomaly patterns of surface temperature and precipitation for each season (boreal spring, summer, autumn and winter) as seen in past warmer/cooler SST events in the area of NINO.3 (corresponding to El Niño/La Niña events), NINO.WEST and IOBW. The figures below are examples for El Niño and La Niña impacts in boreal winter (from December through February). These results are based on observation and Japanese 55-year Reanalysis (JRA-55) data from 1958 through 2012 (a period of 55 years).



More schematic charts are available on the pages shown below.

Previous temperature and precipitation anomalies:

- El Niño events
- La Niña events
- Warmer SST events in the western tropical Pacific (NINO.WEST)
- Cooler SST events in the western tropical Pacific (NINO.WEST)
- Warmer SST events in the tropical Indian Ocean (IOBW)
- Cooler SST events in the tropical Indian Ocean (IOBW)



The "Detailed Charts" page shows anomaly patterns of three-month-mean temperature and precipitation fields centered on each calendar month for previous warmer/cooler SST events in each of the three tropical areas with 5° x 5°-grid representation, from which the schematic charts described above were derived.

<https://ds.data.jma.go.jp/tcc/tcc/products/climate/ENSO/index.htm>

## 2. Climate System Monitoring

Home	World Climate	Climate System Monitoring	El Niño Monitoring	NWP Model Prediction	Global Warming	Climate in Japan	Training Module	Press release
------	---------------	---------------------------	--------------------	----------------------	----------------	------------------	-----------------	---------------

HOME > Climate System Monitoring

### Climate System Monitoring

JMA monitors the climate system focusing on atmospheric circulation, tropical convection, oceanographic conditions and snow cover to understand backgrounds and factors of the present climate conditions including extreme events.

#### Main Products

#### Report on Climate System

- › Reports on Specific Events (11 Apr 2019)
- › Monthly Highlights on the Climate System (September 2019)
- › Seasonal Highlights on the Climate System (Summer, June 2019 - August 2019)
- › Annual Report on the Climate System (2016)

#### Monitoring and Statistical Analysis (Explanation)

- › Analysis Charts and Monitoring Indices
- › Asian monsoon monitoring (31 Oct 2019)
- › Madden-Julian Oscillation (MJO) (31 Oct 2019)
- › Stratospheric circulation (31 Oct 2019)
- › Composite map for El Niño / La Niña events **NEW**

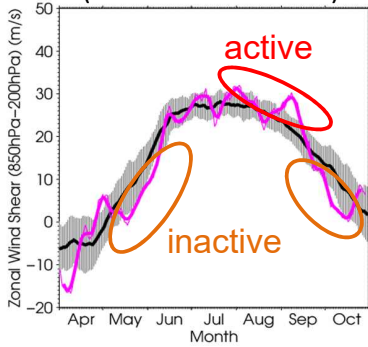
Report on Climate System

- Charts and indices
- Asian monsoon monitoring
- MJO
- Stratospheric circulation
- Composite maps

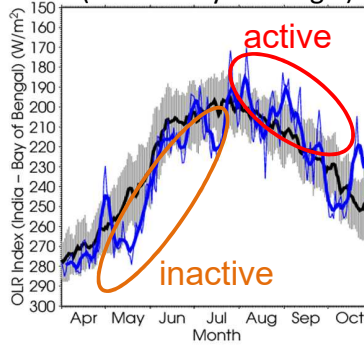


# Asian monsoon monitoring indices (2019)

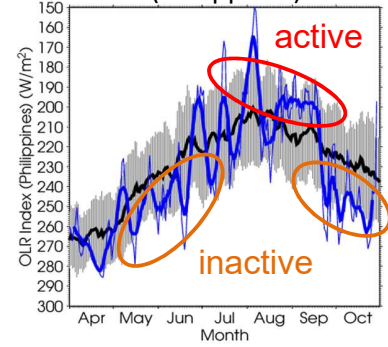
Vertical zonal-wind shear  
(North Indian Ocean)



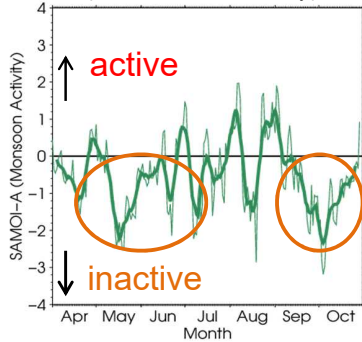
OLR index  
(India - Bay of Bengal)



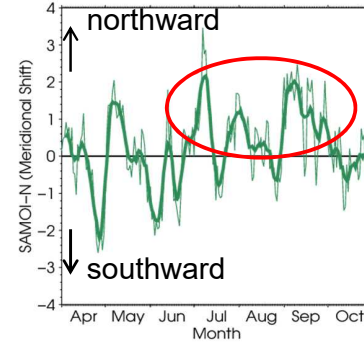
OLR index  
(Philippines)



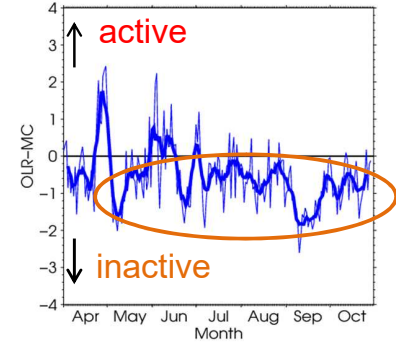
SAMOI-A  
(Monsoon Activity)



SAMOI-N  
(Northward Shift of Monsoon Activity)



OLR-MC  
(Maritime Continent)



These indices are useful in monitoring the strength and expansion of the Asian summer monsoon.

[https://ds.data.jma.go.jp/tcc/tcc/products/clisys/ASIA\\_TCC/monsoon\\_index.html](https://ds.data.jma.go.jp/tcc/tcc/products/clisys/ASIA_TCC/monsoon_index.html)

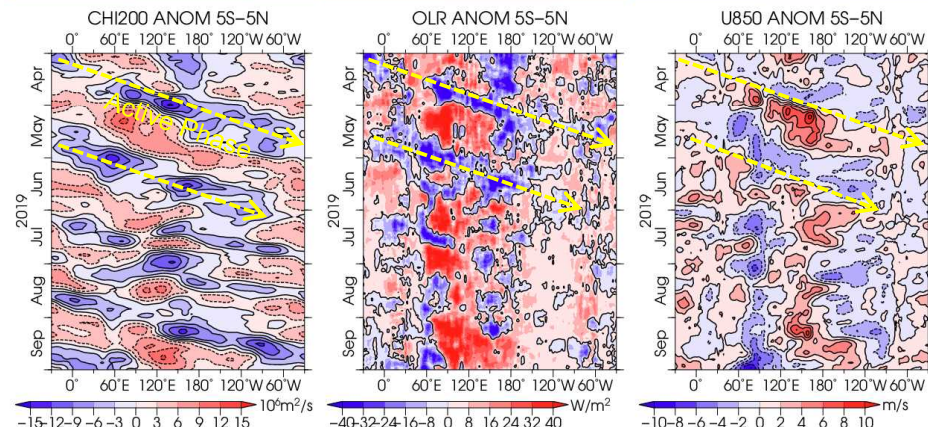
## Time-longitude cross section

This web page provides time-longitude cross sections. These charts are useful in monitoring intraseasonal oscillations such as Madden-Julian Oscillation (MJO).

### Time-Longitude cross section

Checking the right boxes will reflect selected options in the left section to all the other sections. --->  Time  Elements  Hist/Anom  Time Mean  Latitudinal Range  
Clicking on the 'default' button will initialize your setting. --->

<p>The last month to be shown:</p> <p><input type="radio"/> Last month</p> <p>⊙ Select -&gt; Year 2019 Month 9 &lt; &gt;</p> <p>Elements: 200-hPa Velocity Potential</p> <p><input type="radio"/> Hist <input checked="" type="radio"/> Anom <input type="radio"/> Norm</p> <p>Time Mean: <input type="radio"/> 3-day <input checked="" type="radio"/> 7-day</p> <p>Latitudinal Range: Equator (5S-5N) ▾</p>	<p>The last month to be shown:</p> <p><input type="radio"/> Last month</p> <p>⊙ Select -&gt; Year 2019 Month 9 &lt; &gt;</p> <p>Elements: Outgoing Longwave Radiation (OLR)</p> <p><input type="radio"/> Hist <input checked="" type="radio"/> Anom <input type="radio"/> Norm</p> <p>Time Mean: <input type="radio"/> 3-day <input checked="" type="radio"/> 7-day</p> <p>Latitudinal Range: Equator (5S-5N) ▾</p>	<p>The last month to be shown:</p> <p><input type="radio"/> Last month</p> <p>⊙ Select -&gt; Year 2019 Month 9 &lt; &gt;</p> <p>Elements: 850-hPa Zonal Wind</p> <p><input type="radio"/> Hist <input checked="" type="radio"/> Anom <input type="radio"/> Norm</p> <p>Time Mean: <input type="radio"/> 3-day <input checked="" type="radio"/> 7-day</p> <p>Latitudinal Range: Equator (5S-5N) ▾</p>
--	---	--



### Elements:

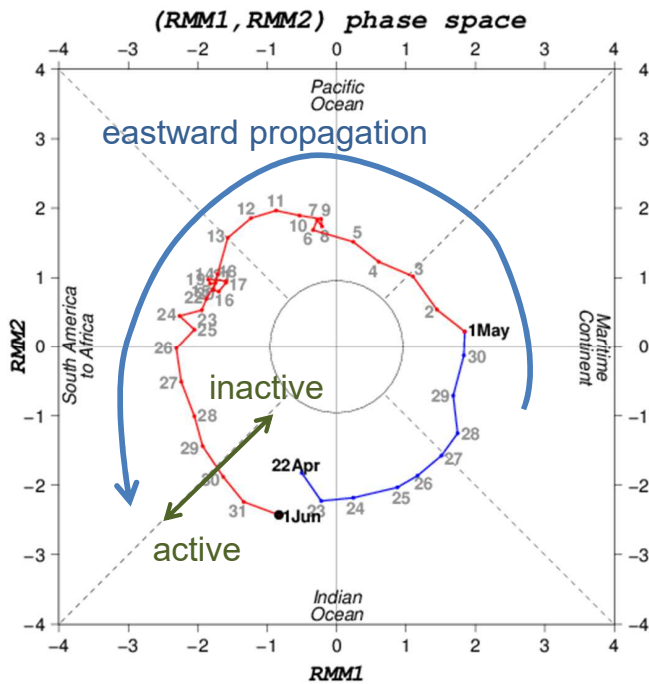
OLR, 200hPa velocity potential, 10m/850hPa/200 hPa zonal wind and SST

Average period:  
3-day and 7-day average

Latitude Range:  
15-25N, 5-15N, 5S-5N (equator), 15-5S

# MJO phase and amplitude monitor

The indices defined by Wheeler and Hendon (2004) are convenient for monitoring MJO phase and amplitude.



In the phase space, the equatorial zones are divided into 8 phases and each phase indicates the active phase of the MJO propagation.

In association with the eastward propagation of MJO, trajectory of RMM1 and RMM2 draws anti-clockwise circles in the phase space.

<https://ds.data.jma.go.jp/tcc/tcc/products/clisys/mjo/monitor.html>

## Composite map for El Niño / La Niña events

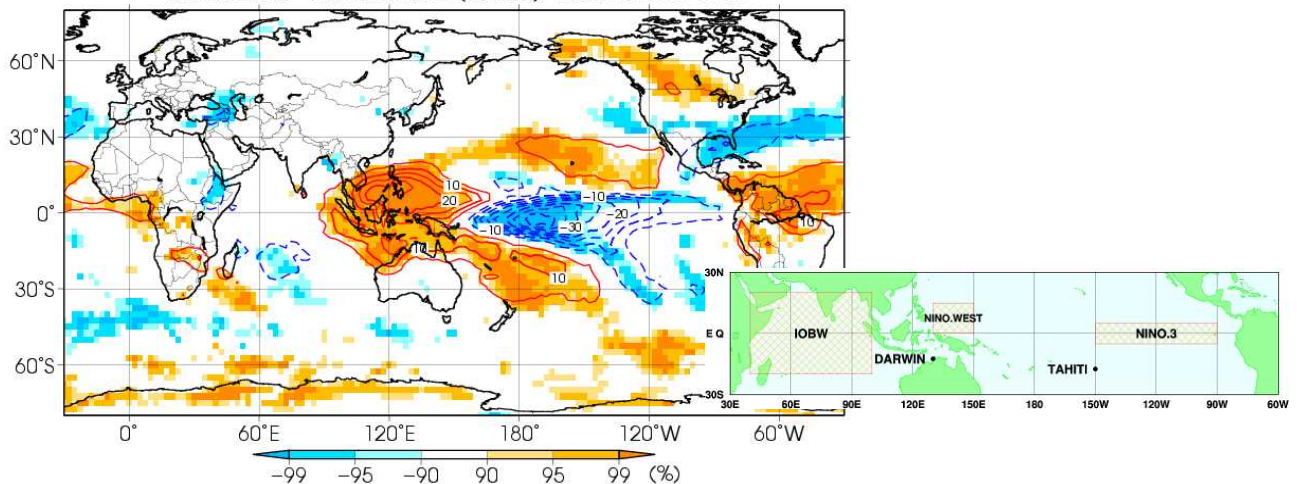
HOME > Climate System Monitoring > Composite map for El Niño / La Niña events

### Composite map for El Niño / La Niña events

Commentary (data and methods, statistical characteristics)

Elements:  ENSO Index:  Phases:   
 Month:  Time Mean:

Element:olr Index:NINO.3(Warm) Period:Dec-Feb



This product provides the statistical analysis on the relationship between warmer/cooler SST event in the areas of NINO.3, NINO.WEST and IOBW and atmospheric circulation.

[https://ds.data.jma.go.jp/tcc/tcc/products/clisys/enso\\_statistics/index.html](https://ds.data.jma.go.jp/tcc/tcc/products/clisys/enso_statistics/index.html)

# Reports on specific events

## Summary of the 2018/2019 Asian Winter Monsoon

### Summary of the 2018/2019 Asian Winter Monsoon

This report summarizes the characteristics of the surface climate and atmospheric/oceanographic considerations related to the Asian winter monsoon for 2018/2019.

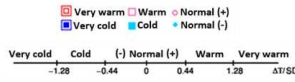
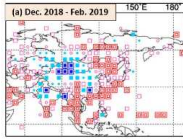
Note: The Japanese 55-year Reanalysis (JRA-55; Kobayashi et al., 2015) atmospheric circulation data and COBE-SST (Shi et al., 2005) sea surface temperature (SST) data were used for this investigation. NOAA Interpolated Outgoing Longwave Radiation (OLR) data (Lietmann and Smith 1996) provided online by the U.S. NOAA Earth System Research Laboratory (ESRL) at <https://www.esrl.noaa.gov/psd/> was referenced to infer tropical convective activity. The base period for the normal is 1981–2010. The term "anomaly" as used in this report refers to deviation from the normal.

#### 1. Surface climate conditions

Temperatures for December 2018 to February 2019 were generally above normal from the eastern part of East Asia to the southern part of South Asia, and were below normal in and around the northwestern part of East Asia (Figure 15). In particular, seasonal mean temperatures were extremely high from the Okinawa/Amami region of Japan to southern China and from the central part of Southeast Asia to the southern part of South Asia, and were extremely low from western Mongolia to northwestern China. Precipitation amounts during this period were above normal in and

around southern and western parts of East Asia and the northwestern part of Southeast Asia, and were below normal in the northeastern part of East Asia (Figure 16). Drier-than-normal conditions in and around the Philippines and warmer-than-normal conditions in and around Southeast Asia, as seen in typical anomaly patterns of past El Niño events, were observed around February.

Figure 17 shows the extreme climate conditions observed between December 2018 and February 2019. In December, extremely high temperatures were seen from the Okinawa region of Japan to Southeast Asia, and extremely low temperatures were seen in the northwestern part of East Asia. Extremely high precipitation amounts were observed from western Japan to eastern China and from Myanmar to northwestern Sumatra. In January, extremely high temperatures were seen from northeastern China to the southern part of Central Siberia and from southern China to the central part of Southeast Asia. Extremely high precipitation amounts were observed from southern China to western Thailand, and extremely low precipitation amounts were observed from northern Japan to the southern Korean Peninsula. In February, extremely high temperatures were seen from the Ogawara Islands of Japan to southern China and from the central part of Southeast Asia to the southern part of South Asia.



## Primary Factors behind the Heavy Rain Event of July 2018 and the Subsequent Heatwave in Japan from Mid-July Onward

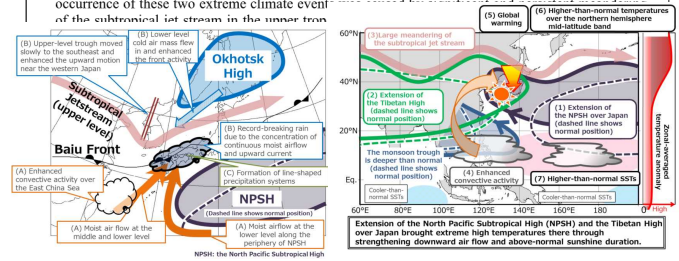
22 August 2018

Tokyo Climate Center, Japan Meteorological Agency  
<https://ds.data.jma.go.jp/tcc/tcc/index.html>

Abstract

Japan experienced significant rainfall particularly from western Japan to the Tokai region mainly in early July (The Heavy Rain Event of July 2018), which caused widespread havoc nationwide. Extremely high temperatures subsequently persisted throughout most of Japan from mid-July onward.

In this context, the Japan Meteorological Agency (with the help of the Tokyo Climate Center Advisory Panel on Extreme Climatic Events) investigates atmospheric and oceanic conditions considered to have contributed to such climate extremes and summarizes related primary factors. Based on this work, the Heavy Rain Event of July 2018 is attributed to an ongoing concentration of two massively moist air streams over western Japan and persistent upward flow associated with the activation of a stationary Baiu front. The related heatwave is attributed to the expansion of a persistent North Pacific Subtropical High and Tibetan High to the Japanese mainland. The serial occurrence of these two extreme climate events



<https://ds.data.jma.go.jp/tcc/tcc/products/clisys/reports/index.html>

## Monthly and seasonal highlights on the climate system

JMA monitors the global atmospheric circulation, convection, ocean conditions and snow/ice coverage. 'Monthly (Seasonal) Highlights on the Climate System' is a monthly (seasonal) bulletin focusing on the monthly (seasonal) highlights of the monitoring results.

HOME > Climate System Monitoring > Monthly Highlights on the Climate System

### Monthly Highlights on the Climate System

'Monthly Highlights on the Climate System' has been issued in PDF format since March 2007 as a monthly bulletin focusing on the monthly highlights of the monitoring results.

#### Highlights in September 2019

- Monthly mean temperatures were significantly above normal from northern to western Asia, and from the western part of Western Africa to the western part of Middle Africa, from the eastern USA to southern Mexico, and in and around central Brazil.
- In the equatorial Pacific, remarkably positive SST anomalies were observed in the eastern equatorial Indian Ocean, the sea northeast of the Philippines, and the eastern Pacific, and was suppressed from the southeastern tropical Indian Ocean to the western equatorial Indian Ocean.
- In the 500-hPa height field, positive anomalies were seen over the northern polar region, the sea south of Alaska, the eastern USA, and the sea west of Europe, and northeast of the Caspian Sea and over Eastern Siberia.

#### Full version (PDF)

▶ [Monthly Highlights on the Climate System \(September 2019\)](#)

▶ [Back Number](#)

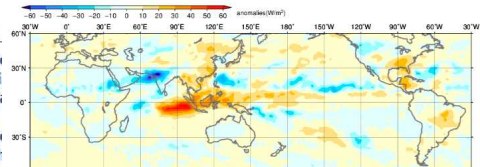


Fig. 6 Monthly mean Outgoing Longwave Radiation (OLR) anomaly (September 2019)

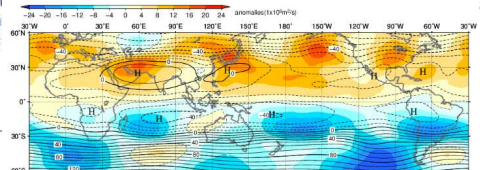


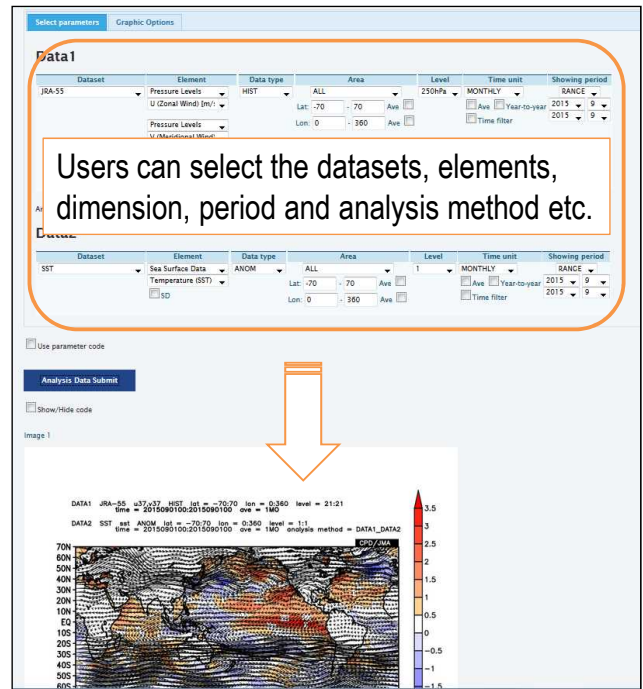
Fig. 8 Monthly mean 200-hPa stream function and anomaly (September 2019). The contour interval is  $10 \times 10^6 \text{ m}^2 \text{ s}^{-1}$ . The base period for the normal is 1981–2010.

Monthly Highlights: <https://ds.data.jma.go.jp/tcc/tcc/products/clisys/highlights/index.html>

Seasonal Highlights: [https://ds.data.jma.go.jp/tcc/tcc/products/clisys/season\\_highlights/index.html](https://ds.data.jma.go.jp/tcc/tcc/products/clisys/season_highlights/index.html)

# iTacs: Interactive Tool for Analysis of the Climate System

- The iTacs (Interactive Tool for Analysis of the Climate System) is a web-based application for climatological analysis.
- The output of analysis can be downloaded in the form of gridded data (GrADS format).
- This tool is available for registered NMHS staffs only.
- Applicants are requested to contact TCC via E-mail ([tcc@met.kishou.go.jp](mailto:tcc@met.kishou.go.jp)).



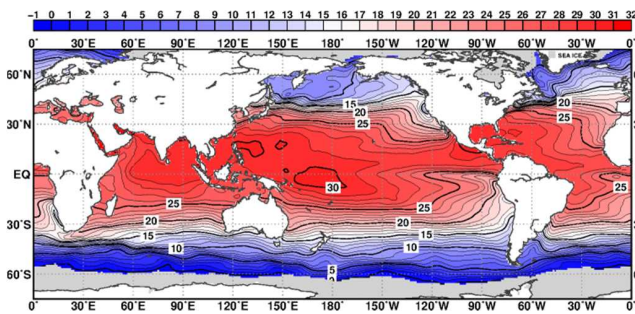
<https://extreme.kishou.go.jp/tool/itacs-tcc2015/>

## 3. El Niño Monitoring

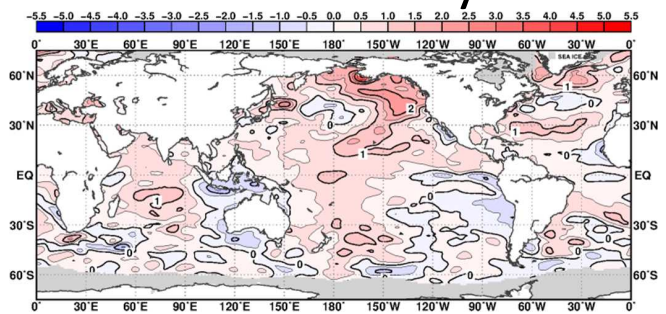
The screenshot shows the JMA El Niño Monitoring website. The navigation bar includes 'Home', 'World Climate', 'Climate System Monitoring', 'El Niño Monitoring' (highlighted with a red box), 'NWP Model Prediction', 'Global Warming', 'Climate in Japan', 'Training Module', 'Press release', and 'Links'. Below the navigation bar, the page title is 'El Niño Monitoring and Outlook'. The main content area includes a paragraph about JMA's operations, a 'Main Products' section, and several sub-sections: 'Latest Products' (last updated: 10 Oct 2019), 'ENSO Impacts', 'Model Descriptions & Analysis Procedures', and 'Decadal Oscillation'. Callouts with arrows point to specific items: 'Latest analysis and outlook' points to 'El Niño Outlook'; 'Historical El Niño and La Niña Events' points to 'Historical El Niño and La Niña Events'; 'Monthly maps and longitude-depth cross sections' points to 'Longitude-Depth Cross Section along the Equator'; and 'Pacific Decadal Oscillation index' points to 'Pacific Decadal Oscillation (15 Feb 2019)'.

# SST (JJA 2019)

## SST



## SST anomaly



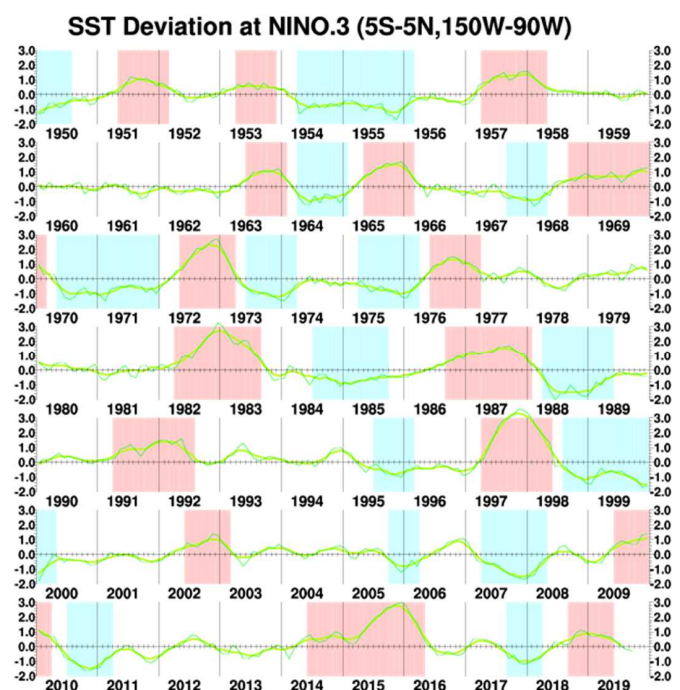
- In the equatorial Pacific, remarkably positive SST anomalies were observed near the date line.
- In the North Pacific, remarkably positive SST anomalies were widely observed.
- In the Indian Ocean, remarkably positive SST anomalies were observed in almost the entire region west of 100°E, and remarkably negative SST anomalies were observed south of Java and in the southwestern coast of Australia.

# Historical El Niño and La Niña Events

Historical El Niño and La Niña Events

El Niño	La Niña
	summer 1949 - summer 1950
spring 1951 - winter 1951/52	
spring 1953 - autumn 1953	spring 1954 - winter 1955/56
spring 1957 - spring 1958	
summer 1963 - winter 1963/64	spring 1964 - winter 1964/65
spring 1965 - winter 1965/66	autumn 1967 - spring 1968
autumn 1968 - winter 1969/70	spring 1970 - winter 1971/72
spring 1972 - spring 1973	summer 1973 - spring 1974
	spring 1975 - spring 1976
summer 1976 - spring 1977	
spring 1982 - summer 1983	summer 1984 - autumn 1985
autumn 1986 - winter 1987/88	spring 1988 - spring 1989
spring 1991 - summer 1992	summer 1995 - winter 1995/96
spring 1997 - spring 1998	summer 1998 - spring 2000
summer 2002 - winter 2002/03	autumn 2005 - spring 2006
	spring 2007 - spring 2008
summer 2009 - spring 2010	summer 2010 - spring 2011
summer 2014 - spring 2016	autumn 2017 - spring 2018
autumn 2018 - spring 2019	

Time series of NINO.3 SST deviation



# **Climate condition at extreme climate events**



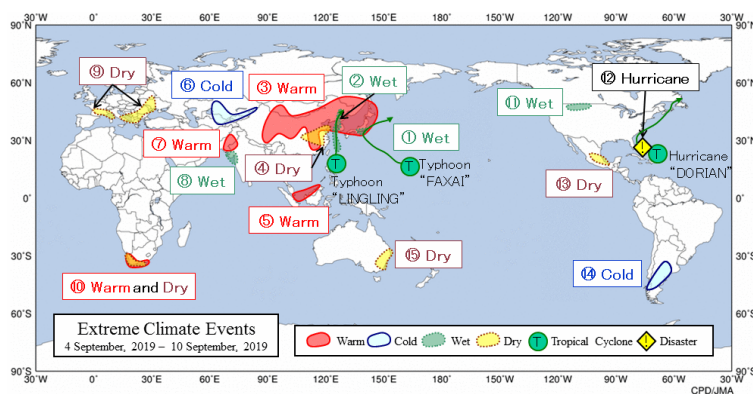
## Climate condition at extreme climate events

TCC monitors the global climate with CLIMAT and SYNOP reports from National Meteorological and Hydrological Services (NMHSs) through the Global Telecommunication System (GTS) of the World Meteorological Organization (WMO). This document briefly introduces monitoring reports on extreme climate events in the world and related products, which are regularly updated and available on the TCC website.

### 1. Reports on global extreme climate events

Extreme climate events are rarely experienced; they include massive storms, heat waves, cold spells, prolonged droughts and other phenomena with various temporal ranges, and often cause weather-related disasters that influence socio-economic activity. Statistically, TCC defines such events as phenomena occurring once every 30 years or less. Weekly reports (Fig. 1(a)) are based on SYNOP data submitted by NMHSs around the world, while monthly (Fig. 1(b)), seasonal and annual reports are based on CLIMAT data from the same organizations.

(a) Weekly



(b) Monthly

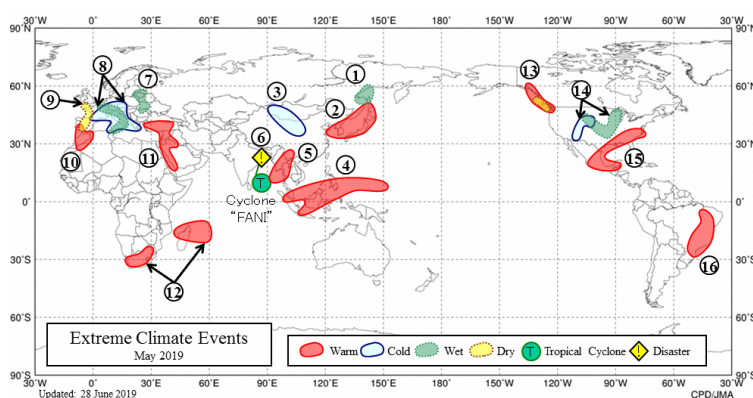


**Fig. 1.** Examples of (a) weekly and (b) monthly reports on global extreme climate events (Weekly reports: <https://ds.data.jma.go.jp/tcc/tcc/products/climate/weekly/index.html>) (Monthly reports: <https://ds.data.jma.go.jp/tcc/tcc/products/climate/monthly/index.html>)

In addition to these reports provided regularly, TCC provides special reports for specific extreme climate events with primary factors in terms of atmospheric and oceanic conditions related to the events, when these extreme climate events are considered to influence socio-economic activities.

It is noted that SYNOP reports provide real-time weather data from one specific weather stations, while CLIMAT reports contain monthly statistics relating to various meteorological elements from individual weather stations for specific month, such as monthly mean temperature and monthly precipitation totals.

### **1.1 Extreme warm/cold events**

Extreme warm/cold events for each weather station are identified from normalized mean temperature anomalies in the target period. Anomalies are deviations from the climatological normals, and standard deviations for normalization are based on interannual variability over the same 30 years as for climatological normals.

- Weekly: Extreme warm (cold) events are identified if weekly mean temperature anomalies from observation are estimated to exceed (or fall below)  $+3\sigma$  ( $-3\sigma$ ), where  $\sigma$  is the standard deviation of mean temperatures in a 31-day period with the target week at its center. (e.g., if the target period is from Dec. 9th to Dec. 15th, the 31-day period is from Nov. 27th to Dec. 27th).
- Monthly: Extreme warm (cold) events are identified if monthly mean temperature anomalies from observation exceed (or fall below)  $+1.83\sigma$  ( $-1.83\sigma$ ), where  $\sigma$  is the standard deviation of monthly mean temperatures.
- Seasonal: Extreme warm (cold) events are identified if seasonal mean temperature anomalies from observation exceed (or fall below)  $+1.83\sigma$  ( $-1.83\sigma$ ), where  $\sigma$  is the standard deviation of seasonal mean temperatures.

### **1.2 Extreme wet/dry events**

Extreme wet/dry events for each weather station are identified from precipitation totals in the target period and their ratio to the climatological normals.

- Weekly (wet): Extreme wet events are identified if weekly precipitation totals from observation exceed the relevant thresholds, which depend on the climatological normals of precipitation totals in a 29-day period (referred to here as X) with the target week as its center (e.g., if the target period is from Dec. 9th to Dec. 15th, the 29-day period is from Nov. 28th to Dec. 26th). For example, if the X value are 10, 100, 200, and 500 mm, the corresponding thresholds are 153, 98, 81 and 59% of X, respectively. The thresholds are fixed at 59% if X exceeds 500 mm.

- Weekly (dry): Extreme dry events are identified if precipitation totals from observation are lower than any value in the climatological normal base period during a 30-day period starting 29 days before the end of the target week (e.g., if the target week is from Dec. 9th to Dec. 15th, the 30-day period is from Nov. 16th to Dec. 15th).
- Monthly: Extreme wet (dry) events are identified if monthly precipitation totals from observation are more (less) than any value in the climatological normal base period for the month.
- Seasonal: Extreme wet (dry) events are identified if seasonal precipitation totals from observation are more (less) than any value in the climatological normal base period for the season.

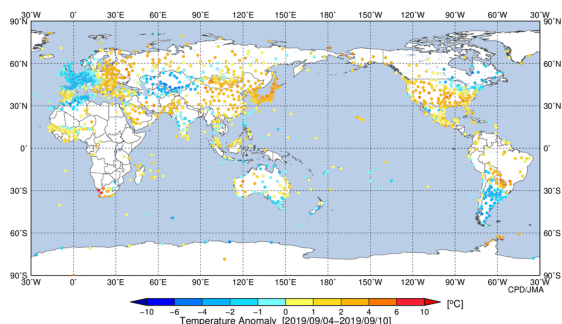
## 2. World climate charts using CLIMAT/SYNOP reports

A variety of temperature and precipitation climate charts using CLIMAT and SYNOP reports are available on the TCC website, which are the basis of the reports on global extreme climate events provided by TCC.

### 2.1 (Weekly) weekly mean temperatures and anomalies, 7-day precipitation and ratio, 30-day precipitation and ratio

Weekly and 30-day averaged/cumulative values are based on SYNOP reports from NMHSs around the world. Weekly mean values and anomalies are calculated for temperatures (Fig. 2(a)), and 7-day (Fig. 2(b)) and 30-day totals and ratios are calculated for precipitation. Anomalies are deviations from the climatological normal, and ratios are derived by dividing precipitation totals for a certain period by the climatological normal for the corresponding period.

(a) Weekly (7-day) mean Temperature anomaly (°C)



(b) Weekly (7-day) precipitation total ratio (%)

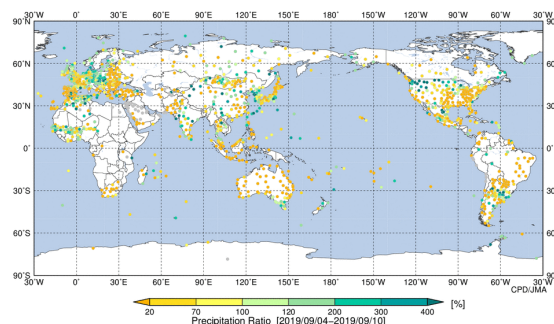


**Fig. 2.** Examples of weekly (7-day) (a) mean temperature anomalies (°C) and (b) precipitation total ratios (%)

(Weekly: <https://ds.data.jma.go.jp/tcc/tcc/products/climate/climfig/?tm=weekly>)

## 2.2 (Monthly) monthly mean temperature anomalies and precipitation totals

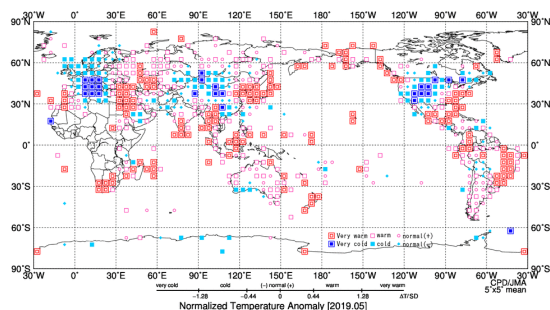
Monthly mean temperatures are based on CLIMAT reports from NMHSs around the world. Anomalies are deviations from the climatological normal. Monthly precipitation totals are also based on CLIMAT reports and are shown after area-averaged over each 5°x5° grid box.

## 2.3 (Monthly, seasonal, and annual) normalized temperature anomalies

Monthly (Fig. 3(a)), seasonal and annual mean temperature anomalies normalized by their standard deviations are shown after the application of averaging in 5°x5° grid boxes. The data used are from CLIMAT reports submitted by NMHSs around the world. Anomalies are deviations from the climatological normal, and standard deviations for normalization are based on interannual variability over the same 30 years as for climatological normals.

The category thresholds are  $\pm 1.28$ ,  $\pm 0.44$ , and 0. For example, a normalized anomaly magnitude exceeding 1.28 (0.44) represents the likelihood of its appearance once every 10 years (3 years) or less, where temperature frequency is assumed to follow Gaussian distribution. For seasonal and annual maps, no marks are shown if insufficient data are available for the period.

(a) Monthly normalized temperature anomaly (°C)



(b) Monthly precipitation ratio (%)

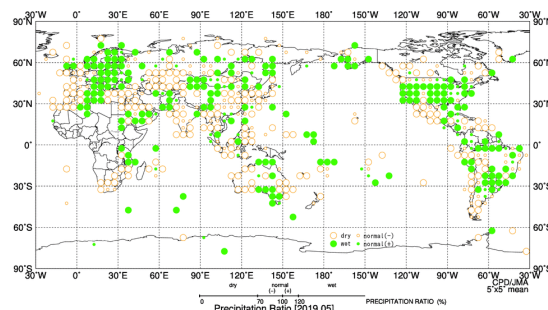


**Fig. 3.** Examples of monthly (a) normalized temperature anomaly (°C) and (b) precipitation ratio (%)

(Monthly: <https://ds.data.jma.go.jp/tcc/tcc/products/climate/climfig/?tm=monthly>)

(Seasonal: <https://ds.data.jma.go.jp/tcc/tcc/products/climate/climfig/?tm=seasonal>)

(Annual: <https://ds.data.jma.go.jp/tcc/tcc/products/climate/climfig/?tm=annual>)

## 2.4 (Monthly, seasonal, and annual) precipitation ratios

Monthly (Fig. 3(b)), seasonal, and annual precipitation ratios to the climatological normals are shown after the application of averaging in 5°x5° grid boxes. The data used are from CLIMAT reports submitted by NMHSs around the world.

The category thresholds are 70%, 100%, and 120%. For seasonal and annual maps, no marks are shown if insufficient data are available for the period.

## 2.5 (Monthly) distribution of extreme climate stations

For each  $5^{\circ}\times 5^{\circ}$  grid box in extreme climate conditions (warm/cold and wet/dry), the weather station reporting the most extreme value is marked as per the legend in the chart (Fig. 4).

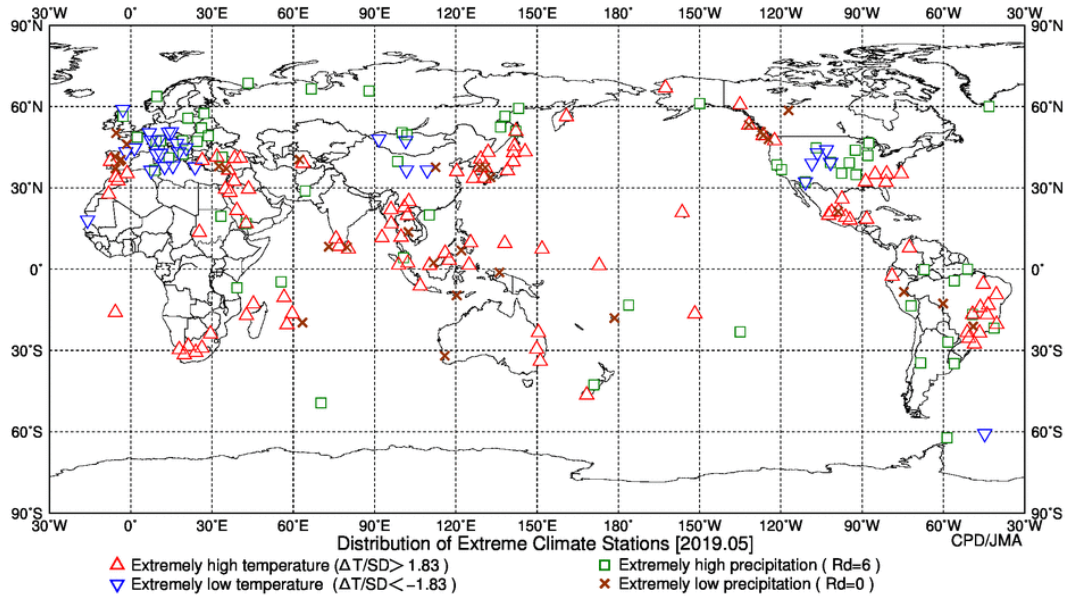


**Fig. 4.** Example of monthly distribution of extreme climate stations  
(Monthly: <https://ds.data.jma.go.jp/tcc/tcc/products/climate/climfig/?tm=monthly>)

## 2.6 (Annual) frequencies of extremely high/low temperature and heavy/light precipitation

Frequencies of extremely high/low temperature or heavy/light precipitation months based on monthly observation data. The frequencies are calculated by dividing the total number of extremely warm/cold months by the total number of data-available months in each  $5^{\circ}\times 5^{\circ}$  grid box. Frequencies are indicated by semicircle scale. Given that extreme climate events are defined as phenomena occurring every 30 years or less, frequencies are normally expected to be about 3% and values exceeding 10-20% are considered to be above normal.

### 3. ClimatView – a tool for viewing monthly climate data

The ClimatView tool (Fig. 5) enables viewing and downloading of monthly world climate data, giving users access to statistics on monthly mean temperatures, monthly total precipitation amounts and related anomalies or ratios for all stations where such data are available. Statistics on monthly means of daily maximum/minimum temperatures and Standardized Precipitation Index (SPI) are also provided. These data are derived from CLIMAT messages reported via the GTS line from WMO Members around the world.

Data are available for the period since June 1982, when JMA started receiving CLIMAT messages. Current data are from the previous month or the month before it, and are usually updated around the 9th of each month. CLIMAT data received at the German Meteorological Service (Deutscher Wetterdienst; DWD) are also included in the database. Since 1999, DWD and JMA have jointly operated the GCOS Surface Network Monitoring Centre (<http://www.gsncmp.dwd.de/>) and exchanged CLIMAT data. Statistics on climatological normals for monthly mean temperature and monthly total precipitation are based on the period 1981 - 2010. The data sources for the normals are CLIMAT messages received by JMA and GHCN data distributed by National Oceanic and Atmospheric Administration (NOAA)'s National Centers for Environmental Information (NCEI).

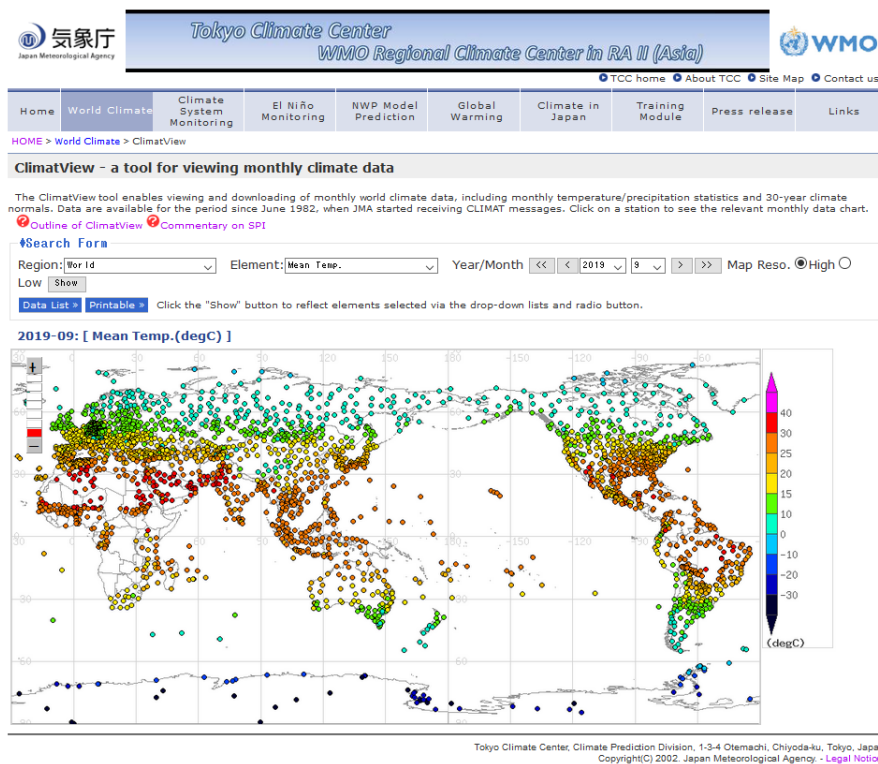


**Fig. 5.** ClimatView  
(<https://ds.data.jma.go.jp/tcc/tcc/products/climate/climatview/frame.php>)

### 3.1 Distribution map

On the distribution map, temperature, precipitation data and Standardized Precipitation Index (SPI) for each station are displayed as colored round marks for selected areas. A color legend is shown on the right. Basic usage of the distribution map is as follows:

- Hover over a station on the distribution map to show data on the chosen element and the name of the station in a pop-up balloon (Fig. 6(a)).
- Use the drop-down lists and radio button at the top of the page to change the region, element, year/month, and map resolution (Fig. 6(a)).
- Click the [- Click the "Show" button to reflect elements selected via the drop-down lists and radio button (Fig. 6(a)).
- Drag the scroll bars on the right side and the bottom of the map to adjust the display area (Fig. 6(a)).
- Click the "Printable" button to display a figure in a new window for printing (Fig. 6(a)).
- Select "Low" for the map resolution if map drawing takes a long time due to a slow connection (Fig. 6(a)).
- Click the buttons on the zoom bar on the left to zoom in/out of the map (Fig. 6(b)).
- The red mark between the zoom bar buttons shows the degree of zoom (a higher position indicates a larger map) (Fig. 6(b)).
- The white buttons on the bar can also be clicked to zoom in/out (Fig. 6(b)).

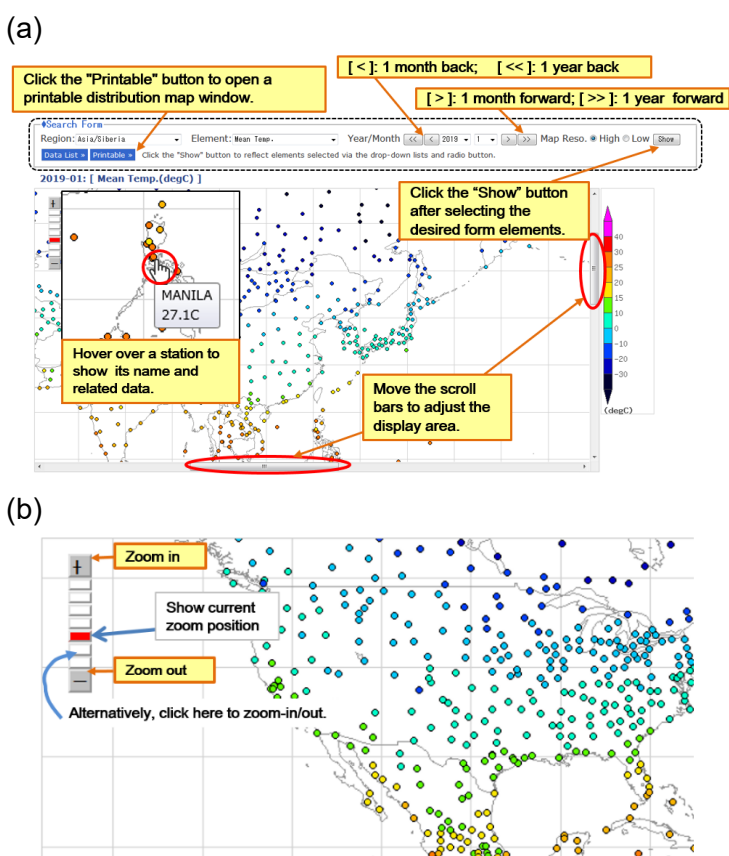


**Fig. 6.** How to use distribution maps on the ClimatView

### 3.2 Historical graphs and data lists for individual stations

From the distribution map, historical graphs and data lists for selected individual stations can be shown on the ClimatView. Basic usage of the historical graphs and data lists for individual stations is as follows (Fig. 7):

- Click a station on the distribution map to display a time-series graph covering a period of two years.
- Change the period of the graph as desired by selecting from the "Term" list (1 year, 2 years, 5 years or all years).
- Change the SPI time scale of the graph as desired by selecting from the "SPI time scale" list (3-month, 6-month, 12-month or ALL display).
- Data used for the graph are listed below it, and can be downloaded in comma-separated value (csv) format by clicking the "Download" button.

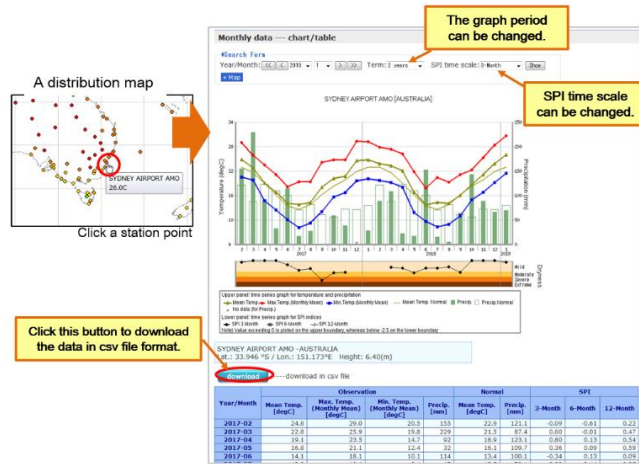


**Fig. 7.** How to use historical graphs and data lists for individual stations on the ClimatView

### 3.3 Data lists for individual regions

In addition to showing data lists for individual stations, a data list for all stations in the selected region can be displayed. Basic usage to show a data list for all stations in the selected region is as follows (Fig. 8):

- Clicking the "Data list" button on the distribution map.
- If "World" is selected as the region, Asia/Siberia stations are displayed for the data list in place of all stations worldwide.
- If "Normal" is selected as an element on the distribution map, normal values are displayed in the data list.

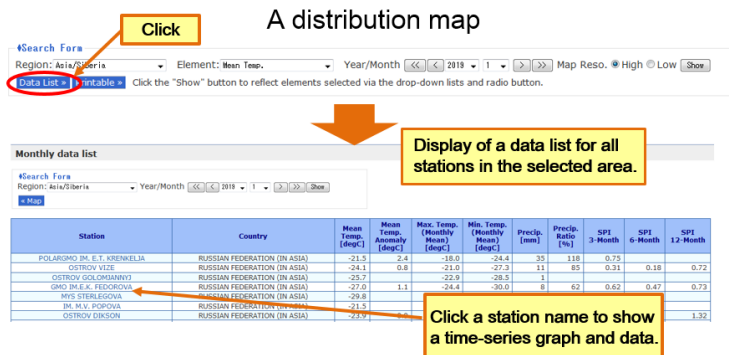


**Fig. 8.** How to use data lists for stations in the selected region on the ClimatView

- Click a station name in the list to show a time-series graph and data for the station. For details, see "3.2 Historical graphs and data lists for individual stations."
- The region and year/month can be changed via the form options at the top of the page.

### 3.4 Standardized Precipitation Index (SPI)

#### (a) What is the SPI?

The Standardized Precipitation Index (SPI) is commonly used for operational drought monitoring by NMHSs around the world to quantify precipitation deficits on multiple timescales. Related calculation for specific locations is based on long-term precipitation records for the target period. The ability to compute index values on numerous time scales makes this metric useful in the quantification of risk regarding various types of droughts (e.g., meteorological, agricultural and hydrological). The need for only precipitation data as an input parameter facilitates SPI computation. However, it should be noted that no evapotranspiration effect is considered. On the ClimatView, dry condition for each station is categorized as Table. 1. Refer to the WMO's SPI User Guide (WMO, 2012) for details of the background of the index, its introduction and a related description.

SPI	Category	Severity of event
0 ~ -0.99	Mild dryness	1 in 3 years
-1.00 ~ -1.49	Moderate dryness	1 in 10 years
-1.5 ~ -1.99	Severe dryness	1 in 20 years
< -2.0	Extreme dryness	1 in 50 years

**Table.1.** SPI values and corresponding states in ClimatView (cited from WMO (2012))

#### (b) Data and method

Calculation of the SPI indices shown in the ClimatView tool is based on monthly precipitation totals from CLIMAT data for states worldwide and on GHCN data provided by the NCEI/NOAA. Both sets of data are based on observations conducted at surface weather stations worldwide, but CLIMAT data are available only as far back as June 1982. Where both are available for the same station, CLIMAT data are applied. To derive probability distribution for past precipitation amounts, monthly precipitation data are used wherever possible for the period from 1950 to 2010. SPI values are not calculated if the available data span is shorter than 30 years. The ClimatView tool shows SPI values only as far back as June 1982.

TCC uses the SPI calculation program provided by Colorado State University in the USA. In SPI computation, the long-term record of past precipitation is fitted to probability distribution before transformation to normal distribution (Fig. 9). Accordingly, the mean SPI for the location and desired period is zero (Edwards and McKee, 1997). Negative SPI values indicate precipitation below the median value. Drought events may occur when the SPI is continuously negative and reaches a certain value, such as -1.0 or less (McKee et al., 1993).

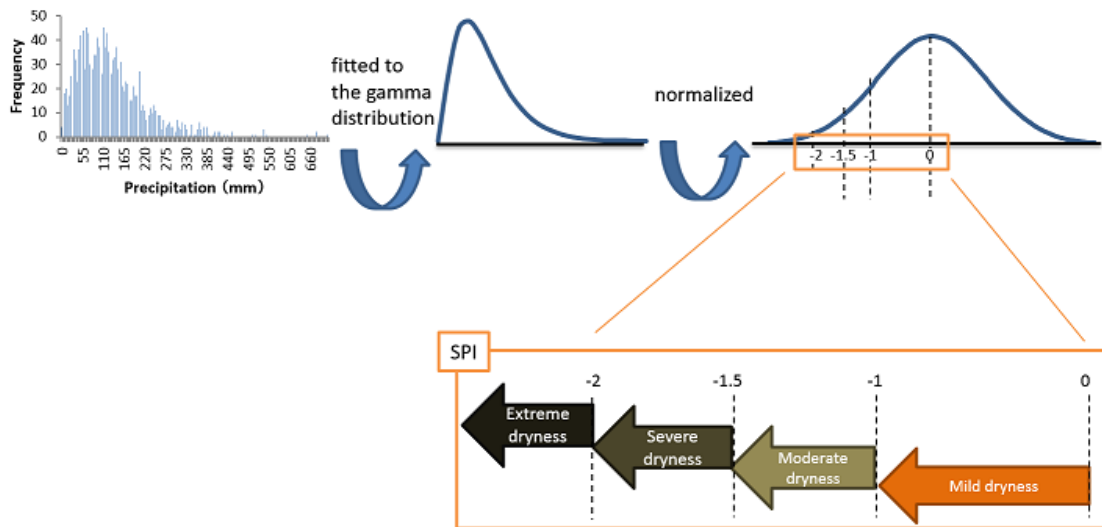


**Fig. 9.** Schematic representation of SPI calculation

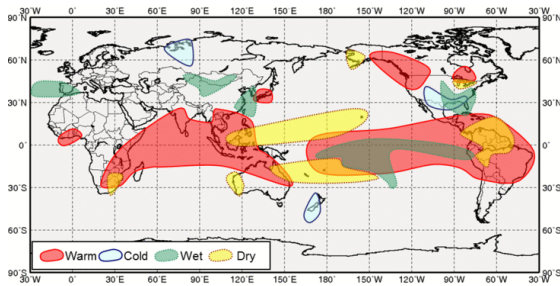
#### **4. Composite maps – impacts of tropical sea surface temperature (SST) variability on the global climate**

Sea surface temperature (SST) variability in the tropics can significantly impact on the global climate through atmospheric circulation. El Niño/La Niña events, which are identified by SST fluctuations from the central to the eastern equatorial Pacific (NINO.3), are widely-known examples of this. In addition, SST variability in the western tropical Pacific (NINO.WEST) and the tropical Indian Ocean (IOBW) may also have significantly affect climate conditions around the world. JMA surveyed these impacts and summarized them in schematic chart form.

Schematic charts indicate typical anomaly patterns of surface temperature and precipitation for each season (boreal spring, summer, autumn and winter) as seen in past warmer/cooler SST events in the area of NINO.3 (corresponding to El Niño/La Niña events), NINO.WEST and IOBW. Fig. 10(a) and (b) are examples for El Niño and La Niña impacts in boreal winter (from December through February). These results are based on observation and Japanese 55-year Reanalysis (JRA-55; Kobayashi et al, 2015) data from 1958 through 2012 (a period of 55 years).

In addition, anomaly patterns of three-month-mean temperature and precipitation fields are available on the TCC website, centered on each calendar month for previous warmer/cooler SST events in each of the three tropical areas with 5°x5°-grid representation, from which the schematic charts were derived.

(a) Impacts of El Niño in boreal winter



(b) Impacts of La Niña in boreal winter

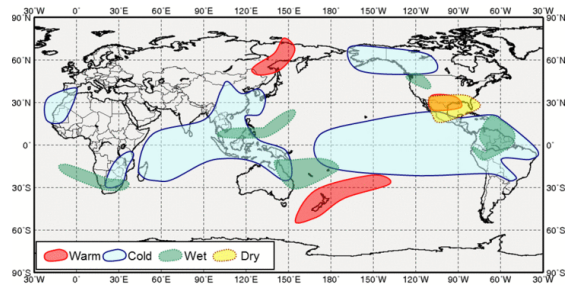
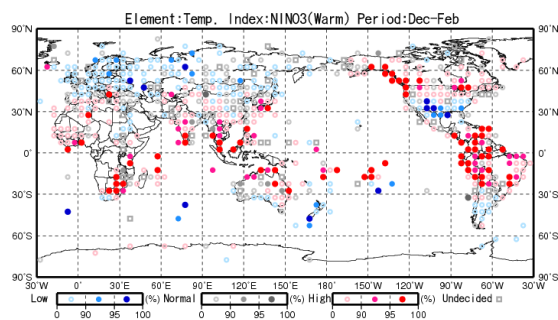


**Fig. 10.** Schematics to show impacts of (a) El Niño and (b) La Niña events in boreal winter (December-January-February)  
(<https://ds.data.jma.go.jp/tcc/tcc/products/climate/ENSO/index.htm>)

(a) Temperature anomalies



(b) Precipitation anomalies

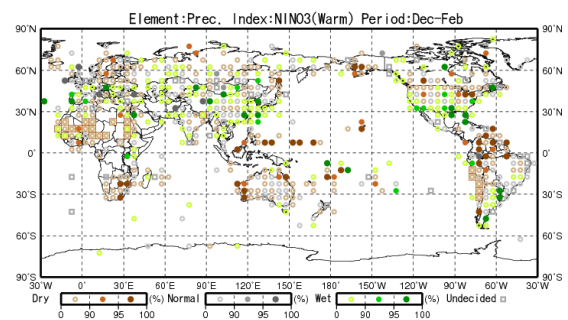


**Fig. 11.** (a) Temperature and (b) precipitation anomalies appeared in the past El Niño events in boreal winter (December-January-February)  
(<https://ds.data.jma.go.jp/tcc/tcc/products/climate/ENSO/month.html>)

## References

- Edwards, D. C. and T. B. McKee, 1997: Characteristics of 20th century drought in the United States at multiple time scales. Climatology Report 97-2, Department of Atmospheric Science, Colorado State University, Fort Collins, Colorado.
- Kobayashi, S., Y. Ota, Y. Harada, A. Ebata, M. Moriya, H. Onoda, K. Onogi, H. Kamahori, C. Kobayashi, H. Endo, K. Miyaoka, and K. Takahashi, 2015: The JRA-55 Reanalysis: General Specifications and Basic Characteristics. *J. Meteorol. Soc. Japan*, **93**, 5 - 48.
- McKee, T.B., N.J. Doesken and J. Kleist, 1993: The relationship of drought frequency and duration to time scale. In: Proceedings of the Eighth Conference on Applied Climatology, Anaheim, California, 17–22 January 1993. Boston, American Meteorological Society, 179–184.
- World Meteorological Organization, 2012: Standardized Precipitation Index User Guide (WMO-No.1090), Geneva.



## **Climate analysis information**

**– Examples of analysis of past extreme events –**



## Climate analysis information – Examples of analysis of past extreme events –

This document introduces two examples of analysis of past extreme events: (1) influences of the El Niño event in 2014-2016 on the global climate (JMA, 2017) and (2) the Heavy Rain Event of July 2018 and the persistent heatwave of summer 2018 in Japan (JMA, 2019; Shimpo et al., 2019).

### 1. Influences of the El Niño event in 2014-2016 on the global climate

An El Niño event started in summer 2014, peaked in winter 2015/2016 and ended in spring 2016. Sea surface temperatures (SSTs) in the Indian Ocean trailed the event by a couple of months and remained above normal toward spring/summer 2016. Influences from the resulting SST anomalies were extensively felt across the globe, with effects including dry conditions in Southeast Asia, extremely heavy precipitation along the Yangtze River basin.

#### 1.1 Development of the El Niño event and associated atmospheric circulation

Atmospheric circulation anomalies associated with the event are briefly described here for the period from May to October 2015 (the Asian summer monsoon season) during the development phase and before the peak, and for the period from April to June (around the onset of the Asian summer monsoon), when SST anomalies in the Indian Ocean peaked in the wake of the event. Also shown are results from statistical analysis of atmospheric circulation observed during the past El Niño events and high-SST events in the Indian Ocean.

Figure 1 shows changes in the NINO.3 index and the IOBW index, which are defined as SST departures from the climatological mean based on the latest sliding 30-year period averaged over the eastern equatorial Pacific and the tropical Indian Ocean, respectively. The NINO.3 index turned positive around spring 2014 and began to increase rapidly in spring 2015. Values began to decline after peaking in winter 2015/2016, returned to near-normal in spring 2016, and turned negative in summer 2016. The IOBW index surged on the heels of NINO.3, peaking in spring 2016 before declining throughout summer.

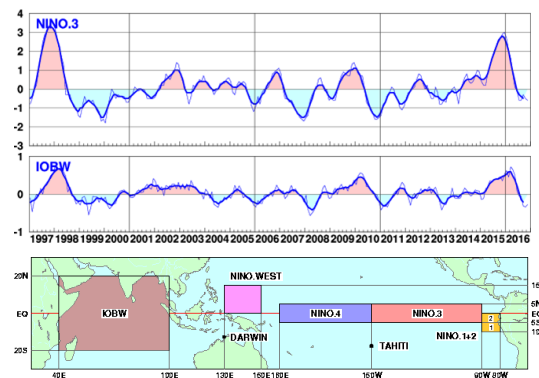


**Fig. 1.** NINO.3 and IOBW index fluctuations

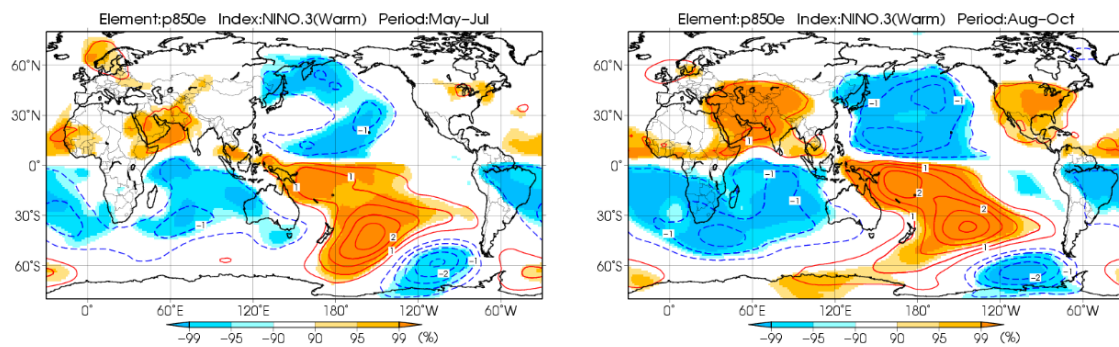
Thin lines indicate monthly values and thick lines indicate the five-month moving average. These indices are defined as SST anomalies averaged over the areas shown in the bottom panel.

Figure 2 shows stream function anomalies at 850 hPa composited over the three-month periods of May to July (early Asian summer monsoon) and August to October (late Asian summer monsoon) of El Niño years from 1958 – 2012 based on JRA-55 (Kobayashi et al., 2015). The figures show that, during Asian summer monsoon periods, equatorial symmetric cyclonic and anticyclonic circulation anomalies tend to develop in the Pacific and in the area from the Indian Ocean to the Maritime Continent, respectively, in response to convection anomalies associated with El Niño events. This anomaly pattern leads to weaker-than-normal southwesterlies and suppressed monsoon precipitation over Southeast Asia.

A composite map of stream function anomalies at 850 hPa for the three-month periods of April to June in positive IOBW years based on JRA-55, as shown in Fig. 3, indicates cyclonic circulation anomalies north of the equator in the Indian Ocean and equatorial symmetric anticyclonic circulation anomalies over the area from Indochina to the western North Pacific. These anticyclonic anomalies are likely related to equatorial Kelvin waves, which propagate from the Indian Ocean where SSTs remain above normal in the aftermath of an El Niño event, toward the western Pacific and induce Ekman divergence north and south of the equator (Xie et al., 2009).

(a) May - July

(b) August - October



**Fig. 2.** Composite map for stream function at 850 hPa during El Niño events. Three-month mean for (a) early Asian summer monsoon (May to July) and (b) late Asian summer monsoon (August to October). Anomalies are represented as deviations from the zonal mean. Contours are at intervals of  $0.5 \times 10^6 \text{ m}^2/\text{s}$ . Shading denotes statistical confidence.

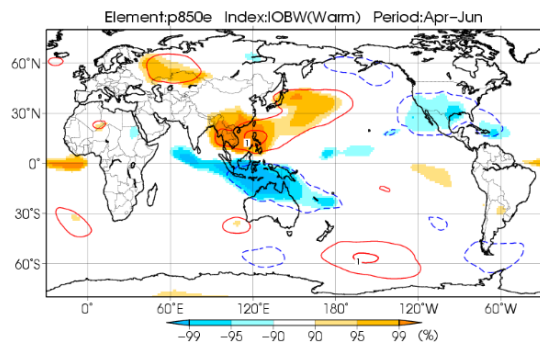
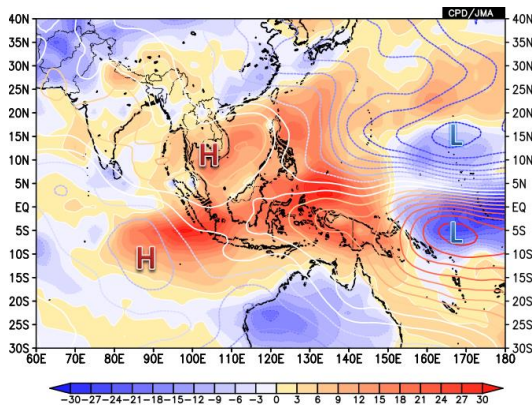


**Fig. 3.** Composite map for stream function at 850 hPa during warm IOBW events. Three-month mean for April to June. Anomalies are represented as deviation from the zonal mean. Contours are at intervals of  $0.5 \times 10^6 \text{ m}^2/\text{s}$ . Shading denotes statistical confidence.

Anomalies of outgoing longwave radiation (OLR) and stream function at 850 hPa for May to October 2015 are shown in Fig. 4 (a). The circulation pattern of this period is characterized by cyclonic circulation anomalies over the Pacific and anticyclonic circulation anomalies centered over Indochina, which is quite similar to the situation of anomalies observed in past El Niño summers as shown in Fig. 2.

Anomalies of OLR and stream function at 850 hPa for April to June 2016 (around the monsoon onset) are shown in Fig. 4 (b). The anomaly pattern closely resembles that for the positive IOBW shown in Fig. 3, with cyclonic circulation anomalies in the Indian Ocean and anticyclonic anomalies and suppressed convection over the area from Indochina to the western tropical North Pacific.

(a) May - October 2015



(b) April - June 2016

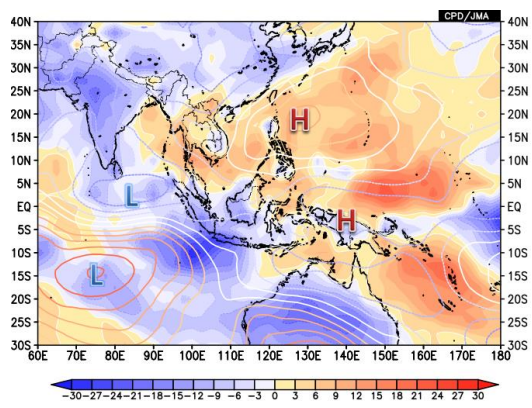


**Fig. 4.** Anomalies of outgoing longwave radiation (shading) and stream function at 850 hPa (contours)

(a) May to October 2015, and (b) April to June 2016. H and L denote anticyclonic and cyclonic circulation anomalies, respectively. Contours are at intervals of  $0.5 \times 10^6 \text{ m}^2/\text{s}$ .

## 1.2 Influences on the global climate

Some pronounced influences on the global climate from atmospheric circulation anomalies associated with the El Niño event and positive SST anomalies in the Indian Ocean are described below.

### (1) Suppressed precipitation over Southeast Asia

Southeast Asia experienced below-normal precipitation from spring 2015 to spring 2016, which adversely affected water resource management and agriculture. In addition to the worst drought conditions for 90 years in Viet Nam (United Nations Food and Agriculture Organization), a state of emergency was declared for the Mekong Delta in relation to damage caused by sea water running up the water-deprived river (United Nations Country Team Viet

Nam). Wildfires were frequently reported in Indonesia and Malaysia (United States National Aeronautic and Space Administration).

Daily cumulative precipitation calculated from Indochina observation station data is shown in Fig. 5 for the period from April 1 2015 to March 31 2016 along with the same period in recent years for comparison. In 2015, precipitation remained below normal from around May, and cumulative precipitation for the 12-month period ending March 2016 was the lowest since 2000 at that time.

Precipitation totals for the 12 months from April 2015 to March 2016 were lower than 60% of the normal for some stations in Borneo and 60 – 70% for stations in Indochina (Fig. 6). Precipitation was also below normal for the southern part of the Philippines.

As mentioned previously, southwest summer monsoon activity in Southeast Asia tends to be weak during El Niño events. The anticyclonic anomalies in the lower troposphere centered over Indochina (Fig. 4 (a)), which are considered to be responses to the weak monsoon and similar to atmospheric characteristics seen in past El Niño events (Fig. 2), were a factor behind below-normal precipitation from 2015 to 2016.

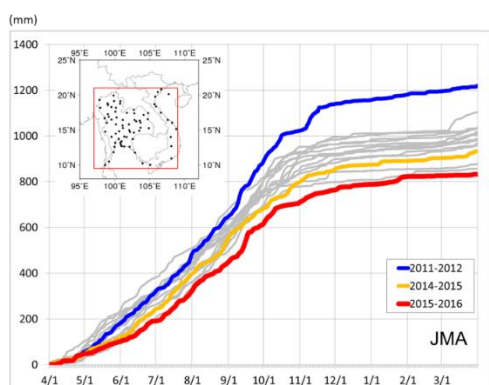


**Fig. 5.** Cumulative precipitation averaged over stations in Indochina. Observation stations are shown on the inset map. The red, yellow and blue lines indicate cumulative precipitation for 12-month periods starting April 2015, April 2014 and April 2011, respectively. Grey lines indicate other years after 2000. All data are from SYNOP.

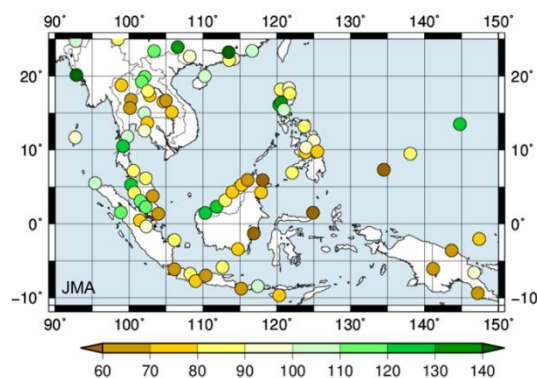


**Fig. 6.** 12-month precipitation anomalies for April 2015 to March 2016. Anomalies are based on CLIMAT reports and represented as ratios against the normal.

## (2) Heavy precipitation in the Yangtze River basin

Areas along the middle and lower Yangtze River experienced above-normal precipitation starting in April 2016. Cumulative precipitation from April 1 averaged over the stations in the basin was the highest since 1997 at that time (Fig. 7). Amounts soared from late June onward in particular, with the highest cumulative 30-day precipitation among the stations for June 21 to

July 20 exceeding 900 mm (Fig. 8). More than 200 fatalities were reported in relation to heavy rainfall and landslides from late June to early July, according to the government of China.

Such an extended period of extremely heavy precipitation was caused by strong convergence of moist air flow from the South China Sea over the Yangtze River (Fig. 9). This was induced by anticyclonic circulation anomalies over the western tropical North Pacific associated with the high SSTs in the Indian Ocean (Fig. 4 (b)).

This pattern of high SSTs in the Indian Ocean, the anticyclonic circulation anomalies over the western tropical North Pacific, moist air intrusion from the South China Sea and water vapor convergence over southern China resembled the conditions seen in 1998 – another year when the Yangtze River basin was hit by heavy precipitation.

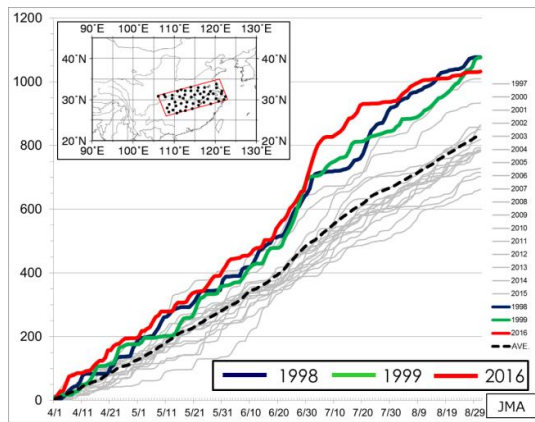


**Fig. 7.** Cumulative precipitation averaged over stations in the middle and lower Yangtze River basin. Observation stations are shown on the inset map. The red, blue and green lines indicate cumulative precipitation for the periods starting on April 1 of 2016, 1998 and 1999, and grey lines indicate the same period for all other years since 1997. The dashed black line indicates the average over the 19 years from 1997 to 2015.

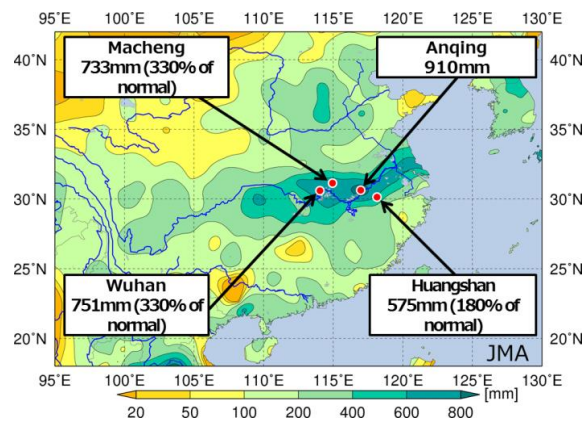


**Fig. 8.** 30-day precipitation in the middle and lower Yangtze River basin. The map indicates 30-day precipitation for June 21 to July 20, 2016, when particularly heavy rainfall was recorded. Red dots denote stations recording the three highest precipitation amounts for the 30-day period (Anqing, Wuhan and Macheng) and the highest amount for April 1 to July 24 (Huangshan).

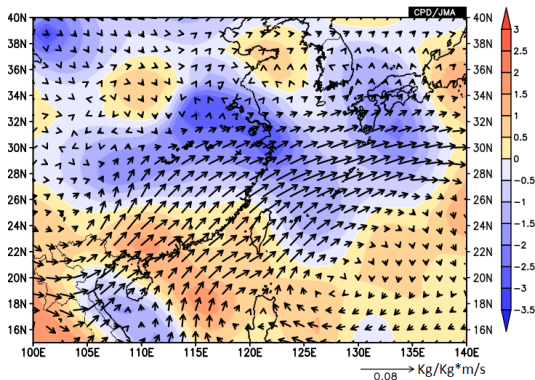


**Fig. 9.** Water vapor flux (arrows) and normalized divergence (shading) anomalies at 850 hPa for April to June 2016. Warm and cool colors indicate divergence and convergence anomalies, respectively.

## 2. The Heavy Rain Event of July 2018 and the persistent heatwave of summer 2018 in Japan

In summer 2018, Japan experienced significant rainfall particularly from western Japan to Tokai region mainly in early July causing widespread havoc nationwide, followed by extremely high temperatures subsequently persisted throughout most of Japan.

### 2.1 The Heavy Rain Event of July 2018 in Japan

#### (1) Characteristics of climate condition

Japan experienced an extreme climate event that brought unprecedented amounts of precipitation especially over western Japan and Tokai region from June 28 to July 8, 2018, which was officially named “The Heavy Rain Event of July 2018” by the Japan Meteorological Agency (JMA), in the presence of the stationary Baiu front and Typhoon Prapiroon (T1807). Some of the JMA Automated Meteorological Data Acquisition System (AMeDAS) stations in Shikoku and Tokai regions recorded more than 1,800 and 1,200 mm, respectively, during the period. Some areas experienced two to four times the precipitation of the monthly climatological normal for July (Fig. 10 (a)). Overall precipitation at 966 selected AMeDAS stations throughout Japan in early July 2018 reached 208,035.5 mm (215.4 mm per station), which was the highest among any 10-day period starting 1st, 11th, and 21st of the months since 1982, highlighting the nationwide significance of this event.

In comparison with past heavy rainfall events caused by frontal systems and typhoons, a prominent characteristic of this rain event is that the record-breaking local precipitation, particularly within 48 to 72 hours, was observed extensively over western Japan and Tokai region, including the Seto Inland Sea side of Chugoku and Shikoku regions, where monthly precipitation normal are lower than in the surroundings (Fig. 10 (b)).

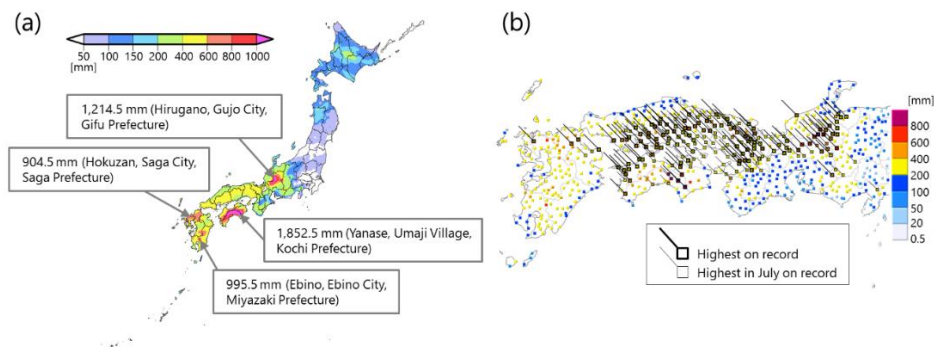


**Fig. 10.** Precipitation amounts (mm) observed during the Heavy Rain Event of July 2018 for the period from June 28 to July 8, 2018. (a) 11-day total over Japan. (b) Maximum 72-hour precipitation during the 11-day event over western Japan and Tokai region

Thick and thin squares with short lines in (b) indicate stations at which the 72-hour maxima during the event were the highest ever any time since 1982 and the highest in July, respectively.

## (2) Characteristics of atmospheric circulation

During the heavy rainfall observed over western Japan and Tokai region from July 5 to 8, the Baiu front was distinct over western Japan in association with the development of the Okhotsk High to the west of Japan and expansion of the North Pacific Subtropical High (NPSH) to the southeast of Japan (Fig. 11 (b)). The persistent confluence of two massively moist air streams over the south of Japan brought unprecedented amounts of moisture to western Japan (Fig. 11 (c)). In addition, persistent ascent was associated with the stationary Baiu front around western Japan. Some areas were also affected by line-shaped convective precipitation systems.

The synoptic-scale conditions observed around Japan were attributable to pronounced meanders of the upper-level Polar-front Jet (PFJ) and the Subtropical Jet (STJ). The development of the Okhotsk High and the expansion of the NPSH were associated with northward meanders of the PFJ around Eastern Siberia and the STJ over the east of Japan, respectively, with upper-level quasi-stationary anticyclonic anomalies there (Fig. 11 (a)). In addition, the upper-level trough lingering around the Korean Peninsula was associated with the southward meander of the STJ in the area (Fig. 11 (a)).

The primary synoptic-scale factors and large-scale atmospheric circulation contributing to the heavy rainfall observed over western Japan and Tokai region from July 5 to 8 are summarized in Figs. 12 and 13, respectively.

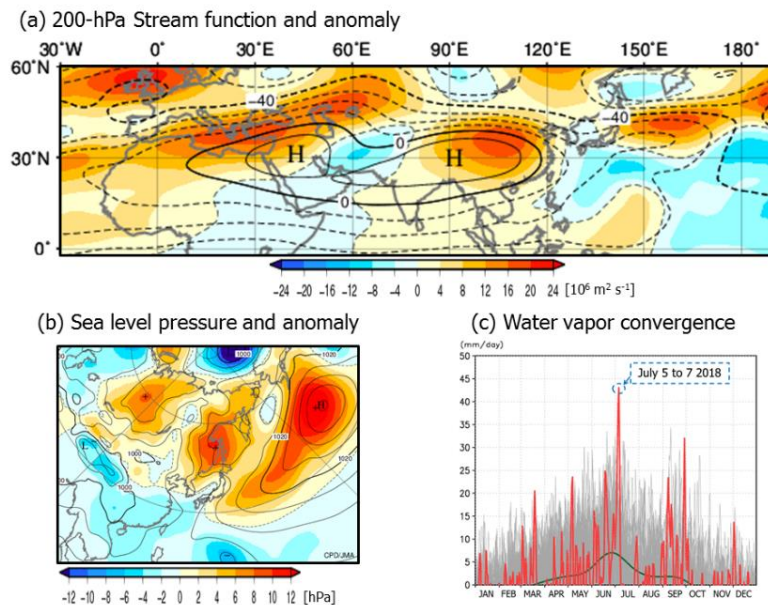


**Fig. 11.** (a) 200-hPa stream function (contours) and anomaly (shade), (b) sea level pressure (contours) and anomaly (shade) for the period from July 4 to 8, 2018, (c) three-day running-mean timeseries representation of vertically integrated horizontal moisture flux convergence (mm per day) within  $31.25 - 35^\circ\text{N}$ ,  $130 - 135^\circ\text{E}$ . The contours are drawn at intervals of (a)  $10 \times 10^6 \text{ m}^2 \text{ per s}$  and (b) 4 hPa. In (c), red, grey and green lines are annual timeseries representations for 2018, other individual years from 1958 to 2017 and the normal. The base period for the normal is 1981 – 2010.

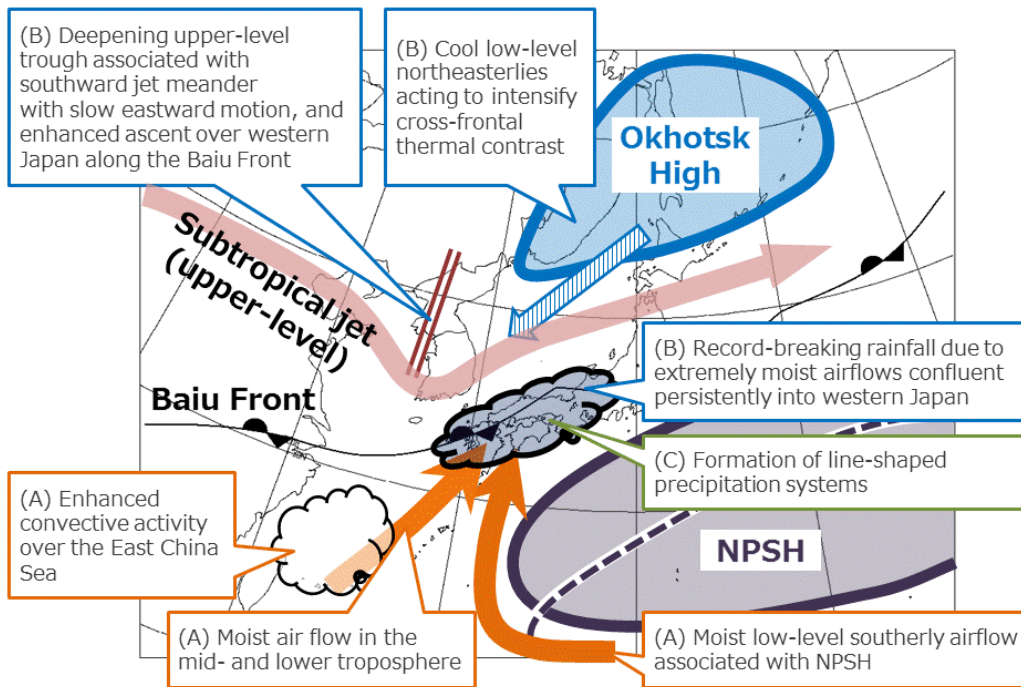


**Fig. 12.** A schematic for primary synoptic-scale factors behind the extreme rainfall event that occurred over western Japan and Tokai region from July 5 to 8, 2018  
NPSH stands for the North Pacific Subtropical High. Purple dashed line shows normal position of the NPSH.

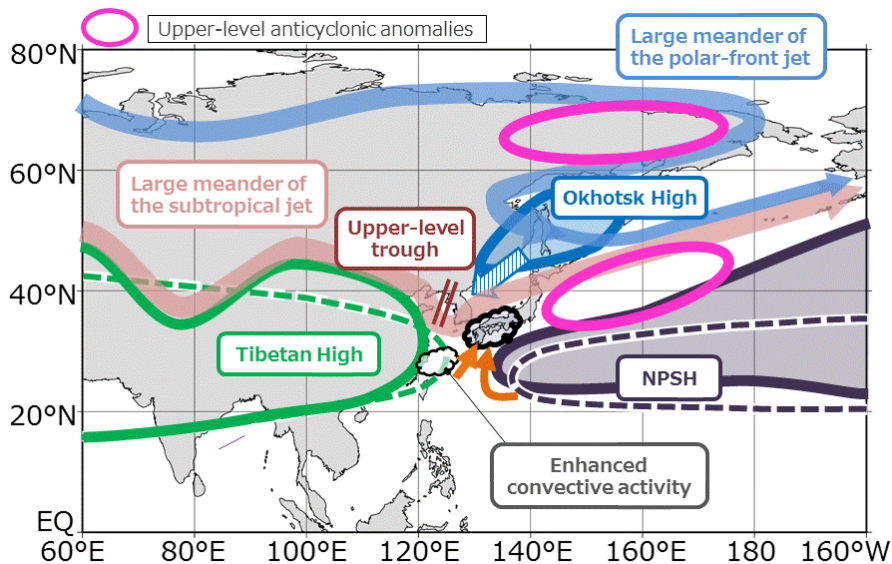


**Fig. 13.** A schematic for large-scale atmospheric circulation behind the extreme rainfall event that occurred over western Japan and Tokai region from July 5 to 8, 2018  
NPSH stands for the North Pacific Subtropical High. Purple and green dashed lines show normal position of the NPSH and the Tibetan High, respectively.

## 2.2 Heat wave in summer 2018 in Japan

### (1) Characteristics of climate condition

In summer 2018, eastern and western Japan experienced unprecedentedly hot summer conditions. The July-mean and seasonal-mean temperature anomalies for 2018 in eastern Japan were the highest on record since 1946 at +2.8°C and +1.7°C above the normal, respectively (Fig. 14), and 48 of 153 surface observation stations in Japan reported record or joint-record maximum temperatures for summer. Several reported maximum temperatures exceeding 40°C at the peak of the heatwave, and a new national record maximum temperature of 41.1°C was recorded at Kumagaya in Saitama Prefecture on July 23. At many observation stations, daily maximum temperatures often exceeded 30°C and sometimes even 35°C. A cumulative total of 6,483 AMeDAS stations observed daily temperatures of 35°C or higher from June to September 2018, exceeding the previous record in 2010 among data going back to 1976 (not shown).

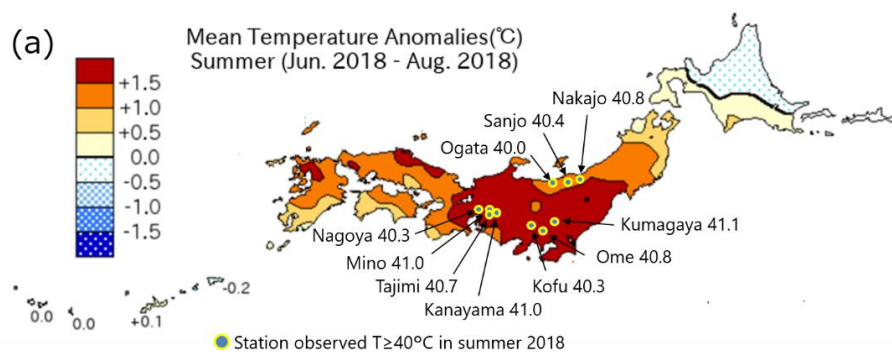


**Fig. 14.** Seasonal mean temperature anomaly (°C) for Japan in summer 2018. Stations observed daily maximum temperatures of 40 °C or higher in 2018 summer are also shown. The base period for the normal is 1981 – 2010.

### (2) Characteristics of atmospheric circulation

From mid-July to August, both the surface NPSH and the upper-tropospheric Tibetan High persisted in their extension to the main islands of Japan (Figs. 15 (a), (b)). Surface temperatures in Japan increased, due mainly to high-pressure systems with warmer-than-normal air covering the islands, predominantly sunny conditions and downward flow associated with the pressure systems.

The expansion of the Tibetan High to Japan was attributable to the northward meandering of the STJ in the vicinity of Japan with varying but persistent extents (Fig. 15 (a)). The expansion of the NPSH in the vicinity of Japan was attributable to enhanced convective activity over and around the Philippines (Fig. 15 (c)) as well as the significant meandering of the STJ.

In addition to the above effects associated with anomalous circulation, suspected factors behind the heatwave over Japan include marked tropospheric warmth over the Northern Hemisphere mid-latitudes from spring 2018 and a long-term rising trend of surface air

temperatures against a background of global warming.

Primary factors behind the unprecedentedly hot conditions observed in summer, especially in the middle and late July 2018, are summarized in Fig. 16.

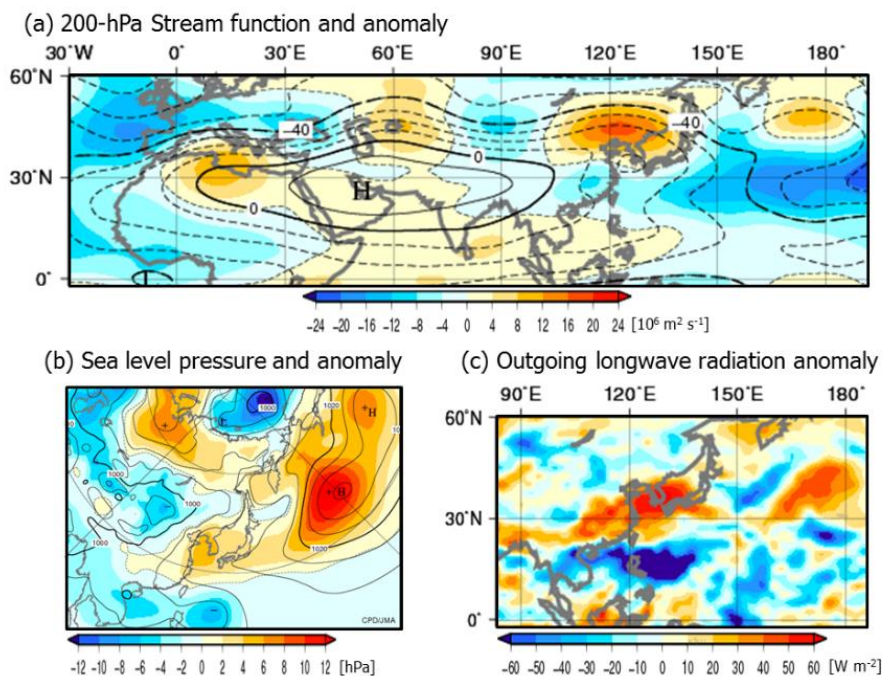


**Fig. 15.** (a) 200-hPa stream function (contours) and anomaly (shade), (b) sea level pressure (contours) and anomaly (shade), (c) outgoing longwave radiation (OLR) anomaly for the period from July 15 to 19, 2018.

The contours are drawn at intervals of (a)  $10 \times 10^6 \text{ m}^2/\text{s}$  and (b) 4 hPa. The base period for the normal is 1981 – 2010.

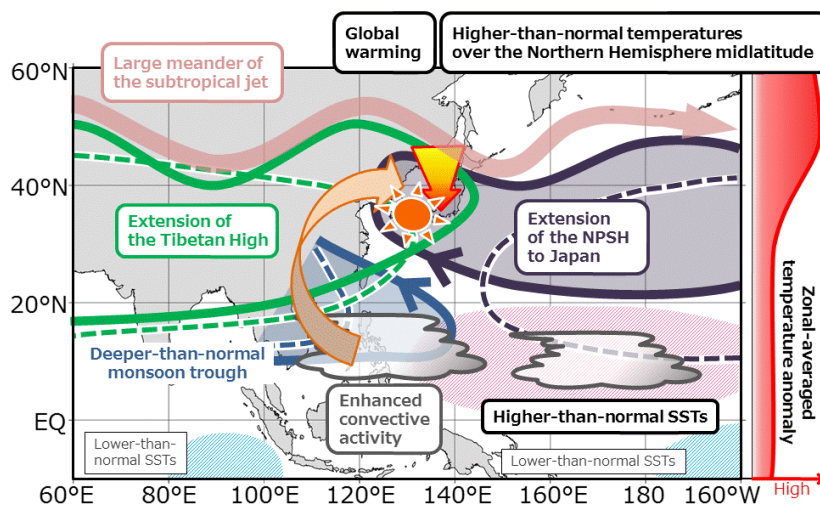


**Fig. 16.** A schematic for large-scale atmospheric circulation behind the heat wave in summer 2018, especially in the middle and late July 2018.

NPSH and SST stand for the North Pacific Subtropical High and sea surface temperature, respectively. Purple, green and blue dashed lines show normal positions of the NPSH, the Tibetan High and the monsoon trough, respectively.

## References

- Japan Meteorological Agency, 2017: *Annual Report on the Climate System 2016*, 74pp (Available on line at <https://ds.data.jma.go.jp/tcc/tcc/products/clisys/arcs/arcs2016.pdf>, accessed 5 November 2019).
- Japan Meteorological Agency, 2019: *Climate Change Monitoring Report 2018*, 92pp.
- Kobayashi, S., Y. Ota, Y. Harada, A. Ebita, M. Moriya, H. Onoda, K. Onogi, H. Kamahori, C. Kobayashi, H. Endo, K. Miyaoka and K. Takahashi, 2015: The JRA-55 Reanalysis: General Specifications and Basic Characteristics. *J. Meteorol. Soc. Japan*, **93**, 5 – 48.
- Shimpo, A., and co-authors, 2019: Primary factors behind the Heavy Rain Event of July 2018 and the subsequent heat wave in Japan. *SOLA*, **15A**, 13–18
- Xie, S.-P., K. Hu, J. Hafner, H. Tokinaga, Y. Du, G. Huang, and T. Sampe, 2009: Indian Ocean Capacitor Effect on Indo-Western Pacific Climate during the Summer following El Niño. *J. Climate*, **22**, 730 – 747.